Linear and nonlinear optics of dye-doped thin films

Cnossen, Gerard

LINEAR AND NONLINEAR OPTICS OF DYE-DOPED THIN FILMS

GERARD CNOSSEN

RIJKSUNIVERSITEIT GRONINGEN

LINEAR AND NONLINEAR OPTICS OF DYE-DOPED THIN FILMS

Proefschrift

ter verkrijging van het doctoraat in de
Wiskunde en Natuurwetenschappen
aan de Rijksuniversiteit Groningen
op gezag van de
Rector Magnificus Dr. S.K. Kuipers
in het openbaar te verdedigen op
vrijdag 13 november 1992
des namiddags te 4.00 uur

door

GERARD CNOSSEN

geboren op 2 september 1965
te Sneek

Promotor: Prof. Dr. D.A. Wiersma

Oan heit en mem,
foar Alie

This work was generously supported by AKZO Inc, Arnhem, The Netherlands, and by the Dutch Ministry of Trade and Industry (I.O.P. Programme on Polymer Composites and Special Polymers).

VOORWOORD

Op deze plaats wil ik graag een groot aantal mensen en instellingen bedanken die hebben bijgedragen aan de totstandkoming van dit proefschrift.

In de eerste plaats wil ik mijn promotor Douwe Wiersma bedanken voor het in mij gestelde vertrouwen en de wetenschappelijke vrijheid die mij werd geboden. Deze vrijheid en zelfstandigheid heb ik als bijzonder leerzaam ervaren.

Veel dank ben ik verschuldigd aan Karel Drabe, die in de afgelopen periode heeft zorg gedragen voor een zeer plezierige en directe begeleiding. De nimmer aflatende bereidheid zijn eigen werk opzij te leggen om vragen mijnerzijds te beantwoorden heb ik bijzonder gewaardeerd. Hierdoor heb ik zowel op theoretisch als op experimenteel gebied zeer veel geleerd. Zonder zijn inzet en medewerking zou dit proefschrift dan ook veel moeizamer tot stand zijn gekomen.

De enthousiaste steun van Arend Jan Schouten bij de preparatie van monolagen en polymere films was onmisbaar bij de in dit proefschrift beschreven experimenten. Ook voor het beantwoorden van de vele vragen op chemisch gebied ben ik hem dank verschuldigd. In dit kader wil ik ook Monique Schoondorp bedanken voor de plezierige samenwerking. Het bestuderen van verschillende soorten monolagen werd aanzienlijk vergemakkelijkt door de beschikbaarstelling van de azobenzenen gesynthetiseerd door Jos Hulshof uit de groep van Prof. Dr. B.L. Feringa. Het I.O.P. project betreffende Bijzondere Polymeren en Polymere Composieten wil ik, afgezien van de financiele ondersteunig, met name bedanken voor het katalyseren van bovengenoemde samenwerking.

De afdeling Electronen Microscopie ben ik zeer erkentelijk voor het spontaan beschikbaarstellen van een overbodig geworden opdampapparaat, hetgeen mij veel tijd en loopwerk heeft bespaard.

Foppe de Haan wil ik graag bedanken voor het schrijven van de uitstekende programma's voor de Monte–Carlo berekeningen en de aansturing van de verschillende laser – opstellingen.

De haastklusjes van technische aard werden altijd vakkundig geklaard door Bert van Dammen en Willem Zevenberg van de instrumentmakerij.

Alle post–doc.'s promovendi, a.i.o.'s, o.i.o.'s en studenten van de groepen Wiersma, Duppen, Kommandeur, Jonkman en Schouten wil ik bedanken voor hun bijdrage aan de prettige werksfeer op het lab.

CONTENTS

Chapter 1: ***Introduction*** 12

1.1 Background 13

1.2 Outline 14

References 18

Chapter 2: ***Localization of spontaneous emission in front of a mirror*** 19

(published in *Opt. Commun.* **73**, 91 (1989), by K.E. Drabe, G. Cnossen, and D.A. Wiersma)

2.1 Abstract 20

2.2 Introduction 20

2.3 Experimental 21

2.4 Results and discussion 22

References 28

Chapter 3: ***Spontaneous emission and dephasing in front of a mirror: Measurement of the ultrafast dynamics of nile blue in a polymer*** 30

(published in *Chem. Phys. Lett.* **169**, 416 (1990), by K.E. Drabe, G. Cnossen, and D.A. Wiersma)

3.1 Abstract 31

3.2 Introduction 31

3.3 Theory 32

3.4 Experimental 36

3.5 Results and discussion 37

References 40

Chapter 4: ***Reflection-induced source correlation in spontaneous emission*** 41

(published in *Phys. Rev. Lett.* **65**, 1427 (1990), *ibid.* **66**, 675 (1991), by K.E. Drabe, G. Cnossen, D.A. Wiersma, H.A. Ferwerda, and B.J. Hoenders)

4.1 Abstract 42

4.2 Introduction 42
4.3 Results and discussion 43
4.4 Comment by Daniel F.V. James 50
4.5 Reply 51
References 52

Chapter 5: *Fluorescence properties of rhodamine 6G physisorbed to aluminum* 54
5.1 Abstract 55
5.2 Introduction 55
5.3 Experimental 57
5.4 Results an discussion 58
References 65

Chapter 6: *Nonlinear optical properties of Langmuir-Blodgett monolayers: Local-field effects* 67
(published in *J. Chem. Phys.* **97**, ... (1992), by G. Cnossen, K.E. Drabe, and D.A. Wiersma)
6.1 Abstract 68
6.2 Introduction 68
6.3 Theory and numerical calculations 72
6.3.1 General aspects 72
6.3.2 The crystal model 76
6.3.3 The isotropic monolayer model 77
6.3.4 Numerical results 80
6.4 Experimental 85
6.5 Experimental results 87
6.5.1 General aspects 87
6.5.2 Aggregation 89
6.5.3 The tilt angle 91
6.5.4 Microscopic local-fields: dependence of $\chi^{(2)}$ on surface density 94
6.6 Discussion and conclusions 100
Appendix 101
References 103

Chapter 7: ***Second-harmonic generation in front of a mirror*** 107

7.1 Abstract 108

7.2 Introduction 108

7.3 Experimental 109

7.4 Results and discussion 110

7.4.1 Second-harmonic generation as a function of surface density 110

7.4.2 Second-harmonic generation as a function of distance to the mirror 116

References 120

Samenvatting 123

CHAPTER 1

Introduction

1.1 Background

1.2 Outline

References

1.1 Background

In this thesis optical experiments are described in which the effect of quantum electrodynamical interactions between dye–molecules and the radiation field on the linear and first–order nonlinear optical properties is studied. A separation is made between (A) the interaction of dye–molecules with their own radiation field, and (B) the interaction of dye–molecules with the emitted field of neighbouring dye–molecules. In case (A) spectral properties are studied of fluorescing molecules placed in front of metallic mirrors. Interference effects are observed, due to reflections from the mirror–surface. In the second type of experiments (B), intermolecular interactions in dye–doped monolayers are studied by means of second–harmonic generation. The efficiency of second–harmonic generation is studied as a function of the distance between, and as a function of the mutual orientation of the dye–molecules. The effect of a nearby metallic surface on the first–order nonlinear optical properties is considered.

The interest in the fluorescence properties of dye molecules in front of a mirror originated from the work of De Martini et al. [1,2]. In their work the angular dependence of the spontaneous emission of a thin Ruby crystal in front of a mirror was interpreted in terms of changes in the zero–point electromagnetic field density, caused by the presence of a nearby mirror. The observed emission pattern is explained as a clear evidence for the physical reality of the zero–point electromagnetic field. In chapter 2 of this thesis, however, it is shown that the angular and spectral localization effects observed can be explained also classically as resulting from self–interference in spontaneous emission from a Wiener–fringe pattern [3]. These interference effects were found to be useful also in a study of the optical dynamics of excited dye–molecules in polymer films (chapter 3), and in a study of the coherence properties of light emitted by molecules placed in front of a mirror (chapter 4).

In connection to the work on luminescence in front of highly reflecting surfaces ideas developed to study also second–harmonic generation in front of

these surfaces. Especially, we were interested in the influence of a mirror on the macroscopic and microscopic local-fields, for which second-harmonic generation can act as a very sensitive probe. Knowledge of the local-field is important for the interpretation of experimental results in terms of molecular properties. In order to observe strong second-harmonic signals asymmetric dye-molecules were arranged in a non-centrosymmetric way by means of the Langmuir-Blodgett monolayer technique [4]. As a reference point we first started to analyse the (microscopic) local-field inside monolayers by using glass substrates (chapter 6). The microscopic local-field is altered by varying the distance between, and by changing the mutual orientation of the dye-molecules. The effect of a metal substrate could then be compared to results obtained on glass substrates (chapter 7).

1.2 Outline

In this section a short description of the contents of each chapter is given. The relation between successive chapters is discussed.

In *chapter* 2 the effect of a mirror on the fluorescence spectra of molecules contained in a 1-2 μm thick polymer layer is discussed. Two kinds of interference effects need to be considered for a correct description of the fluorescence spectrum. In the first place interference occurs between the directly emitted wave and the wave reflected by the mirror (see Fig.1.1), also called wide-angle interference [5]. Secondly, fringes are formed upon interference between the direct and reflected wave of the exciting laser beam. A spatially modulated pattern of excited molecules is formed (Wiener grating) [6]. In case of micron thick layers this grating is essential in the detection of the wide-angle interference. In the absence of this grating wide-angle interference cannot be resolved spectrally.

The other way around, using a pulsed excitation source, wide-angle interference can be used to study the effect of phase relaxation (dephasing) [7] during the formation of the Wiener grating, the subject of *chapter* 3. Dephasing causes a loss in coherence in the ensemble of excited molecules, and

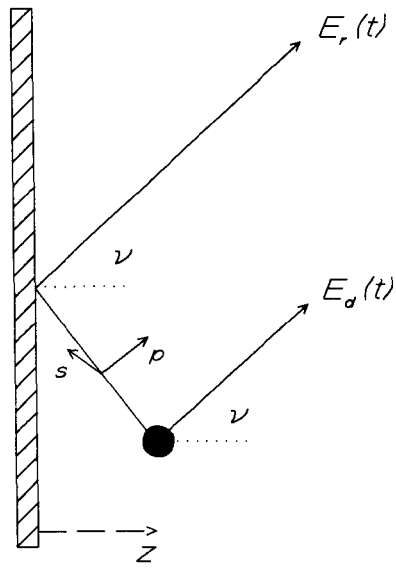

Figure 1.1: *Wide–angle interference: interference between direct and reflected rays emitted by a molecule at a distance z from the mirror. Also shown are the electric–field polarization directions parallel (p) and perpendicular (s) to the plane of incoming and outgoing beams.*

consequently reduces the visibility of the Wiener grating. By measuring the visibility of the observed interference fringes in the fluorescence spectrum as a function of the time delay between the direct and the reflected laser pulse, a dephasing time of 100 fs at room temperature could be measured for the dye molecule nile blue dissolved in poly(4–vinylpyridine). The time delay between the two pulses was varied by changing the distance between the emitting layer and the mirror. The distance could be determined from the observed interference period. A major advantage of this new technique is that only low–excitation powers are needed; it suffices to detect the spontaneous emission of the sample.

In *chapter* 4 we discuss coherence properties of light emitted by a thin fluorescing film (1–2 μm) placed in front of a mirror. The field correlation between different points in space and time is calculated, and is found to

deviate from a general scaling law, as first formulated by E. Wolf [8]. The consequence of this deviation from the scaling law is that the detected emission spectrum is not invariant on propagation, in contradiction to normal light sources (i.e. blackbody radiation) [9]. Emission spectra of a fluorescent film in front of a mirror have been measured at different points in space, and were found to depend on the distance from the light source, and the angle of observation. The observations agree well with theory.

In the above described experiments the distance between the fluorescing molecules and the metallic mirror surface was larger than the wavelength of emission ($\approx 0.6\,\mu$m). Energy transfer to the metal substrate could therefore be neglected. The effect of energy transfer on fluorescence properties of molecules separated less than 10 nm from the mirror is the subject of *chapter* 5. Energy transfer is caused by the coupling of the oscillating dipole with its fictitious image dipole in the metal substrate [10]. The coupling is brought about by the near-field of the radiating dipole. This situation is comparable to the case of two coupled pendulums [11]; the amplitude oscillates back and forth between these two pendulums. However, the difference is that the image dipole is strongly damped compared to the inducing dipole. The image dipole dissipates energy into the metal substrate by various scattering processes [10], leading to a decrease of the excited state lifetime by several orders of magnitude. In case the excited state lifetime becomes as short as the pure dephasing time, a broadening of the fluorescence spectrum is observed. This broadening has not been noticed before. The distance dependence of the above mentioned phenomena is described in chapter 5. A comparison with theory is made.

In the second part of this thesis intermolecular interactions in monolayers of dye molecules are studied by means of second-harmonic generation. In a second-harmonic generation experiment the effective surface nonlinear polarization $P_i(2\omega)$ at frequency 2ω is measured, where $P_i(2\omega)$ is given by [12]:

$$P_i(2\omega) = \sum_{j,k} \chi^{(2)}_{ijk}(2\omega,\omega,\omega) E_j(\omega) E_k(\omega) \ , \qquad (1.1)$$

here $E_{j,k}(\omega)$ is the field strength at frequency ω along the j,k axis. The quantity of interest is the second-order surface susceptibility $\chi^{(2)}_{ijk}(2\omega,\omega,\omega)$, a

proportionality constant relating the nonlinear polarization $P_i(2\omega)$ to the applied fields. Molecular parameters are contained in this term according to [13]:

$$\chi^{(2)}_{ijk}(2\omega,\omega,\omega) = N_s < T^{\lambda\mu\nu}_{ijk} > \beta_{\lambda\mu\nu} \ , \qquad (1.2)$$

where N_s is the surface density of nonlinear active molecules, $T^{\lambda\mu\nu}_{ijk}$ the coordinate transformation matrix connecting the molecular axis system to the laboratory frame, the angular brackets $< >$ denote an average over the molecular orientations, and $\beta_{\lambda\mu\nu}$ is a tensor component of the molecular nonlinear polarizability. Eq.(1.2) is only valid in case interactions between molecules can be neglected, i.e. the microscopic local-field can be neglected. In case of interactions significant deviations from linearity of $\chi^{(2)}_{ijk}(2\omega,\omega,\omega)$ in surface density N_s can be expected.

In *chapter* 6 the macroscopic surface susceptibility of dye-doped Langmuir-Blodgett monolayers is studied as a function of surface density. Deviations from a linear behaviour of $\chi^{(2)}_{ijk}(2\omega,\omega,\omega)$ with surface density are found. The experimental results are confirmed by theoretical calculations assuming a certain ordering of the molecules at the surface. The ordering of the molecules is revealed by second-harmonic generation and by linear absorption spectroscopy.

In *chapter* 7 second-harmonic generation in front of a metallic mirror is studied. The frequency doubling efficiency is again measured as a function of surface density. In front of a mirror the applied field components differ in magnitude from the applied fields in front of a glass substrate. Therefore induced dipole moments have different directions, leading to different interactions within the monolayer. Less pronounced deviations from linearity are found. Also described are experiments in which the distance between the mirror and the optical nonlinear monolayer is varied over a range from 1 to 6 nm. The efficiency of second-harmonic generation is found to decrease for small distances from the mirror. The results are explained in terms of energy transfer. Here energy transfer again leads to an enhanced damping rate of the

optical transition, which is expected to reduce the molecular nonlinearity.

References

[1] F. De Martini, *Phys. Lett.* **A115**, 421 (1986).

[2] F. De Martini and G. Innocenti, *Quantum Optics*, edited by J.D. Harvey and F.D. Walls (Springer–Verlag, Berlin, 1986), Vol. IV.

[3] M. Born and E. Wolf, *Principles of Optics* (2^{nd} edition, Pergamon Press LTD, Oxford, 1964).

[4] *Langmuir–Blodgett films*, edited by G. Roberts (Plenum Press, London, 1990).

[5] O. Halpern and F.W. Doermann, *Phys. Rev.* **52**, 937 (1937).

[6] O. Wiener, *Ann. d. Phys.* **40**, 203, (1890).

[7] see for example L. Allen and J.H. Eberly in *Optical Resonance and Two–Level Atoms* (John Wiley & Sons, Inc., New York, 1975).

[8] E. Wolf, *Phys. Rev. Lett.* **56**, 1370 (1986).

[9] E. Wolf, *J. Opt. Soc. Am.* **68**, 6 (1978).

[10] Th. Arvidis and B.N.J. Persson, *J. Phys. Chem.* **88**, 837 (1984).

[11] see for example R.P. Feynman, R.B. Leighton, and M. Sands in *The Feynman Lectures on Physics* (Addison–Wesley Publishing Compagny, London, 1977).

[12] Y.R. Shen, *Annu. Rev. Phys. Chem.* **40**, 327 (1989).

[13] Th. Rasing, G. Berkovic, Y.R. Shen, S.G. Grubb, and M.W. Kim, *Chem. Phys. Lett.* **130**, 1 (1986).

CHAPTER 2

Localization of spontaneous emission in front of a mirror

2.1 Abstract

2.2 Introduction

2.3 Experimental

2.4 Results and discussion

References

2.1 Abstract

We show that the fluorescence emitted in front of a mirror exhibits angular and spectral localization effects that are caused by self–interference in the spontaneous emission from a Wiener–fringe pattern. A semi–classical description is given and found to be in good agreement with the observations.

2.2 Introduction

About two decades ago it has been shown that the lifetime of spontaneous emission of a molecule or atom in front of a mirror can be influenced by the presence of a mirror at a distance comparable to the wavelength of the emitted light [1]. The influence of boundary conditions on radiation was pointed out by Purcell [2] and first observed by Drexhage [1] in a pioneering study of the fluorescence of organic dyes close to a mirror. Drexhage et al. [1] showed that the fluorescence lifetime of a dye molecule close to a mirror exhibits an oscillatory behaviour as a function of distance between the molecule and the mirror. This effect has been explained classically [3,4] as arising from the coupling between the molecule's radiating dipole and its fictitious mirror image. At some distances the two dipoles oscillate in phase, leading to a shorter fluorescence lifetime; at other distances they oscillate out of phase and the lifetime is lengthened. One can also consider the effect to arise from the self–interference between the wave packet emitted into the solid angle of observation with its reflection from the mirror in the same direction [5]. Quantum electrodynamically, spontaneous emission results from the coupling of the excited molecule to the vacuum states of the electromagnetic field. The effect of a mirror near a radiating molecule is explained as a change of the mode density of the vacuum field to which the excited molecule is coupled by the molecule–radiation field hamiltonian. If the density of resonant "vacuum" states is reduced lifetime lengthening occurs, if the density is increased the

spontaneous emission lifetime decreases.

Recently it has been suggested by De Martini [6] and Innocenti [7] that the observed angular dependence of the spontaneous emission of a thin ruby slab in front of a mirror provides clear evidence for "the physical reality of the zero-point electromagnetic field". In other words, they claimed that this angular dependence of the spontaneous emission could only be explained quantum electrodynamically. This remarkable statement inspired us to reinvestigate this phenomenon, using a thin polymer film doped with the strongly fluorescing molecule Rhodamine 6G as a probe. We show in this chapter that the angular and spectral localization effects observed in the luminescence of atoms and molecules near a mirror can be explained also classically as resulting from self-interference in spontaneous emission from a Wiener-fringe pattern [8,9]. We further show that the observed enhancements in the spontaneous emission at long wavelengths rule out the importance of Lippmann fringes [9] in the observed effects.

2.3 Experimental

Fig. 2.1 shows schematically the outline of the experiment. A low-divergence (<0.5mr), expanded laser beam (≈ 20mm diameter, power density $17\,\mathrm{mW/cm^2}$) is used to excite the fluorescence of a thin polymer film doped with Rhodamine 6G (R6G). As excitation source we used the frequency-doubled output of a modelocked Nd-YAG or a cw Ar^+ laser. The exciting light beam was polarized perpendicular to the plane of incidence with an angle v_p with respect to the mirror normal.

The polymer poly(4-vinylpyridine) film doped with R6G was oriented parallel to the mirror. The polymer films were prepared by spin-coating a solution of 14 weight% polymer, 0.8 weight% R6G in 2-chloro ethanol either directly onto an aluminum mirror or on a pre-existing polystyrene layer on the mirror. The thickness of the films and intermediate polystyrene lasers used in these experiments varied between 1 to 10 μm; the concentration of R6G was adjusted to an optical density of about 0.2 in a single pass for all films.

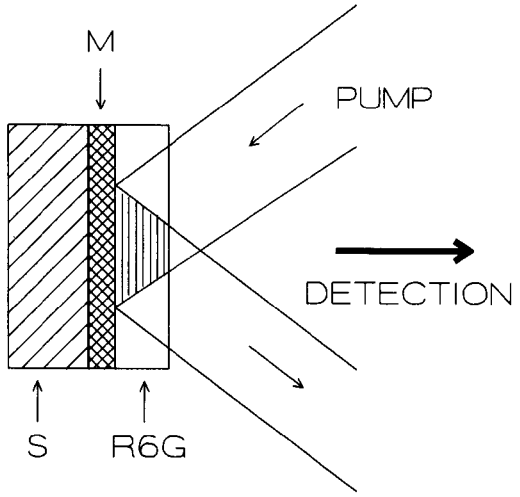

Figure 2.1: *Schematical outline of the geometry of the experiment. S, M and R6G denote substrate, mirror and the polymer film doped with R6G, respectively.*

The emission of the R6G film was angularly resolved with a resolution better then 0.5 mr using a 155 mm focal length lens and a 0.05 mm diameter pinhole. A polarizer was placed behind the the pinhole, and was oriented such that s-polarization of the emission was also wavelength resolved using a 1 m grating spectrometer (Spex 1704). Special care was taken to insure that the emission properly filled the mirrors and grating of the spectrometer, as misalignment affected the results.

2.4 Results and discussion

Fig. 2.2 shows a typical R6G fluorescence spectrum observed in a direction perpendicular to the mirror. The 7 μm thick R6G film was directly spin-coated onto the Al mirror and excited by a Nd-YAG laser beam at an angle of 40 degrees with the mirror normal in air. On comparing this spectrum with that of a film

spincoated on an optical flat, one notes an enhancement of the emission intensity at about 16750 cm^{-1}. This enhancement of the emission intensity is certainly not due to stimulated emission, as all spectra at any detection angle v could be reproduced with a tenfold decrease in pump intensity (i.e. $1.5 mW/cm^2$). We note that De Martini et al. [6,7] observed a similar localization effect in the case of a ruby crystal when the total emission in the perpendicular direction was monitored as a function of pump angle v_p.

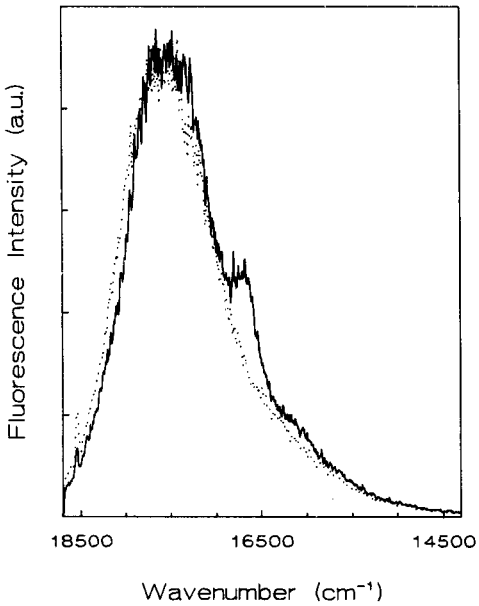

Figure 2.2: *Fluorescence spectrum of R6G in a polymer film: on top of a mirror (solid line), and without mirror (dashed line).*

In order to explain these angular and spectral localization effects, consider an emitter at a distance z from the mirror. The total field $E_t(t)$ is detected at distances much larger than z, in which case the direct ($E_d(t)$) and reflected field ($E_r(t)$) have nearly the same weight, i.e.

$$E_t(t) = E_d(t) + E_r(t) \tag{2.1}$$

(in the above equation E_t is the projection onto the s-polarized polarizer).

When the emission is detected at an angle v with respect to the mirror normal, a simple geometrical consideration gives for the path difference between the direct and reflected light $2z\cos v$. We then may write for the reflected field

$$E_r(t) = R\exp(i\Delta)E_d(t-\tau_m)\,, \tag{2.2}$$

where R is the reflectivity, $\Delta \equiv \Delta(v)$ the phase jump due to the mirror in the direction v, v the angle with the mirror normal ($v=0$ is perpendicular to the mirror), and $\tau_m = 2z\cos v/c$, with c the speed of light in the R6G film. In the present experiments the spectral content $I_t(\omega)$ of the total field (consisting of both the direct and reflected light) is determined. The spectral intensity is proportional to the Fourier transform of the auto-correlation function of $E_t(t)$ [10], i.e.

$$I_t(z,\omega) \propto |\hat{E}_t(\omega)|^2 = (1/4\pi)^2 \int_{-\infty}^{+\infty} dT \exp(i\omega T) < E_t^*(t)E_t(t+T) > \,. \tag{2.3}$$

In the above equation, the coherence time of the auto-correlation function of the spontaneous emission is determined by the decay time of the homogeneously broadened transition, averaged over the static inhomogeneous distribution of the center-frequencies of the emitters, and summed over the vibronic transitions. In working out the above equation one easily obtains for the spectral content of an emitter located at z

$$I_t(z,\omega) = I_d(\omega) + R^2 I_d(\omega) + 2RI_d(\omega)\cos(\omega\tau_m - \Delta)\,, \tag{2.4}$$

where $I_d(\omega)$ corresponds with the spectral intensity of the field $E_d(t)$ only.

Interestingly enough, the interference term given by the last term in Eq.(2.4) is independent of any factors which determine the coherence length of the emission of R6G. This despite the fact that the emission is allowed to interfere before its spectral content is determined. The above result is

identical to the results of Drexhage [1] and Fleck [11] derived under the limiting condition of a monochromatic emitter. The result of Eq.(2.4) is also very similar to the case where wide angle interference is studied [12,13]. In order to obtain the emission of the R6G film, the Wiener fringes [8,9] formed by the incident and reflected pump beam should be taken into account. The resulting density of excited molecules as a function of z is given by

$$\rho(z) = 1 + R^2 - 2R\cos(2k_{pz}z)\,, \tag{2.5}$$

where $k_{pz} = k_p \cos v_p$. It is assumed that the index of refraction of the R6G film is about the same as the transparent film, and that the phase jump is π upon reflection.

The total emission of the sample then follows simply by adding the intensities of Eq.(2.4) with a weight given by Eq.(2.5), i.e.

$$I_t(\omega) = \frac{1}{L_2 - L_1}\int_{L_1}^{L_2} \mathrm{d}z\, \rho(z)\, I(z,\omega)\,, \tag{2.6}$$

where $L_1 = 0$ if the R6G film is on top of the mirror and $(L_2 - L_1)$ the thickness of the sample. In writing out Eq.(2.6) many terms arise; the dominant terms are

$$I_t(\omega)/I_d(\omega) = (1+R^2)^2 + 2R^2\cos[(k_{pz}-k_z)(L_2+L_1)]\,\mathrm{sinc}[(k_{pz}-k_z)(L_2-L_1)]\,, \tag{2.7}$$

where $\mathrm{sinc}x = (\sin x)/x$, $k_z = k\cos v$, and k the wavevector of the emission. Eq.(2.7) is the central result of this chapter.

We first note that when $L_1 = 0$ and $R = 1$, Eq.(2.7) reduces to the expression obtained by De Martini et al. [6,7] (vide infra). These authors, however, derived this result quantum electrodynamically whereby explicitly a zero-point standing-wave field perpendicular to the mirror was introduced. The observed angular dependence of the ruby luminescence, as described by the second term of Eq.(2.7), was interpreted by them as a clear indication of the physical reality of a zero-point vacuum field in front of a boundary. This interpretation is

certainly not unique as Eq.(2.7) was derived entirely classical without explicit reference to the existence of a zero-point field.

Eq.(2.7) predicts that for R6G films spin-coated directly on top of the mirror the fluorescence spectrum consists of two components: (a) the normal fluorescence spectrum with weight $(1+R^2)^2$, and (b) an interference term given by $2R^2\mathrm{sinc}[2(k_{pz}-k_z)L_2]$. The maximum of the sinc function is located at $k_z=k_{pz}$. Thus by varying the pump angle v_p, one changes $k_{pz}=k_p\cos v_p$ which causes a shift of the top of the sinc function to a different region of the emission spectrum. Similarly, if v_p is held constant, changing the angle v at which the emission is viewed also moves the top of the sinc function to another wavelength (recall that $k_z=k\cos v$).

The above mentioned features were found to be in agreement with the experimental results. In general, Eq.(2.7) was found to be in quantitative agreement, provided that for large angles v or v_p the appropriate phase jump upon reflection is used. Notable exceptions were found only for films directly spincoated on the mirror and having a thickness less than about 1.5 μm. The explanation of this anomaly is outside the scope of the present chapter.

It is of interest to note that by integrating Eq.(2.7) over ω space, the total emission intensity as a function of pump angle v_p is obtained. In the special case of $L_1=0$ and a sample thickness much less than the coherence length of the emission, one can easily see that Eq.(2.7) remains valid with $I_t(\omega)$ replaced by $I_t\equiv\int I_t(\omega)\,\mathrm{d}\omega$. These conditions were actually met in De Martini's experiments on ruby [6,7].

Eq.(2.7) further predicts that for films separated from the mirror an additional cosine modulation should be present. The emission spectra obtained were found to be in quantitative agreement with Eq.(2.7). An example is shown in Fig. 2.3 where the R6G film was separated from the Al mirror by a transparent polystyrene film. Larger separations between the R6G film and the mirror (up to about 0.5 mm) have been realized by spin-coating the R6G film on a Separate optical flat (flatness better than $\lambda/10$). The film faced the reflective surface of an Al or dielectric mirror. The interference patterns were also found to be remarkably insensitive to mechanical vibrations, despite the fact the total length of optical path was in excess of 5 m. This stability basically results

from the presence of Wiener fringes, which keep the excited molecules at a fixed distance from the mirror.

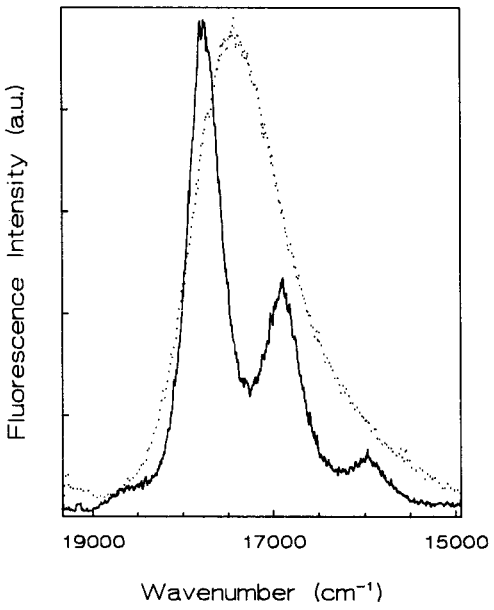

Figure 2.3: *Fluorescence spectra of R6G in a 2 μm thick polymer film: 2.2 μm separated from the mirror by a transparent film (solid line), and without mirror (dashed line). From the periodic modulation, described by the cosine term in Eq.*(2.7), *one obtains the distance of the film to the mirror.*

Finally, we have also used the interference effect to asses the importance of Lippmann fringes [9,14,15] in these type of experiments. A Lippmann fringe arises from energy transfer among near resonant molecules in front of a mirror. The spatial fringe pattern is similar to the Wiener one of Eq.(2.5) except for an additional factor z^{-2} [14,15]. Two conclusions can immediately be drawn: (a) Lippmann fringes will only be formed in spectral regions where absorption and emission overlap, (b) the effect of Lippmann fringes will rapidly diminish for thicker layers. Our experiments clearly show that for sample thickness between 1.5 and 20 μm the observed emission enhancements are in accord with Eq.(2.7).

Using thick samples ($>10\,\mu$m) the fluorescence interference effect can be shifted to spectral regions where absorption and emission do not overlap. In this case we also found the predicted enhancement.

We therefore conclude that Lippmann fringes are of no importance to the description of the interference effects discussed in this paper.

Whether Lippmann fringes play a role in the observed anomalous emission spectra from thin samples ($<1.5\,\mu$m) deposited on mirrors, remains to be studied.

In conclusion: we have shown that the angular and spectral localization effects observed in the spontaneous emission of molecules in front of a mirror can be explained satisfactorily using classical theory. It was further shown that Wiener and not Lippmann fringes determine the observed enhancement of the spontaneous emission.

References

[1] K.H. Drexhage, *Progress in Optics*, edited by E. Wolf (North–Holland, Amsterdam, 1974), Vol. XII, p165.

[2] E.M. Purcell, *Phys. Rev.* **69**, 681 (1946).

[3] H. Kuhn, *J. Chem. Phys.* **53**, 101 (1970).

[4] P.W. Milonni and P.L. Knight, *Opt. Commun.* **9**, 119 (1973).

[5] H. Morawitz, *Phys. Rev.* **187**, 187 (1969).

[6] F. De Martini, *Phys. Lett.* **A115**, 421 (1986).

[7] F. De Martini and G. Innocenti, *Quantum Optics*, edited by J.D. Harvey and F.D. Walls (Springer–Verlag, Berlin, 1986), Vol. IV.

[8] F.A. Jenkins and H.E. White, *Fundamentals of Optics* (4^{th} edition, McGraw–Hill, New York, 1987).

[9] M. Born and E. Wolf, *Principles of Optics* (2^{nd} edition, Pergamon Press LTD, Oxford, 1964).

[10] R. Loudon, *The Quantum Theory of Light*, (2^{nd} edition, Clarendon Press, Oxford, 1983).

[11] M. Fleck, *Dissertation*, University of Marburg (1969), Germany.

[12] E. Schrödinger, *Ann. d. Phys.* **61**, 69 (1920).

[13] O. Halpern and F.W. Doermann, *Phys. Rev.* **52**, 937 (1937).

[14] E. Fermi, *Rev. Mod. Phys.* **4**, 87 (1932).

[15] G.S. Agarwal, *Phys. Rev.* **A12**, 1987 (1975).

CHAPTER 3

Spontaneous emission and dephasing in front of a mirror: Measurement of the ultrafast dynamis of nile blue in a polymer

3.1 Abstract

3.2 Introduction

3.3 Theory

3.4 Experimental

3.5 Results and discussion

References

3.1 Abstract

We show that the spontaneous emission spectrum of a thin sample in front of a mirror exhibits Wiener–type fringes that contain information on the dephasing dynamics of the excited molecules. In order to probe these dynamics, the molecules must be excited with a short optical pulse or with a light field that has a correlation time shorter than the dephasing time constant T_2. The technique is used to study the ultrafast dephasing of nile blue in a polymer matrix at room temperature. A homogeneous dephasing time constant T_2 of 100 ± 10 fs is obtained.

3.2 Introduction

At the end of the last century Wiener [1] observed that when a photosensitive material in front of a mirror is illuminated with a well–collimated light beam, fringes are formed that run parallel to the flat mirror surface. When lasers became available, several new optical phenomena were discovered, such as the photon echo [2] and transient–grating scattering [3]. The physical basis for these techniques depends on the formation of Wiener–type fringes. The fringe pattern or grating in these experiments is formed by interference of two (non–parallel) pulses in the sample. When the excitation pulses are time–coincident a grating is formed in real space and its decay can be monitored by a third probe pulse. When the excitation pulses are time–delayed with respect to one another, a grating is formed in *frequency* space. When this frequency grating is excited with a third pulse a stimulated photon echo is generated. It has been shown that a two–pulse photon echo can be described as a self–diffraction effect from a frequency grating [4].

In the last decade transient–grating and photon–echo experiments on the picosecond time scale have been extensively used to study condensed–phase molecular dynamics [5,6]. When femtosecond excitation pulses are used for these

type of experiments, sample damage quite often occurs because of the high electrical fields associated with these short pulses. High intensities, however, are often needed to produce sufficient coherence in the sample to enable detection of the coherent signal, such as a femtosecond photon echo [7]. Therefore it is desirable to have optical probes available having the same information content, but not relying on the formation of a macroscopic polarization.

In this chapter we report a new technique to probe femtosecond dephasing dynamics, requiring only low-excitation intensities. The method is based on the measurement of the *spontaneous emission* spectrum of a thin sample (about 2 μm) in front of a mirror. The sample is excited by a 40 fs pulse from a colliding-pulse mode-locked (CPM) laser or by a 5 ns pulse of a spectrally broad-band dye laser that has a field correlation time of 55 fs. The presence of a mirror has two effects: Firstly, it leads to the creation of a transient Wiener-fringe pattern; secondly, it leads to an interference effect in spontaneous emission spectrum. The amplitude of this fringe pattern as a function of distance between the sample and the mirror is determined by the optical-dephasing time constant T_2. Experiments on the dye molecule nile blue doped into a thin film of poly(4-vinyl pyridine) yield a T_2 of 100 ± 10 fs at room temperature.

3.3 Theory

Prior to discussing the experiments in greater detail, we present the theoretical foundation of our new method. Fig.3.1a shows the simplified level scheme of the dye molecule, and Fig.3.1b gives the schematics of the experimental arrangement. In our experiments on nile blue, a number of vibronic states {2} are optically excited that relax to the vibrationless excited state 3. From this state 3, emission occurs to the vibrational manifold {1} of the ground state. As low-excitation intensities are used, the pulse angles $\theta(\mu E/\hbar)$ are small: $\sin\theta \approx \theta$. Here μ is the transition dipole and E the electric field associated with the pulse and $\hbar$ Planck's constant divided by 2π. The mirror in

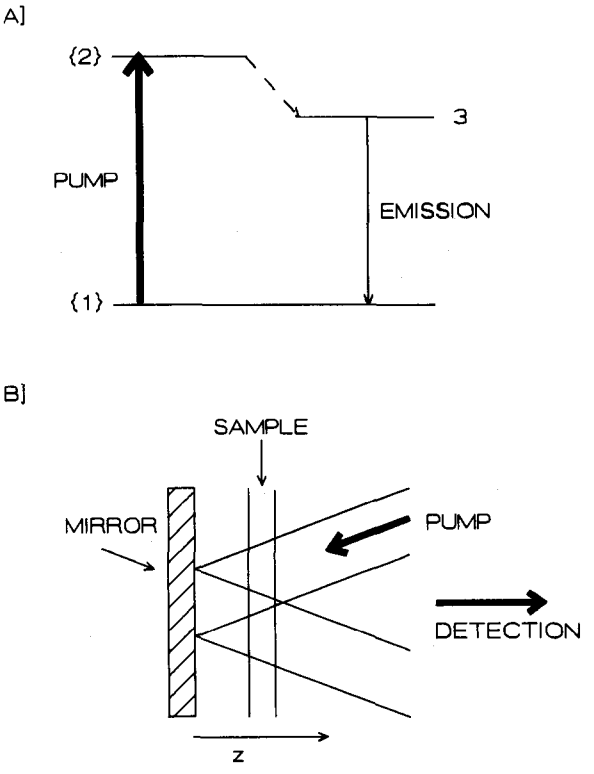

Figure 3.1: (A) *Relevant level scheme for nile blue.* {1} *and* {2} *denote vibrational manifolds in the ground and excited state, while* 3 *stands for the vibrationless excited singlet state.* (B) *Schematics of the experimental arrangement. Note that the emission is detected in a direction perpendicular to the mirror.*

our experiments is assumed to be ideal; it has a reflectivity of 1 and imposes a phase shift of π on a reflected light wave. Consider now an ensemble of molecules at a distance z from the mirror and excited at t_0. Due to the presence of a mirror these molecules are again excited by a reflected pulse at a time t_{21}:

$$t_{21} = (2z\cos\upsilon_p)n/c\,, \tag{3.1}$$

where υ_p is the angle of incidence of the pump beam with respect to the mirror normal, c the speed of light in vacuum, and n the refractive index of the sample material. These excitation pulses form a Wiener–fringe pattern in both the ground and excited state. When the inhomogeneous broadening of the vibronic and pure electronic transitions are correlated [8], the Wiener–fringe pattern in the relaxed excited state (ρ_{33}) is proportional to [4]

$$\rho_{33}(z,\Delta,t) \propto \theta^2 \exp(-\Delta^2/\sigma^2)\exp(-t/T_1)[1-\exp(-\Gamma_{21}t_{21})\cos(\Delta t_{21}+2k_{zp}z)]\,, \tag{3.2}$$

where θ is the excitation pulse angle, Δ the detuning from the center of the excitation wavelength, and σ the width of the Gaussian inhomogeneous distribution of optical oscillators. T_1 is the population relaxation time of state 3 and Γ_{21} the homogeneous linewidth of the vibronic $2\leftarrow 1$ transition, $k_{zp} = (\omega_p \cos\nu_p)n/c$ is the projection of the wavevector of the pump beam on the normal to the mirror. In deriving Eq.(3.2) we assumed the excitation pulse duration to be much shorter than the dephasing time constant Γ_{21}. The minus sign preceding the damping term in Eq.(3.2) arises from the phase shift of π between the excitation pulses. Note that the population in level 3 as a function of distance to the mirror exhibits an oscillatory behaviour, known as the Wiener–fringe pattern [1] or grating.

Eq.(3.2) shows that the amplitude of the transient Wiener–fringe pattern is not only damped by a population relaxation (T_1) process, but also by a homogeneous dephasing (Γ_{21}) process. For two–level systems Γ_{21}^{-1} is known as the optical–dephasing lifetime T_2.

In order to obtain the emission spectrum of all molecules in the sample we have to convolute $\rho_{33}(z,\Delta,t)$ with the emission spectrum of a single molecule in the inhomogeneous distribution and then integrate the resulting expression over z and t. It can be seen from Eq.(3.2) that integration over z, in a sample much longer than the wavelength of light, leads to a severe suppression of the fringe pattern in emission. However, in the presence of a mirror, a single photon

interference effect in the spontaneous emission should be taken into account. For the subensemble of molecules located at distance z from the mirror this interference term is $1-\cos(2k_z z)$ [1], where $k_z = k\cos\nu$, with k the absolute value of the wave vector, and ν the angle of observation with respect to the mirror normal. One thus obtains for the emission spectrum angularly resolved in the direction ν:

$$I^{\nu}(t,\omega) = \int_{L_1}^{L_2} \mathrm{d}z\,[\rho_{33}(z,\Delta,t) *_{\Delta} I^{e}_{hom}(\omega,\Delta)]\,[1-\cos(2k_z z)]\,, \tag{3.3}$$

where $I^{e}_{hom}(\omega,\Delta)$ is the homogeneous emission spectrum of a single site at position Δ in the inhomogeneous line, $*_{\Delta}$ means a convolution with respect to Δ, and the integration over z takes the finite thickness of the sample into account. For $L_1 = 0$ the sample is on top of the mirror. Integration over z gives a number of terms, the dominant one arising from the product $\exp(-\Gamma_{21}t_{21})\int \mathrm{d}z \cos(\Delta t_{21} + 2k_{zp}z)\cos(2k_z z)$. In order to obtain an explicit expression for the emission spectrum, we assume that the spectrum of a single site in the inhomogeneous band is Lorentzian:

$$I^{e}_{hom}(\omega,\Delta) = \frac{\Gamma_{31}}{[\omega - (\Omega^{e}_{0} + \Delta)]^2 + \Gamma^2_{31}}\,. \tag{3.4}$$

Here Ω^{e}_{0} is the center of the inhomogeneously broadened emission line and Γ_{31} is the homogeneous decay rate. Two extreme cases will be considered: In the first case (A), the optical transition is predominantly inhomogeneously broadened, meaning that $\sigma \gg \Gamma_{31}$. In the second case (B), the transition is predominantly homogeneously broadened , i.e. $\sigma \ll \Gamma_{31}$.

Using Eqs.(3.3) and (3.4), we calculate for case (A)

$$I^{\nu}(\omega) \propto I^{e}_{inhom}(\omega)\,\{1 + \tfrac{1}{2}\exp[-(\Gamma_{31}+\Gamma_{21})t_{21}]\cos[\kappa(L_1+L_2)]\,\mathrm{sinc}[K(L_2-L_1)]\}\,. \tag{3.5}$$

Here $I^{e}_{inhom}(\omega)$ is the inhomogeneously broadened emission spectrum,

$\kappa = (n/c)[(\omega_p + \omega - \Omega_0^e)\cos\nu_p - \omega\cos\nu]$, $K = k_{zp} - k_z$ and $\mathrm{sinc}x = \sin x/x$. In deriving Eq.(3.5) we have assumed that the sample thickness is such that the transit time $n(L_2 - L_1)/c$ is short compared to $(\Gamma_{21} + \Gamma_{31})^{-1}$. In all our experiments the emission spectrum was detected in the direction perpendicular to the mirror, meaning that $\cos\nu = 1$. We then calculate from Eq.(3.5) that the modulation period of the fringe pattern in emission is $1/n(1 - \cos\nu_p)(L_2 - L_1)$ (in cm^{-1}), where L_1 and L_2 are expressed in centimeters. For the homogeneous case (B) we obtain an expression of the same form as Eq.(3.5) but with a damping term $\exp(-\Gamma_{21}t_{21})$ instead of $\exp[-(\Gamma_{31} + \Gamma_{21})t_{21}]$ and with $\kappa = K = k_{zp} - k_z$. In the homogeneous case we thus find a modulation period in the emission spectrum of $1/n(L_1 + L_2)$. Note that exactly the same modulation period is found when the emission spectrum is excited with a cw laser; in this case the fringe amplitude, however, does not depend on dephasing [9].

Eq.(3.5) is the main result of this chapter. It predicts that for short pulse excitation of a thin sample in front of a mirror the emission spectrum exhibits fringes that are damped by the sum of the dephasing constants Γ_{21} and Γ_{31} (case A) or by the dephasing constant Γ_{21} only (case B). Moreover, whether we are dealing with case (A) or case (B) can be ascertained from the modulation period in the emission spectrum.

In closing this section we note that it has been shown [10] that Eq.(3.5) also holds for excitation with a stochastic light source for which the correlation time is much less than the dephasing time.

3.4 Experimental

The experiments were performed on thin (about 2μm thick) polymer films, prepared by spincoating a solution of poly(4–vinylpyridine) (P4VP) doped with the fluorescent molecule nile blue. The concentration of nile blue in the dry film was about 10^{-3}M. The sample was separated from the Al mirror by a transparent poly(styrene) film. A glass plate with index–matching oil was mounted on top of the sample to circumvent etalon effects in the measurement of the emission spectrum. The emission spectra were angularly resolved in a

direction perpendicular to the mirror with a resolution of 25 cm^{-1}.

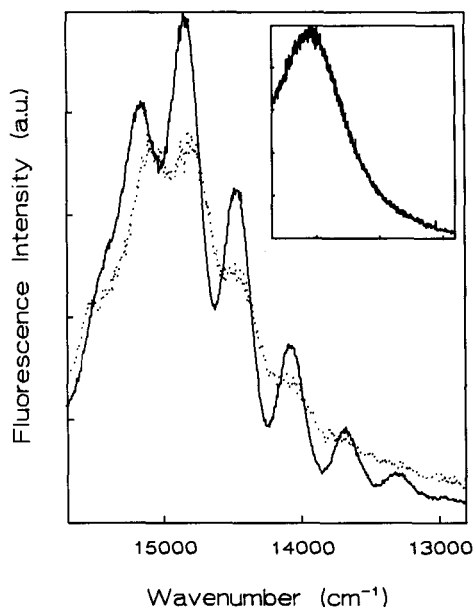

Figure 3.2: *Room-temperature emission spectra of nile blue doped in a thin film of poly(4-vinylpyridine). The solid is the spectrum obtained in front of a mirror and excited with a cw HeNe laser operating at 632.8nm. The dashed spectrum is obtained when under the same conditions a 40fs pulse from a CPM laser is used for excitation. The insert shows the spectrum obtained without a mirror.*

3.5 Results and Discussion

Fig. 3.2 displays two emission spectra of nile blue in front of a mirror: one excited with a HeNe laser, the other with 40fs pulses from a CPM laser. The first thing to note is that the fringe period in both spectra are identical, consistent only with the case of a *homogeneously* broadened emission spectrum. If the emission spectra was predominantly *in*homogeneously broadened the modulation

period would have been 10 times larger ($\cos\nu_p \approx 0.9$) than in the present experiment. The reduced intensity of the fringes in the emission spectrum when the CPM laser is used for excitation, is attributed to homogeneous dephasing between the excitation pulses. To measure the homogeneous dephasing time constant Γ_{21} a number of samples were made with varying thickness of the spacer layer and their emission spectra recorded using the CPM and a HeNe laser as excitation source. Identical conditions regarding excitation spot size, detection angle and detection aperture were used.

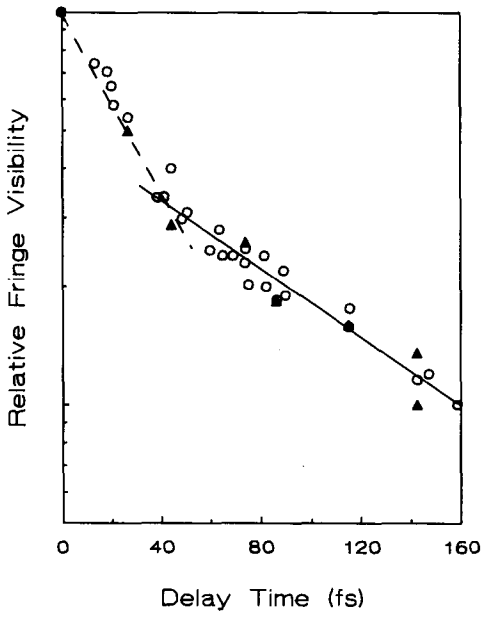

Figure 3.3: *Relative fringe visibility in emission of nile blue doped in poly(4-vinylpyridine) as a function of delay between the incident and reflected pulse from the mirror. The delay times were calculated from the modulation period in emission and use of Eq.*(3.1). *The open circles are data points obtained using the CPM laser; the closed triangles are data points obtained by stochastic excitation with a spectrally broad-band dye laser*

Fig. 3.3 shows a plot (open circles) of the *relative* fringe visibility in

emission as a function of distance between the emitting layer and the mirror for CPM versus HeNe excitation. The fringe visibility is defined as $(I_{max}-I_{min})/(I_{max}+I_{min})$, where I_{max} is a maximum and I_{min} a minimum of the modulation in the emission spectrum. For short pulse delays (dashed line in Fig. 3.3) the fringe intensity follows closely the excitation pulse correlation function. For pulse-delay times greater than 40 fs, the decay of the fringe intensity is fitted to an exponential with a time constant of 100 ± 10 fs (solid line in Fig. 3.3). The closed triangles in Fig. 3.3 are data points obtained by stochastic excitation using a dye-laser pulse with a field-correlation time nearly identical to that of the CPM-laser pulse. As can be seen the results obtained with a stochastic and coherent light source are identical. We therefore conclude that the homogeneous dephasing time for the lowest singlet transition of nile blue in P4VP is 100 ± 10 fs at room temperature. For nile blue in solution at room temperature, Becker et al. [7] measured an optical T_2 of 65 fs, using the photon-echo technique. It is surprising to find that in a polymer the bath fluctuations occur on a comparable time scale as in a solution. This raises the following question : To what extent, in a polymer at room temperature, can one separate the time scales for homogeneous and inhomogeneous broadening?

De Silvestri et al. [11] concluded from femtosecond three-pulse scattering experiments that dye-doped polymer systems are homogeneously broadened at room temperature. This conclusion is supported by excitation-wavelength-dependent emission spectra of nile blue in P4VP. Only a small spectral shift ($\leq 25\ cm^{-1}$) of the emission band is observed upon varying the wavelength of an exciting light source (bandwidth $6\ cm^{-1}$) over the spectral range of the 40 fs CPM-laser pulse From consideration of these facts, the question arises of what the relationship is between the measured optical-dephasing time of 100 ± 10 fs and a "relaxation time" of 7 fs (calculated from the $1450\ cm^{-1}$ "homogeneous" width in the emission spectrum. We propose that the apparent "homogeneity" of the emission spectrum is caused by overlap of spectra from many different initial vibronic states. As our method relies on the interference effect of a single photon emitted from a particular vibronic state, it measures the vibration-averaged dynamics of a wavepacket on the excited-state potential-energy surface.

In conclusion: a new technique to measure ultrafast dephasing processes has

been demonstrated and discussed. In this method a mirror aids in the formation and detection of a frequency and spatial grating excited by a light field with a short correlation time. A major advantage of the method is that only low-excitation powers are needed; it suffices to detect the spontaneous emission of the sample. An interesting aspect of the method is that it also provides information on the homogeneous and inhomogeneous contributions to the spectrum. Since the detected emission arises from an incoherently populated state, the measured decay is not complicated by quantum beats as in femtosecond photon-echo-decay experiments

References

[1] O. Wiener, *Ann. d Physik* **40**, 203 (1890).

[2] N.A. Kurnit, I.D. Isabella, and S.R. Hartmann, *Phys. Rev. Lett.* **18**, 567 (1964).

[3] H.J. Eichler, *Opt. Acta* **24**, 631 (1977).

[4] K. Duppen and D.A. Wiersma, *J. Opt. Soc. Am.* **B3**, 614 (1986).

[5] M.D. Fayer, *Ann. Rev. Phys. Chem.* **33**, 63 (1982).

[6] D.A. Wiersma and K. Duppen, *Science* **237**, 1147 (1987).

[7] P.C. Becker, H.L. Fragnito, J.Y. Bigot, H. Brito Cruz, R.L. Fork, and C.V. Shank, *Phys. Rev. Lett.* **63**, 505 (1989).

[8] K. Duppen, D.P. Weitekamp, and D.A. Wiersma, *Chem. Phys. Lett.* **106**, 147 (1984).

[9] K.E. Drabe, G. Cnossen, and D.A. Wiersma, *Opt. Commun.* **73**, 91 (1989).

[10] K.E. Drabe, G. Cnossen, and D.A. Wiersma, to be published.

[11] S. De Silvestri, A.M. Weiner, J.G. Fujimoto, and E. Ippen, *Chem. Phys. Lett.* **112**, 195 (1984).

CHAPTER 4

Reflection-induced source correlation in spontaneous emission

4.1 Abstract

4.2 Introduction

4.3 Results and discussion

4.4 Comment by Daniel F.V. James

4.5 Reply

References

4.1 Abstract

We present fluorescence spectra showing that the spontaneous–emission spectrum of a molecule in front of a mirror is not invariant on propagation. We also calculate the cross–spectral density of this light source and show that it does not obey Wolf's scaling law [*Phys. Rev. Lett.* **56**, 1370 (1986)].

4.2 Introduction

Wolf [1] recently showed that the spectrum of a light source cannot generally be expected to be invariant on propagation through free space. Wolf also showed that for a planar, quasihomogeneous light source the normalized spectrum in the far–field zone is only identical to the source spectrum if the spectral coherence of the light source obeys a certain scaling law. The light source satisfies the scaling law if the complex degree of coherence $\mu^{0}(\omega,\boldsymbol{r}_2-\boldsymbol{r}_1)$ is only a function of the variable $k(\boldsymbol{r}_2-\boldsymbol{r}_1)$, where ω is the angular frequency, $\boldsymbol{r}_2-\boldsymbol{r}_1$ is the vectorial distance between two points in the source plane, and k is the absolute value of the wave vector.

It is obvious that it is quite important to investigate which light sources do or do not obey the scaling law. For instance, the question may be raised whether light sources of great cosmological interest such as stars and quasars obey the scaling law [2]. If not, then, as Wolf [2] showed, the interpretation of spectral redshifts as solely arising from the Doppler effect in an expanding universe must be reexamined. A deviation from the invariance on propagation can also be a complicating factor in obtaining frequency standards.

Bocko, Douglass, and Knox [3] recently showed that source correlations can lead to marked frequency shifts of spectral lines. Their experiments were performed using two acoustic sources that were partly correlated. Morris and Faklis [4,5] recently demonstrated that by using a Fourier achromat one can generate a light source that also violates Wolf's scaling law. Wolf [2]

suggested that the superradiance and superfluorescence may lead to source correlations and hence to light sources that are variant on propagation. An entirely different physical mechanism for source correlations might arise from correlations between the refractive index of pairs of points in a spatially random medium [2].

In this chapter we show that spontaneous emission in front of a mirror presents a light source that violates Wolf's scaling law. Fig. 4.2 shows two fluorescence spectra obtained at two different points in space. It is clear that these spectra are rather different. The physical origin of this effect is easily understood as arising from interference between the direct and reflected light into a certain direction ν (see also the inset of Fig. 4.1). If a molecule is situated at a distance z from the mirror, the path difference between the interfering rays in the direction ν is $2z\cos\nu$, leading to constructive or destructive interference depending on the wavelength of the emitted light. This interference effect is basically a wide-angle interference effect as studied by Schrödinger [6], by Halpern and Doermann [7], and more recently by Drexhage [8] and De Martini [9].

4.3 Results and discussion

In order to understand the propagation effect in greater detail we have to examine the cross-spectral density of a single emitter; in the second step we account for the mode of excitation and spatial extent of our light source and sum over all emitters in the sample.

The cross-spectral density is defined as [1]

$$W(\boldsymbol{r}_1,\boldsymbol{r}_2,\omega)=\int_{-\infty}^{+\infty} d\tau \exp(i\omega\tau)<E^*(\boldsymbol{r}_1,t)E(\boldsymbol{r}_2,t+\tau)> , \qquad (4.1)$$

where $E(\boldsymbol{r},t)$ represents the complex analytical signal at the space-time point $(\boldsymbol{r},t)$, the angular brackets indicate an ensemble average, $\boldsymbol{r}_1$ and $\boldsymbol{r}_2$ denote two positions, and ω denotes the angular frequency ($\omega=kc$, where k is the absolute

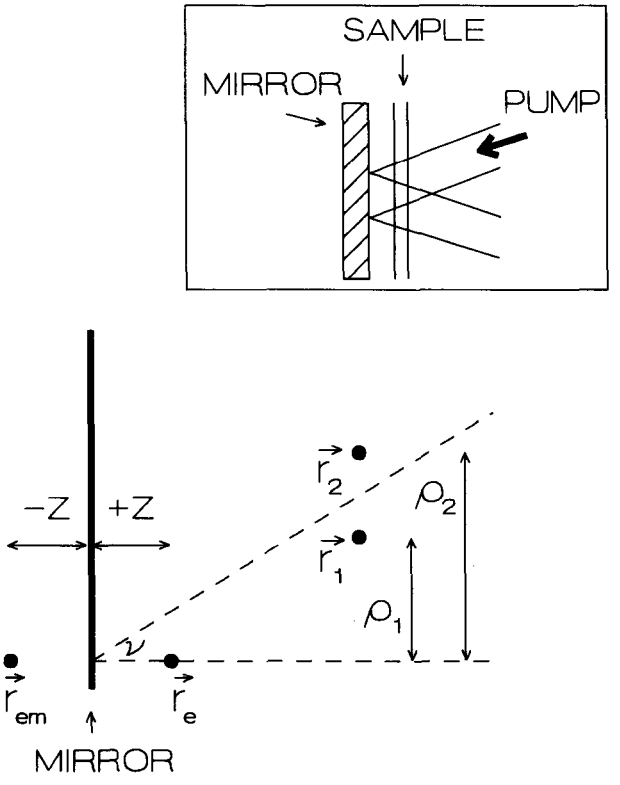

Figure 4.1: *Illustration of notation. Inset: A schematical outline of the geometry of the experiment.*

value of the wave vector, and c the speed of light). In the case of spontaneous emission, it is appropriate to replace the classical fields in Eq.(4.1) by field operators. Particularly convenient is the Heisenberg representation of the

source field given by [10]

$$E^{+}(\boldsymbol{r}_1,t) = (A/|\boldsymbol{r}-\boldsymbol{r}_e|)\prod(t-|\boldsymbol{r}-\boldsymbol{r}_e|/c)\,, \tag{4.2}$$

where $\boldsymbol{r}_e$ is the position of the emitter, $\boldsymbol{r}$ the observation point (which should be sufficiently far away), and $\prod$ a deexcitation operator of the emitter. In the above expression we have contracted several constants into A and have also omitted the orientational dependence of the field. Eq.(4.1) then becomes

$$W_{mol}(\boldsymbol{r}_1,\boldsymbol{r}_2,\omega) = \int_{-\infty}^{+\infty} d\tau \exp(i\omega\tau) < E(\boldsymbol{r}_1,t)E^{+}(\boldsymbol{r}_2,t+\tau) > \,. \tag{4.3}$$

We may write for the electric-field operator at position $\boldsymbol{r}_1$ [10],

$$E^{+}(\boldsymbol{r}_1,t) = E^{+}_{direct}(\boldsymbol{r}_1,t) - RE^{+}_{reflected}(\boldsymbol{r}_1,t)\,, \tag{4.4}$$

where R is the reflectivity of the mirror, and the minus sign arises from a phase jump of π on reflection. The subscripts "direct" and "reflected" indicate the different trajectories the spontaneous emission takes. From the functional dependence of the source-field expression on $\boldsymbol{r}_1$ and t in Eq.(4.2), it is clear that we can relate E_{direct} and $E_{reflected}$ in Eq.(4.4) according to

$$E^{+}_{reflected}(\boldsymbol{r}_1,t) = E^{+}_{direct}(\boldsymbol{r}_1,t-\tau_{1d})\,, \tag{4.5}$$

where τ_{1d} is given below. In precisely the same way we can relate the field operator $E(\boldsymbol{r}_2,t)$ to the space point $\boldsymbol{r}_1$,

$$\begin{aligned} E(\boldsymbol{r}_2,t) &= E_{direct}(\boldsymbol{r}_2,t) - RE_{reflected}(\boldsymbol{r}_2,t) \\ &= E_{direct}(\boldsymbol{r}_1,t-\tau_{12}) - E_{direct}(\boldsymbol{r}_1,t-\tau_{2d})\,, \end{aligned} \tag{4.6}$$

where τ_{12}, τ_{2d}, and τ_{1d} are related to path differences which follow from geometrical considerations (see also Fig. 4.1):
$c\tau_{12} = |\boldsymbol{r}_2-\boldsymbol{r}_e| - |\boldsymbol{r}_1-\boldsymbol{r}_e| \approx (\rho_2-\rho_1)\sin\nu$,

$c\tau_{2d} = |\boldsymbol{r}_2 - \boldsymbol{r}_{em}| - |\boldsymbol{r}_1 - \boldsymbol{r}_e| \approx (\rho_2 - \rho_1)\sin\nu - 2z\cos\nu$,
$c\tau_{1d} = |\boldsymbol{r}_1 - \boldsymbol{r}_{em}| - |\boldsymbol{r}_1 - \boldsymbol{r}_e| \approx 2z\cos\nu$, where $\boldsymbol{r}_{em}$ is the position of the mirror image of the emitter located at $\boldsymbol{r}_e$. It is to be noted that we have assumed that both $\boldsymbol{r}_1$ and $\boldsymbol{r}_2$ are sufficiently large such that in Eq.(4.2) differences in $1/|\boldsymbol{r}_i - \boldsymbol{r}_j|$ ($\boldsymbol{r}_i = \boldsymbol{r}_1, \boldsymbol{r}_2$ and $\boldsymbol{r}_j = \boldsymbol{r}_e, \boldsymbol{r}_{em}$) can be neglected.

Denoting the emission spectrum of an emitter in free space by $S_{mol}(\boldsymbol{r},\omega)$ [which is the Fourier transform of the expectation value $<E_{direct}(\boldsymbol{r},t)E^{+}_{direct}(\boldsymbol{r},t)>$], one obtains for the cross-spectral density of a single emitter in front of a mirror,

$$W_{mol}(\boldsymbol{r}_1,\boldsymbol{r}_2,\omega) = S_{mol}(\boldsymbol{r}_1,\omega)\exp\{ik(\rho_2 - \rho_1)\sin\nu\}\{(1+R^2) - 2R\cos(2kz\cos\nu)\} . \tag{4.7}$$

Note that the cross-spectral density is not only a function of $k(\rho_2 - \rho_2)$, but also depends on the distance z of the emitter to the mirror.

The above equation has been derived for the case of a single emitter. In case of an ensemble of independent emitters we may obtain the cross-spectral density by summing over all emitters:

$$W_{ens}(\boldsymbol{r}_1,\boldsymbol{r}_2,\omega) = \int \mathrm{d}x\mathrm{d}y\mathrm{d}z\,\kappa(x,y,z)W_{mol}(\boldsymbol{r}_1,\boldsymbol{r}_2,\omega) , \tag{4.8}$$

where $\kappa(x,y,z)$ is the density of emitters as a function of coordinates x,y,z. The evaluation of this integration is rather cumbersome and depends on the geometry of the sample. However, sufficient insight into its functional behaviour can be obtained in the following way. First, consider a monolayer of emitters parallel to the mirror. It is readily seen from Fig. 4.1 that the integration over x and y in Eq.(4.8) can be replaced by an integration over the angle ν only, and it follows that the cross-spectral density remains a function of $k(\rho_2 - \rho_1)$ and kz. In particular, we find that for large distances the sample can be approximated by a (two-dimensional) point source, in which case an integration over ν is unnecessary. In addition to the spatial extent of our light source, we must also integrate over the thickness of the sample. In particular, we must account for the periodic density $\kappa(z)$ of excited molecules,

which is simply proportional to the Wiener fringes formed upon excitation [11,12],

$$\kappa(z) = 1 + R^2 - 2R\cos(2k_{pz}z)\,, \tag{4.9}$$

where $k_{pz} = k_p \cos\nu_p$ and the phase jump upon reflection is again taken to be equal to π. Eq.(4.8) then becomes, for $\boldsymbol{r}_1, \boldsymbol{r}_2$ in the far field (with the *spatial* extent of the source approximated by a point),

$$W_{ens}(\boldsymbol{r}_1, \boldsymbol{r}_2, \omega) = \frac{1}{L_2 - L_1} \int_{L_1}^{L_2} \mathrm{d}z W_{mol}(\boldsymbol{r}_1, \boldsymbol{r}_2, \omega)\kappa(z)\,, \tag{4.10}$$

where $L_1 = 0$ means that the fluorescent sample is on top of the mirror and $L_2 - L_1$ is the thickness of the sample. By using Eqs.(4.7) and (4.9) in Eq.(4.10), Many terms are obtained after integration. The dominant ones are easily recognized [13] and given by

$$W_{ens}(\boldsymbol{r}_1, \boldsymbol{r}_2, \omega) = S_{mol}(\boldsymbol{r}_1, \omega)\exp\{ik(\rho_2 - \rho_1)\sin\nu\}$$
$$\times\{(1+R^2)^2 + 2R^2\cos[(k_{pz} - k_z)(L_2 + L_1)]\mathrm{sinc}[(k_{pz} - k_z)(L_2 - L_1)]\}\,, \tag{4.11}$$

where $\mathrm{sinc}x = (\sin x)/x$, $k_z = k\cos\nu$, and k is the absolute value of the wave vector of the emission.

Eq.(4.11) is the main result of this chapter. The emission spectrum is obtained by putting $\boldsymbol{r}_1 = \boldsymbol{r}_2$ (i.e., $\rho_1 = \rho_2$). Note that it is the interference term between direct and reflected light (the second term in the curly braces) that causes a deviation from the scaling law. Indeed if the reflectivity is taken to be zero, the spectrum is invariant on propagation.

In Fig. 4.2 the fluorescence spectrum (lower curve) is shown from the molecule nile blue in front of a mirror. This spectrum is obtained from a position at a large distance from from the sample, in which case the spatial extent can be considered as a point. This spectrum is described by Eq.(4.11) and depends only on the angle of observation. The other spectrum in Fig. 4.2 (upper

curve) is obtained from a position in space closer to the mirror, at a distance such that the spatial extent of the source has to be taken into account. Now the integration over the angle ν should be performed, which tends to wash out the $\cos(2kz\cos\nu)$ term in Eq.(4.7). The relevance of this observation is that in a plane parallel to the mirror and sufficiently close to the fluorescent film, the spectrum is the same at every point in this plane. Spectra taken at points closer to the film than the spectrum of Fig. 4.2 (upper curve) are identical to the spectrum of nile blue obtained without a mirror. In other words, it is possible to define a source plane in which the spectrum is the same at every point across it.

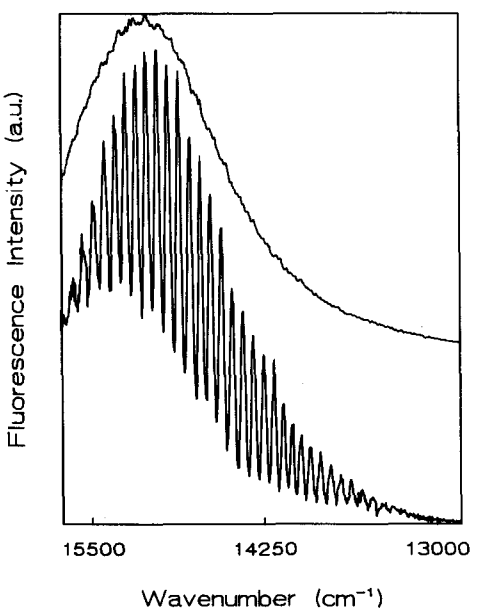

Figure 4.2: *Fluorescence spectra of nile blue at two different points. The upper spectrum is taken at a distance of* 1 *mm from the film; the lower spectrum is taken at a distance of* 100 *mm from the film. Both spectra were obtained from the same sample. Note that the upper spectrum has been shifted for the ease of comparison. The polymer film, containing nile blue, was* 2.5 μm *thick and at a distance of* 54 μm *from the mirror.*

The experiments were performed using polymer layers (1–10 μm thickness) of poly(4–vinylpiridine) doped with the fluorescent molecule nile blue. The films were spincoated on glass plates and placed parallel to an Al mirror. The nile blue molecules were excited by a low divergent HeNe laser having a beam diameter of 1 mm. The low power density (less than 6 mW/mm^2) used precludes any significant contribution from stimulated emission in the spectra. The pump beam, polarized perpendicular to the plane of incidence, is incident at an angle ν_p with respect to the mirror normal. The emission spectrum was detected with an $f/1.6$ lens. The focal point could be located at various points outside the sample. A second lens (210 mm focal length), placed about 500 mm from the first lens, ensures that only light near the focal point of the first lens is properly focused into a 1–m–grating spectrometer. At the exit slit of the spectrometer a photomultiplier tube was used for detection. The particular choice of the laser beam diameter inside the sample and the position of the focal point determines the detection angle and angular resolution.

To summarize, we have shown that spontaneous emission in front of a reflecting surface presents a light source that violates Wolf's scaling law. A noteworthy property of the source is that a plane can be defined in which the spectrum is the same at every point. However, at points outside this plane the spectrum is position dependent. The position dependence basically arises from interference of light traveling directly and via the mirror to the point of observation. However, the effect is not limited by the coherence length of the source (which in our case of nile blue is only a few μm).

As radiation quite often can be expected to be contaminated with reflected light, this violation of the invariance of the spectrum on propagation can occur under rather general conditions. Of course, the *quantitative* extent to which the observed spectrum is dependent on position is determined by a number of factors, of which angular and spectral resolution are most important. As a significant amount of light (about 10%–20%) out of the Universe reaches us via reflection of particles present in interstellar dust [14], it remains a challenge to explore the relevance of our findings.

We gratefully acknowledge discussions with Dr. R. Laureys (Laboratory for Space Research, The Netherlands) on reflective properties of interstellar dust.

4.4 Comment by Daniel F.V. James

In this section a comment [15] written by D.F.V. James is reproduced concerning our work on reflection–induced source correlations [16]. Our reply [17] is presented in the next section.

Drabe et al. have recently presented an important and novel contribution to the study of the spectroscopy of partially coherent sources [17]. However some comments are appropriate with regard to the relationship of their work to Wolf's original theoretical investigations of this subject [1].

Wolf's analysis applies to quasihomogeneous sources. Such sources have the following properties: (1) Their degree of spatial coherence has the functional form $\mu_Q(\boldsymbol{r}_1,\boldsymbol{r}_2,\omega)=g(\boldsymbol{r}_2-\boldsymbol{r}_1,\omega)$, and (2) the spectral intensity $S_Q(\boldsymbol{r},\omega)$ varies so slowly with position that

$$S_Q(\boldsymbol{r}_1,\omega)\approx S_Q(\boldsymbol{r}_2,\omega)\approx S_Q((\boldsymbol{r}_1+\boldsymbol{r}_2)/2,\omega)$$

whenever $|\boldsymbol{r}_1-\boldsymbol{r}_2|\le l$, l being the effective spatial width of $|g(\boldsymbol{r}_1-\boldsymbol{r}_2,\omega)|$, i.e., the coherence length at frequency ω. Under these circumstances the cross–spectral density has the form

$$W_Q(\boldsymbol{r}_1,\boldsymbol{r}_2,\omega)\approx S_Q((\boldsymbol{r}_1+\boldsymbol{r}_2)/2,\omega)\,g(\boldsymbol{r}_2-\boldsymbol{r}_1,\omega)\,.$$

The source described by Drabe et al. consists of an incoherent primary source and its reflection in a plane mirror. This source evidently does not satisfy these requirements.

Further, the authors state that their source violates Wolf's scaling law. This law, which was formulated in Ref.[1], gives a condition for spectral invariance of radiation produced by quasihomogeneous sources. The normalized spectrum of the radiation from such a source will be invariant on propagation if the degree of spatial coherence of the source, assumed to be planar and secondary, has the form $g(\boldsymbol{r}_2-\boldsymbol{r}_1,\omega)=h(\omega(\boldsymbol{r}_2-\boldsymbol{r}_1)/c)$, where c is the speed of light. The authors support their claim by reference to their Eq.(4.11). It is clear,

however, from the analysis presented in their paper that Eq.(4.11) represents the cross-spectral density of the field in the *far zone*, rather than the cross-spectral density of the source. The degree of spatial coherence of their source is rather complicated to describe mathematically. However, even if one derived a mathematical expression for it and it was found to have the form of the scaling law, the spectrum of the emitted radiation would not necessarily be invariant on propagation because, as already mentioned, Wolf's result applies to radiation from quasihomogeneous sources. Of greater relevance to the analysis of the radiation from the system described by the authors is Mandel's investigations regarding cross-spectral purity [18], and more recent studies of spectral changes produced in radiation from two small partially correlated sources [19] and in the Young interference experiment [20].

This work was supported by the Army Research Office.

4.5 Reply

In his comment [15] on our letter [16] James questions the quasihomogeniety and the violation of Wolf's scaling law of the light source we discuss.

In Wolf's [1] analysis the source is defined in the usual way, and is taken to be a plane close to, but not inside, the physical source, which consists in our case of the fluorescent film and its reflection from the mirror. The plane in which our source will be proven to be quasihomogeneous is parallel to the fluorescent film but a distance at least an optical wavelength away from it. To prove the quasihomogeneous character of our light source consider an infinitely large monolayer of fluorescing molecules parallel to the mirror. In a plane parallel and close to this monolayer the ensemble average of the cross-spectral density $W_{ens}(\boldsymbol{r}_1,\boldsymbol{r}_1+\Delta\boldsymbol{r},\omega)$ is basically the sum over all cross-spectral densities of each emitter. Given the infinite extension of the fluorescing monolayer, $W_{ens}(\boldsymbol{r}_1,\boldsymbol{r}_1+\Delta\boldsymbol{r},\omega)$ cannot be dependent on the absolute position $\boldsymbol{r}_1$ in the source plane, simply because all points $\boldsymbol{r}_1$ are equivalent. Therefore W_{ens} is only dependent on $\Delta\boldsymbol{r}$. Similarly, the spectrum $W_{ens}(\boldsymbol{r}_1,\boldsymbol{r}_1,\omega)$ is independent of $\boldsymbol{r}_1$, again simply because all points $\boldsymbol{r}_1$ in the infinitely large source plane are

equivalent. Neither the finite thickness of the fluorescent film nor the distance of the film to the mirror will affect this conclusion. In other words, the source is quasihomogeneous.

In the above arguments, the source plane is taken to be infinitely large, which physically means that edge effects due to the finite spatial extent of excitation can be neglected. This requires that the diameter of the source plane should be considered to be much less than the diameter of the exciting HeNe laser beam. The experimental spectrum shown in Fig. 4.2 (upper spectrum) is taken under these conditions and shows that the spectrum in the vicinity of the fluorescent film is different from the spectrum in the far field. We emphasize that the argument for the violation of Wolf's scaling law in our Letter is not based upon Eq.(4.11) only; we also discuss qualitatively the relevance of the spectra taken close to the fluorescent film.

Finally, we agree with James that it may be relevant to a further analysis of our light source to investigate its cross–spectral purity.

In summary, a quasihomogeneous source can be defined for our system which shows an optical spectrum that is variant with propagation through free space.

References

[1] E. Wolf, *Phys. Rev. Lett.* **56**, 1370 (1986).

[2] E. Wolf, *Nature (London)* **326**, 363 (1987).

[3] M.F. Bocko, D.H. Douglass, and R.S. Knox, *Phys. Rev. Lett.* **58**, 2649 (1987).

[4] G.M. Morris and D. Faklis, *Opt. Commun.* **62**, 5 (1987).

[5] D. Faklis and G.M. Morris, *Opt. Lett.* **13**, 4 (1988).

[6] E. Schrödinger, *Ann. d. Phys.* **61**, 69 (1920).

[7] O. Halpern and F.W. Doermann, *Phys. Rev.* **52**, 936 (1937).

[8] K.H. Drexhage, in *Progress in Optics*, edited by E. Wolf (North–Holland, Amsterdam, 1974), Vol.XII, p165.

[9] F. De Martini, *Phys. Lett.* **A115**, 421 (1986); F. De Martini and G. Innocenti, in *Quantum Optics*, edited by J.D. Harvey and F.D. Walls (Springer–Verlag, Berlin, 1986).

[10] R. Loudon, *The Quantum Theory of Light* (Oxford, London, 1983), 2nd ed..

[11] F.A. Jenkins and H.E. White, *Fundamentals of Optics* (McGraw–Hill, New York, 1987).

[12] K.E. Drabe, G. Cnossen, and D.A. Wiersma, *Opt. Commun.* **73**, 91 (1989).

[13] Terms neglected in Eq.(11) contain sinc functions that can never become unity, in contrast to the term retained in Eq.(11). For example, $\mathrm{sinc}[(k_{pz}+k_z)(L_2-L_1)]$ has a typical value of $1/(k_{pz}+k_z)(L_2-L_1)\approx 10^{-2}$–$10^{-3}$.

[14] R.J. Laureys, K. Matilla, and G. Schnur, *Astron. Astrophys.* **184**, 269 (1987); R.J. Laureys, *thesis*, University of Groningen, 1989 (unpublished), Chap. 4.

[15] D.F.V. James, *Phys. Rev. Lett.* **66**, 675 (1991).

[16] K.E. Drabe, G. Cnossen, D.A. Wiersma, H.A. Ferwerda, and B.J. Hoenders, *Phys. Rev. Lett.* **65**, 1427 (1990).

[17] K.E. Drabe, G. Cnossen, D.A. Wiersma, H.A. Ferwerda, and B.J. Hoenders, *Phys. Rev. Lett.* **66**, 675 (1991).

[18] L. Mandel, *J. Opt. Soc. Am.* **51**, 1342 (1961).

[19] E. Wolf, *Phys. Rev. Lett.* **58**, 2646 (1987); A. Gamliel and N. George, *J. Opt. Soc. Am.* **A6**, 1150 (1989).

[20] D.F.V. James and E. Wolf (to be published).

CHAPTER 5

Fluorescence properties of rhodamine 6G physisorbed to aluminum

5.1 Abstract

5.2 Introduction

5.3 Experimental

5.4 Results and Discussion

References

5.1 Abstract

Fluorescence properties of submonolayers of rhodamine 6G have been measured as a function of distance to an aluminum mirror. For distances less than 5 nm (spacer layers of 1 nm thickness were used) a broadening of the emission spectrum is observed. The fluorescence lifetime has been measured for distances up to 6 nm. The broadening of the fluorescence spectra and the shortening of the lifetime is attributed to efficient energy–transfer to the aluminum substrate. Good agreement with theory is found if volume and surface contributions are included in the energy transfer rate.

5.2 Introduction

The radiative behaviour of luminescing molecules in front of metal surfaces has been studied extensively during the past decades [1–3]. The metal surface influences the radiative as well as the nonradiative properties of emitting molecules. The influence of the mirror shows a marked distance dependence. In case of emitter–mirror distances on the order of the emitted wavelength, an oscillatory behaviour of the fluorescence lifetime with distance is found [2]. This effect is ascribed to the interference between directly emitted waves and partially reflected waves from the mirror. For distances less than about 10 nm the lifetime of the excited state is dominated by radiationless energy transfer to the metal substrate. The excited molecule interacts through the near–field with the electron gas of the metal and the excitation energy is dissipated through various scattering processes into the bulk. A reduction of the excited state lifetime by several orders of magnitude is observed. In case of flat silver surfaces the emission is even completely trapped, and no fluorescence is observable [4].

Absorption of energy by metal electrons requires momentum conservation. Three different sources of momentum can be distinguished [5,6,7]: (A) in the

bulk: scattering by phonons, impurities, and the crystal potential; (B) scattering by the metal surface; (C) from the spatial variation of the near-field of the excited molecule itself. Process (A) dominates at larger distances ($>\sim$5 nm), for which an inverse cube distance dependence is calculated. A d^{-4} dependence is estimated for processes (B) and (C), which are expected to dominate for small molecule-metal distances ($<\sim$5 nm).

A considerable amount of work has been devoted to line shape studies of physisorbed molecules [5,8]. Two different techniques have been applied. By means of infrared reflection-absorption spectroscopy information is obtained about the vibrational frequencies and bandwidths, which are studied as a function of surface coverage [8,9]. The observations are explained in terms of lateral dipole-dipole and dipole-image-dipole interactions [10]. Electron energy-loss spectroscopy has been used to study electronic as well as infrared transitions of adsorbates on metal surfaces [5,11]. In all cases a broadening of the energy levels is observed with respect to multilayer values, which is usually attributed to the reduced excited state lifetime [5,8,11].

For distances shorter than 1 nm chemical effects will also alter the lineshape and line position [3,5]. The chemical bonding to the substrate affects the vibrational frequencies. In addition electron transfer from the adsorbate to the substrate may occur [3,5].

In this chapter we study fluorescence spectra of submonolayers of rhodamine 6G (R6G) spaced by amylose-acetate ester layers from plane aluminum mirrors. Aluminum was chosen because the luminescence is less efficiently quenched compared to, for example, a silver surface. The distance between the mirror and the R6G molecules was varied over a range of 1-6 nm by the application of transparent polymer layers of 1 nm thickness. The advantage of using polymer spacer layers instead of conventional fatty acid monolayers is that a higher spatial resolution is achieved (1 nm versus 5 nm, respectively), caused by the fact that only one polymer spacer layer is transferred per dipping cycle through which the formation of bilayers is prevented [2,12].

We found that the width of the emitted spectrum depends on the distance to the mirror. For small distances a broadening was observed. In addition we measured the fluorescence lifetime and the apparent quantum yield of emission as

a function of emitter–mirror distance. All observations are explained in terms of energy transfer theory, for which acceptable agreement with experimental data is found.

To our knowledge no reports have yet appeared in which the lineshape broadening could be detected via fluorescence emission, and in which the broadening was measured as a function of emitter–metal distance.

5.3 Experimental

R6G was obtained from Lambda Physik, and was used without further purification. R6G monolayers were prepared by the dipping technique. The dipping proceeded at a rate of 0.25 mm/s from a $5*10^{-5}$ M ethanolic solution. As is evident from the absorption spectrum (Fig. 5.1), no sign of aggregation is observed [13].

The substrates were prepared by evaporation, at a pressure of 10^{-5} Torr, of thick aluminum layers onto Corning 7059 microscope slides. The slides were cleaned before use in chromic acid, and were rinsed ultrasonically with milli–Q water, acetone, chloroform, and hexane.

The spacer layer consisted of amylose–acetate ester, and was applied by the Langmuir–Blodgett technique at a surface pressure of 7 mN/m [12]. The subphase was highly purified water (milli–Q), at a temperature of 22 °C. A monolayer was transferred during every upstroke.

Fluorescence spectra were recorded by means of an intensified optical multichannel analyzer (Princeton Instruments), in the direction perpendicular to the substrate surface. The 488 nm line of an argon–ion laser (Spectra Physics) was used as excitation source.

Fluorescence decays of R6G monolayers were measured using a time correlated single photon–counting system. A cavity–dumped mode–locked Argon–ion laser (Coherent, Inc.) operating at a repetition rate of 94 kHz (514.5 nm) was used as excitation source. The photomultiplier used was a Hamamatsu microchannel plate (R1564U–01). The time resolution of the detection system is 33 ps, but due to the rather long pulse duration of the Ar^+–laser the time resolution after

deconvolution was 45 ps.

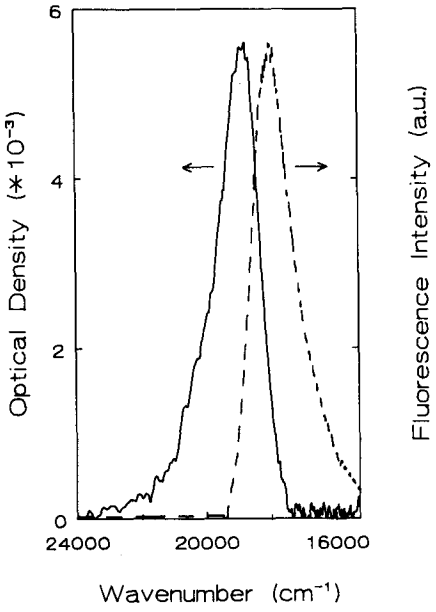

Figure 5.1: *Absorption (solid curve) and fluorescence (dashed curve) spectra of submonolayers of rhodamine 6G on a Corning 7059 glass substrate. Excitation wavelength*: 488 *nm.*

5.4 Results and Discussion

For the calculation of the influence of aluminum substrates on the fluorescence lifetime of physisorbed R6G, we use the theory developed by Persson et al. [5,6,7]. In this theory the excited state lifetime for an oscillating dipole at small distances d from the metal surface ($kd \ll 1$) is given by:

$$T_{1,nr}^{-1}(d) \approx T_{1,\infty}^{-1}\left\{1+\frac{\eta}{8}(dk)^{-3}\left[2\mathrm{Im}\left(\frac{\varepsilon_m(\omega)-\varepsilon_1}{\varepsilon_m(\omega)+\varepsilon_1}\right)+6\xi\frac{1}{k_F d}\frac{\omega}{\omega_p}+18\frac{\omega_F}{\omega_p}\frac{\omega}{\omega_p}\frac{1}{k_F d}\right]\right\}, \tag{5.1}$$

where $T_{1,\infty}$ is the fluorescence lifetime at infinite distance from the mirror, k is the magnitude of the wavevector at the emitted frequency ω, $\varepsilon_m(\omega)$ is the (complex) metal dielectric constant, ε_1 is the dielectric constant of the medium in which the dipole is embedded, and η is an orientational parameter ($\eta = {}^3/_2$ for a perpendicular dipole and $\eta = {}^3/_4$ for a parallel dipole). Some typical metallic electron gas parameters are contained in the last two terms between square brackets, where k_F is the Fermi wavevector, ω_F the Fermi frequency, ω_p the plasma frequency, and $\xi \approx 1$ [7] is a constant which depends on the electron gas density. The last term between square brackets is valid for the limiting case $k_F d \gg \omega_F/\omega$. For a complete derivation and discussion of the different terms in Eq.(5.1) we refer to the work of Persson et al. [5,6,7].

The three terms between square brackets signify the different sources of momentum, as mentioned in the introduction. The first term represents the bulk contribution to the damping rate, and is identical to the classical result where the interaction of the transition dipole of the molecule with the electromagnetic field of its image dipole in the mirror is considered [1]. In this classical theory the out-of-phase (imaginary) part of the reflected field determines the non-radiative lifetime $T_{1,nr}$, while the in-phase (real) part of the reflected field affects the frequency shift $\Delta\omega$. In the derivation a steplike metal surface was assumed. Furthermore, a bulk metal dielectric constant is used, neglecting surface contributions to the energy decay. In Eq.(5.1), however, surface contributions are accounted for by the second term between square brackets, where the required momentum is supplied by the surface potential. In the last term momentum originates from the spatial variation of the near-field of the dipole. The distance behaviour of the three terms between square brackets is different. For the volume scattering a d^{-3} behaviour is calculated, while a d^{-4} behaviour is computed for the other two contributions. Volume contributions are expected to dominate for metallic substrates in the frequency region of strong interband transitions, where indeed an inverse cube distance dependence is found for molecule-surface separations down to 1 nm [3,14]. For nearly free-electron like metals the d^{-4} terms are dominant at small molecule-surface separations ($d \leq 5$ nm), and a fluorescence lifetime is calculated which is about 10 times shorter than one would estimate on ground of bulk

scattering contributions only.

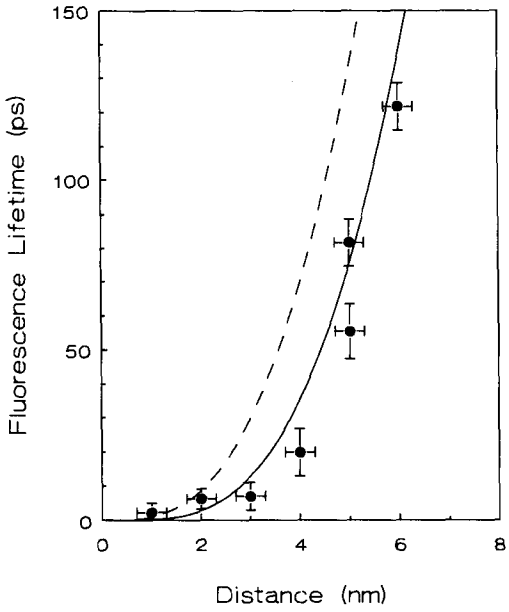

Figure 5.2: *Fluorescence lifetime as a function of emitter–metal distance (closed circular points). The solid line results from the calculation according to Eq.*(5.1), *the dashed curve results in case only bulk contributions to the energy transfer rate are incorporated.*

The results of fluorescence decay measurements of R6G physisorbed to aluminum substrates are given in Fig. 5.2. The fluorescence lifetime is plotted against the distance to the mirror. Fluorescence decay curves could be fitted to a single exponential, in agreement with the work of Leitner et al. [15]. For molecule–surface distances shorter than ≈ 4 nm the fluorescence decay time was shorter than the time resolution of the measuring system (45 ps). For these distances the fluorescence lifetime was determined from quantum yield measurements. The solid line in Fig5.2 is based on Eq.(5.1) using a metal dielectric constant $\varepsilon_m = -39.2 + i11.77$ [16], $\varepsilon_1 = 1.3$, and $T_{1,\infty} = 3$ ns, and $\eta = {}^3/_4$ corresponding to the known parallel orientation of the R6G molecules with

respect to the substrate surface [17]. Furthermore, we used $\omega = 3.3{*}10^{15}$ rad/s, $\omega_p = 2.39{*}10^{16}$ rad/s, $\omega_F = 1.7774{*}10^{16}$ rad/s, and $k_F = 1.75{*}10^{10}\ \mathrm{m}^{-1}$ [18]. The requirement $k_F d \gg \omega_F/\omega$ is met for the whole regime of emitter–metal distances studied, justifying the expression for the last term in Eq.(5.1) (for the smallest distance of 1 nm $(k_F d)/(\omega_F/\omega) \approx 3.2$). The dashed line in Fig. 5.2 is the classical result [1], where surface contributions to the damping rate are neglected. Incorporation of the surface scattering contributions gives a better agreement with experimental data.

In estimating the distance of the emitting layer from the metal surface we presume a native oxide layer of 1 nm thickness to be present at the metal surface [19]. This oxide layer is formed within two hours of exposure to air, and continues to grow very slowly and reaches its final value of about 4 nm after one month. Oxidation is unavoidable due to the application of spacer layers by the Langmuir–Blodgett technique. All measurements were done within one hour after preparation.

In addition to lifetime and quantum yield measurements we measured the distance dependence of the fluorescence spectra for physisorbed R6G monolayers. In Fig. 5.3 emission spectra are shown for R6G monolayers separated by one ($d \simeq 2$ nm), respectively five ($d \simeq 6$ nm) polymer spacer layers. An asymmetric broadening of about $200\ \mathrm{cm}^{-1}$ for the spectrum close to the mirror is observed. The asymmetric broadening is accompanied by a small red shift of the emission maximum of about $50\ \mathrm{cm}^{-1}$. An estimate of the spectral red–shift can be made on ground of the classical interaction of an oscillating dipole with its fictitious mirror image [1], which gives ($kd \ll 1$):

$$\Delta\omega = \omega(d) - \omega(\infty) = -\frac{q\eta}{8}(dk)^{-3} T_{1,\infty}^{-1} \mathrm{Re}\left(\frac{\varepsilon_m(\omega)-\varepsilon_1}{\varepsilon_m(\omega)+\varepsilon_1}\right), \qquad (5.2)$$

where q is the quantum yield of emission at infinite distance from the mirror. On basis of Eq.(5.2) we calculate a red–shift of $17\ \mathrm{cm}^{-1}$ ($d = 2$ nm), which is smaller than the observed red shift of about $50\ \mathrm{cm}^{-1}$ (see Fig. 5.3). Though the right order of magnitude is calculated, the calculated value is a factor of three off from the experimental value.

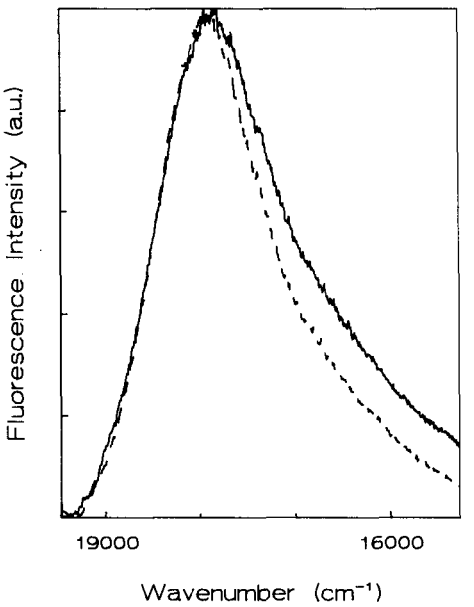

Figure 5.3: *Fluorescence spectra of Rhodamine 6G submonolayers separated from the aluminum surface by one ($d = 2\,nm$, solid line) respectively five spacer layers ($d = 6\,nm$, dashed line). Excitation wavelength*: 488 *nm.*

An estimate of the line broadening can be made on ground of Eq.(5.1). The effect of the reduced excited state lifetime on the homogeneous damping rate Γ_{hom} can be calculated from [20]:

$$\Gamma_{hom} = (2T_1)^{-1} + (T_2^*)^{-1}, \tag{5.3}$$

where T_1 is the excited state lifetime (longitudinal relaxation time), and T_2^* the pure dephasing time (transversal relaxation time) [20]. Any effect of the reduced excited state lifetime on the homogeneous linewidth can be expected if T_1 becomes comparable to T_2^*.

The distance dependence of the width (FWHM) of the fluorescence spectra, normalized with respect to the FWHM at infinite distance from the mirror, is

plotted in Fig. 5.4. The width decreases sharply with increasing distance and remains constant for emitter–mirror distances larger than 5 nm (closed circles). Also shown are measurements of the FWHM for R6G physisorbed directly onto aluminum surfaces (open circles). The distance dependence of the normalized FWHM is calculated according to Eq.(5.3) using the expression of Eq.(5.1) for T_1, where we assume the pure dephasing rate and the inhomogeneous broadening to be independent of emitter–metal distance. The solid line in Fig. 5.4 is the result

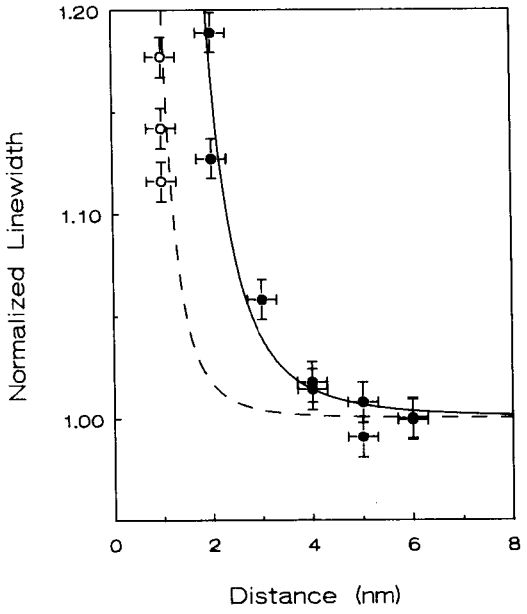

Figure 5.4: *Plot of the FWHM normalized with respect to the FWHM at infinite distance from the mirror, as a function of emitter–mirror distance (closed circles). Open circles are results of measurements of the FWHM for R6G physisorbed directly onto aluminum. Also shown are the results of calculations based on Eqs.*(5.1) *and* (5.3), *using* $T_2^* = 1\,ps$ *(solid line), and* $T_2^* = 100\,fs$ *(dashed line).*

of the above calculations where T_2^* was set to 1 ps. For directly adsorbed R6G agreement with theory is obtained if a pure dephasing time 100 fs was used

(dashed line in Fig. 5.4). The thickness of the oxide layer, which is known to be about 1 nm as argued above, is 1 nm in these calculations.

The difference in pure dephasing times found for R6G directly adsorbed to aluminum and for R6G physisorbed to polymer spacer layers must be attributed to the difference in chemical environment. Incoherent fluctuations in the electric field of conduction electrons as felt by directly adsorbed dye molecules may be a cause for the reduction in dephasing time found.

The estimated pure dephasing time of 1 ps for the polymer-spaced dye monolayers is an order of magnitude longer than the value found for molecules dissolved in, for example, (three dimensional) polymer matrices [21]. However, the value is still orders of magnitude smaller than found for molecules in the gas-phase [20]. The reduced dimensions of our samples is probably the main cause for the long dephasing time found compared to dye molecules dissolved in (three dimensional) polymer matrices.

The excited state lifetime of 200 fs we calculate for a distance of 1 nm from the aluminum surface is of the same order of magnitude as the lifetime estimated by Avouris et al. [11], who studied the $^1B_{2u} \rightarrow {}^1A_1$ transition of pyrazine physisorbed to a Ag(111) surface.

In summary, we studied the fluorescence properties of submonolayers of R6G as a function of distance to the aluminum substrate. A shortening of the fluorescence lifetime and a reduction of the emission quantum yield by several orders of magnitude ($\approx 10^4$) was observed. Also a broadening and red-shift of the emission spectra was observed. The dependence on distance of these results was measured in steps of 1 nm, allowing a detailed test of the distance dependence of the quenching of emission by the aluminum substrate. From the distance dependence of the broadening of the spectra we derive a pure dephasing time of 100 fs for directly adsorbed R6G molecules, and a pure dephasing time of 1 ps for the polymer spaced R6G monolayers. All observations agree favourably with theory, if bulk and surface contributions to the scattering of excited metal electrons are incorporated.

References

[1] R.R. Chance, A. Prock, and R. Silbey, *Adv. Chem. Phys.* **37**, 1 (1978), and references therein.

[2] K.H. Drexhage in *Progress in Optics XII*, edited by E.Wolf (North-Holland, Amsterdam, 1974), p.165.

[3] X.L. Zhou, X.Y. Zhu, and J.M. White, *Surf. Sci. Rep.* **13**, 75 (1991), and references therein

[4] G. Ritchie and E. Burstein, *Phys. Rev.* **B24**, 4843 (1981).

[5] Ph. Avouris and B.N.J. Persson, *J. Phys. Chem.* **88**, 837 (1984).

[6] - B.N.J. Persson and N.D. Lang, *Phys. Rev.* **B26**, 5409 (1982).
- B.N.J. Persson and M. Persson, *Surf. Sci.* **97**, 609 (1980).

[7] B.N.J. Persson, *J. Phys. C.* (*Solid State Phys.*) **11**, 4251 (1978).

[8] A.M. Bradshaw and E. Schweizer in *Spectroscopy of Surfaces*, edited by R.J.H. Clark and R.E. Hester (John Wiley & Sons Ltd, Chichester, 1988), p.413.

[9] P. Hollins and J. Pritchard, *Progr. Surf. Sci.* **19**, 275 (1985).

[10] M. Scheffler, *Surf. Sci.* **81**, 562 (1979).

[11] Ph. Avouris and J.E. Demuth in *Surface Studies with Lasers*, edited by F.R. Aussenegg, A. Leitner, and M.E. Lippitsch (Springer-Verlag, Berlin, 1983), p.24.

[12] M.A. Schoondorp, E.J. Vorenkamp, and A.J. Schouten, *Thin Solid Films* **196**, 121 (1991).

[13] S. Garoff, R.B. Stephens, C.D. Hanson, and G.K. Sorenson, *Opt. Commun.* **41**, 257 (1982).

[14] P.M. Whitmore, H.J. Robota, and C.B. Harris, *J. Chem. Phys.* **77**, 1560 (1982).

[15] A. Leitner, M.E. Lippitsch, S. Draxler, M. Riegler, and F.R. Aussenegg, *Appl. Phys.* **B36**, 106 (1985).

[16] *American Institute of Physics Handbook*, edited by D.E. Gray (McGraw-Hill, New York, 1957), Sec.6, p.103.

[17] H. Sano, G. Mizutani, and S. Ushioda, *Surf. Sci.* **223**, 621 (1989).

[18] N.W. Ashcroft and N.D. Mermin in *Solid State Physics* (Saunders College,

Philadelphia, 1976).

[19] G. Hass and N.W. Scott, *J. Phys. Rad.* **11**, 394 (1950).

[20] see for example L. Allen and J.H. Eberly in *Optical Resonance and Two-Level Atoms* (John Wiley & Sons, Inc., New York, 1975).

[21] K.E. Drabe, G. Cnossen, and D.A. Wiersma, *Chem. Phys. Lett.* **169**, 416 (1990).

CHAPTER 6

Nonlinear optical properties of Langmuir-Blodgett monolayers: Local-field effects

6.1 Abstract

6.2 Introduction

6.3 Theory and numerical calculations
- 6.3.1 General aspects
- 6.3.2 The crystal model
- 6.3.3 The isotropic monolayer model
- 6.3.4 Numerical results

6.4 Experimental

6.5 Experimental results
- 6.5.1 General aspects
- 6.5.2 Aggregation
- 6.5.3 The tilt angle
- 6.5.4 Microscopic local-fields: dependence of $\chi^{(2)}$ on surface density

6.6 Discussion and conclusions

Appendix

References

6.1 Abstract

Detailed measurements of the macroscopic second-order optical nonlinearity $\chi^{(2)}(2\omega,\omega,\omega)$ of Langmuir-Blodgett dye-doped monolayers are reported. The observed deviations from a linear behaviour of $\chi^{(2)}$ with increasing surface density are shown to be due to local-field effects. In order to calculate these local-field factors for disordered systems, a novel Monte-Carlo type calculation is introduced. This calculation not only accounts for density variations in the monolayers but also incorporates the effect of off-diagonal elements of the (microscopic) linear susceptibility-tensor. Quantitative agreement is found between the calculations and the experimental results using only the molecular hyperpolarizability as free parameter

A method is presented to determine the tilt angle of the chromophores in Langmuir-Blodgett monolayers from the anisotropy of the linear absorption. The tilt angle determined this way is in excellent agreement with a determination by second-harmonic generation.

6.2 Introduction

Second-harmonic generation has become one of the most important optical techniques to study the properties of monolayers and interfaces [1]. Due to its great sensitivity to breaking the inversion symmetry, information can be obtained about the structure and ordering of molecules at interfaces.

In order to evaluate the second-harmonic intensity in terms of the structure and ordering of the optically nonlinear molecules, the geometry of the sample is important. The sample can be considered to be build up of three distinct media, namely the substrate, the optically active monolayer, and the superstrate. Each medium has its own dielectric constant. At the interface between the different media an optical beam undergoes reflection and refraction resulting in a change of the electromagnetic field intensity. This change in local-field is often described in terms of *geometric* (or macroscopic)

local-field factors [2-5]. The geometric local-field factors can be found by solving the macroscopic Maxwell equations when the correct boundary conditions are employed.

A clear manifestation of the geometric local-field appears in case of Raman scattering and second-harmonic generation at rough surfaces. Signal enhancement is found due to field resonances in the protrusions at the surface [3-5], and the correct long-range-distance dependence is predicted [6,7]. In case of smooth surfaces the macroscopic local-field manifests itself in the form of a modulated fluorescence spectrum of a one micron thick layer of emitting dye molecules in front of a mirror [8,9]. The modulation pattern in the emission spectrum can be explained in terms of frequency dependent (geometric) local-field factors. Another example of a local-field effect is the enhancement by a factor of 3 to 10 of the signal strength that is observed at the critical angle in an internal reflection experiment [2]. These effects are evident in fluorescence [10] and frequency doubling [11] experiments.

In addition to the geometric local-field factors one has to consider the microscopic local-field caused by dipolar interactions between the molecules. This *microscopic* local-field is much more difficult to handle, because a good knowledge of the system on a molecular level is required. The calculation of this field in a two-dimensional lattice of rigid molecules is the subject of this chapter.

By introducing microscopic local-field factors, the calculation of the response of an interacting ensemble of molecules to an electromagnetic field is reduced to a calculation of the response of isolated molecules interacting with the local-field [12]. At optical frequencies Lorentz-Lorenz type of expressions [13] are often used to describe the microscopic local-field. These expressions are valid for three-dimensional isotropic or cubic media [13].

The adequacy of the Lorentz-Lorenz expressions has been tested for liquids by Levine et al. [14], using static field-induced second-harmonic generation. Good agreement between theory and experiment was found. The Lorentz local-field approach was recently also shown to describe the resonant linear and nonlinear optical response of a dense potassium vapor [15].

In ordered systems of lower dimension like molecular aggregates and Langmuir-Blodgett monolayers, the Lorentz-Lorenz local-field expressions are not

expected to be valid, and explicit numerical calculations involving all molecules need to be performed. However, because of its simplicity [16,17], the Lorentz local–field expression is still often used for Langmuir–Blodgett monolayers. This approximation, however, may fail in case the optical excitations in the film are delocalized. In such cases it is the excitonic rather than molecular nonlinearity that should be accounted for and it has been shown by Spano et al. [18,19]. that a local–field approximation breaks down.

In this chapter we will study the applicability of the local–field concept to a monolayer of dye molecules packed in a two–dimensional lattice. The Langmuir–Blodgett technique provides a way to systematically study the change in local–field as a function of distance between the interacting chromophores. By mixing the optically active molecules with optically inactive ones it is possible to change the distance between the induced dipoles. By applying different surface pressures or by using different types of molecules it is also possible to change the mutual orientation between the interacting dipoles. In this way the intermediate regime between isolated molecular dipoles and the extended exciton state can be studied.

In this chapter we report on the efficiency of frequency doubling of Langmuir–Blodgett monolayers as a function of concentration of the optically active molecules. In order to obtain a specific surface density these dye molecules are mixed with known amounts of inactive fatty–acid molecules.

Recently, several papers have reported on measurements of the second harmonic efficiency as a function of surface density [20–30]. The most popular system is a mixture of a hemicyanine dye and a fatty acid, which, however, is also known for its tendency to form aggregates at higher dye concentrations. Evidence for this aggregation effect is found in the spectrum of this molecule that undergoes a blue shift at high concentration [21–25].

In these systems the second–harmonic efficiency decreases at dye concentrations higher than about fifty mole percent [20–28]. Hayden [20] interprets this decrease solely in terms of the classical microscopic local–field factors as derived by Bagchi et al. [31,32]. Absorption spectra were not reported by Hayden [20], so it is difficult to judge whether aggregation plays a role in the samples used. Furthermore, details about the tilt angle of the dye unit are not provided, so the orientation between the optical dipoles is

unknown. In addition, the interaction between the molecules is supposed to be independent of the mutual orientations of the dipoles [20–23].

A number of groups have attributed the decrease of the second-harmonic intensity at high surface densities, to the centrosymmetric structure of the aggregate [27,28], or to the dispersive effect of aggregation on the nonlinear susceptibility; the blue shift of the spectrum leads to a decrease of the resonance enhancement [24,25]. Others have described this decrease to a combination of aggregation and the classical microscopic local-field effect [21–23].

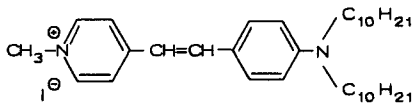

I

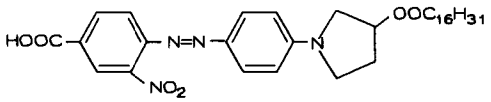

II

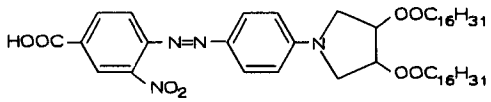

III

Figure 6.1: *Chemical formulas of the studied dye molecules.*

It is obvious that aggregation in monolayers complicates the interpretation of frequency doubling experiments. The optically nonlinear systems dealt with in this chapter show no signature of aggregation and are optically well-characterized. This enables us to interpret the second-harmonic generation

(SHG) efficiency in terms of microscopic local–field factors. The SHG efficiency is studied as a function of surface density for three different dyes (see Fig.6.1). In one system (dye **I**) the molecules are oriented almost parallel to the substrate, in the other two systems the dye molecules attain a more erect position. While the chromophoric groups in dye **II** and **III** are identical, the monolayer structure of these dyes is different due to the presence of a second alkyl chain in compound **III**. In comparing the nonlinear optical behaviour of these two dyes the effect of the tilt angle on the local–field can be studied. In section **6.3** we present a calculation of the microscopic local–field by summing the near–field of the surrounding dipoles in an iterative way, using a Monte–Carlo type procedure. The orientation of the rod–like dye molecules is explicitly incorporated in the calculations. The off–diagonal components of the linear susceptibility tensor are also taken into account. In section **6.4** the experimental details are reported. In section **6.5** we compare the results of calculations with the experimental results on SHG. Finally, in section **6.6** we draw some conclusions.

6.3 Theory and numerical calculations

6.3.1 General aspects

In adopting a theoretical framework for the calculation of the local–field in Langmuir–Blodgett monolayers we make, as stated in the introduction, a distinction between geometrical and microscopic local–field corrections [2–5].

The *geometrical* or macroscopic local–field correction factors relate the field components of the applied field to the corresponding ones in the monolayer and correct for the reflection and refraction of light. These factors are obtained by solving the Maxwell equations, applying the right boundary conditions [2,5].

For later use we list here the expressions for the geometrical local–field correction factors for a monolayer on a flat substrate [2–5],

$$L_{xx}=\frac{2\varepsilon_1 k_{2z}}{\varepsilon_2 k_{1z}+\varepsilon_1 k_{2z}}, \tag{6.1a}$$

$$L_{yy}=\frac{2k_{1z}}{k_{1z}+k_{2z}}, \tag{6.1b}$$

$$L_{zz}=\frac{2\varepsilon_1 k_{1z}(\varepsilon_2/\varepsilon')}{\varepsilon_2 k_{1z}+\varepsilon_1 k_{2z}}. \tag{6.1c}$$

Here x,y,z are the Cartesian laboratory coordinates as shown in Fig.6.2. The z-axis is normal to the substrate surface, while the y-axis is normal to the plane of incidence. In this particular coordinate system the other components L_{ij} of the geometrical local-field tensor are zero. $\boldsymbol{k}_1(\boldsymbol{k}_2)$ is the wavevector for the field in medium 1(2), while $k_{1z}(k_{2z})$ is the projection of $\boldsymbol{k}_1(\boldsymbol{k}_2)$ onto the z-axis. The dielectric constant of medium 1 (the superstrate) is denoted by ε_1, that of medium 2 (the substrate) by ε_2, and that of the monolayer by ε'. Note that these geometrical local-field factors are dependent on, a) the choice of the substrate through ε_2, b) the angle of incidence (through the projection of $\boldsymbol{k}_1$, $\boldsymbol{k}_2$ onto the z-axis), and c) the concentration of the dye-molecules in the monolayer (through ε').

The *microscopic* local-field is a manifestation of the reaction field of the induced dipoles within the monolayer. The local-field along i $(i=x,y,z)$ at site n, denoted as $E^n_{loc,i}$, is calculated from [31-35]:

$$E^n_{loc,i}=L_{ii}E_{0,i}+\sum_{m\neq n}E^m_{dip,i}. \tag{6.2}$$

Here $E_{0,i}$ is the externally applied field along i, and L_{ii} the geometrical correction factor given by Eq.(6.1). The dipolar field $\sum_{m\neq n}E^m_{dip,i}$ in the above equation is the reaction field of the surrounding dipoles, and is calculated from [13]:

$$\boldsymbol{E}^m_{dip}(\boldsymbol{r}_n)=\frac{3\boldsymbol{n}(\boldsymbol{p}^m.\boldsymbol{n})-\boldsymbol{p}^m}{|\boldsymbol{r}_{nm}|^3}. \tag{6.3}$$

Here $\boldsymbol{E}^m_{dip}(\boldsymbol{r}_n)$ is the dipole field at site n due to an induced dipole $\boldsymbol{p}^m$ at site m. In Eq.(6.3) the unit vector $\boldsymbol{n}$ points from $\boldsymbol{r}_m$ to $\boldsymbol{r}_n$, and $|\boldsymbol{r}_{nm}|$ is the distance between sites m and n. The oscillating part of the electric field has not been incorporated in Eq.(6.3). In this near-field approximation the magnetic part of the electromagnetic-field can be ignored [13]. Retardation effects have also been discarded. This assumption is justified by the calculations (section **6.3.3**), where the requirement $\boldsymbol{k}.\boldsymbol{r} \ll 1$ is met.

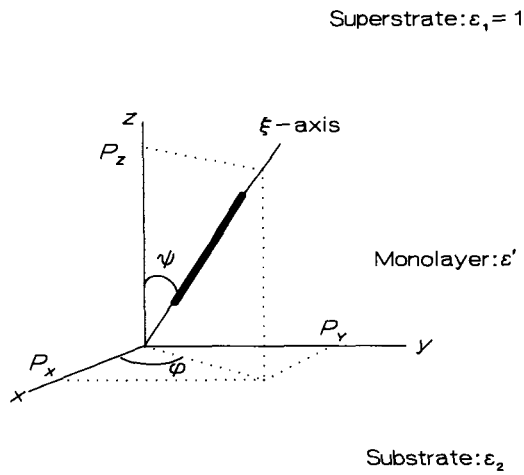

Figure 6.2: *Model system used in the calculations. The substrate surface is denoted by the $x-y$ plane. The $z-$axis is normal to the substrate plane. The tilt angle ψ of the long axis of the dye unit ($\xi-$axis) is assumed to have a site independent fixed value. In the isotropic monolayer case the projection angle ϕ is random at every site. In the crystal model ϕ has a fixed value.*

The microscopic induced dipole moment $\boldsymbol{p}^m$ in Eq.(6.3) is related to the electromagnetic field by:

$$\boldsymbol{p}^m = \boldsymbol{R}\boldsymbol{\alpha}\boldsymbol{R}^{-1}\boldsymbol{E}^m_{loc}\,, \tag{6.4}$$

where $\boldsymbol{E}^m_{loc}$ is the local electromagnetic field at site m, $\boldsymbol{\alpha}$ the linear molecular polarizability tensor, and $\boldsymbol{R}$ the rotation matrix connecting the molecular

coordinate system to the laboratory-frame. The local-field is supposed to be uniform over the dimensions of the dipole (point-dipole approximation).

Note that we assume the induced dipole moment $\boldsymbol{p}^m$ to be determined entirely by the linear polarizability tensor $\boldsymbol{\alpha}$. The dominant component of the linear- as well as the hyper-polarizability for the axially symmetric molecules studied is directed along the ξ-axis (Fig.6.2). Therefore, to an appreciable degree of accuracy the components of $\boldsymbol{\alpha}$ in the molecule-fixed axes system is:

$$\boldsymbol{\alpha} = \begin{pmatrix} 0 & 0 & \\ & & \alpha_{\xi\xi} \end{pmatrix}. \tag{6.5}$$

Usually the other components of $\boldsymbol{\alpha}$ are an order of magnitude smaller for the molecules studied in this work [36]. The linear microscopic polarizability in the laboratory frame, however, is obtained by a similarity transformation $\boldsymbol{R\alpha R^{-1}}$, and is in general non-diagonal. The off-diagonal components of the microscopic linear polarizability are projections of $\alpha_{\xi\xi}$ on the different Cartesian axis (see section **6.3.3**).

It has been shown that for *any* polarizability the local-field at a particular site can be obtained by inversion of the matrix form of Eq.(6.2) [37]. This procedure, however, becomes impractical for large dipole lattices (>1000 dipoles) and is not always necessary either. In order to obtain the sum $\sum_{m \neq n} E^m_{dip,i}$ in Eq.(6.2), we follow an iterative procedure. In the first iteration the applied field $\boldsymbol{LE}_0$ is used to calculate the induced dipole moments $\boldsymbol{p}^m$. The local-field components at site n can now be calculated and are the sum of the applied field $L_{ii}E_{0,i}$ and the total reaction field of the surrounding dipoles $\sum_{m \neq n} E^m_{dip,i}$. In the second iteration the values obtained for the local-field components $E^n_{loc,i}$ are used to recalculate the induced dipole moment $\boldsymbol{p}^m$ and the accompanying reaction field [34,38,39]. As long as the amplitude of the total reaction field at site $\boldsymbol{r}_n$ remains smaller than the applied field, the successive orders ultimately converge to a constant value. If this is not the case than we have to invert the matrix form of Eq.(6.2) to obtain the local-field. In order to calculate the successive orders both the orientation of, and the distances to the neighboring molecules are needed.

Prior to presenting our results we will first provide, as a reference

point, the results obtained from of a crystal-like model. Thereafter we will present the results of a Monte-Carlo calculation. The results of both models for the local-field will be compared in section **6.3.4.**

6.3.2 The crystal model

In the crystal model all dipoles are placed equidistantially on a lattice and are assumed to have the same fixed orientation. For this case an analytical expression can be obtained for the sum of the reaction field of the surrounding dipoles $\sum_{m\neq n} E^{m}_{dip,i}$. The summation in Eq.(6.2) has been carried out by Topping [40], and was used by Bagchi et al. [31,32] to calculate the dipole reaction field in a monolayer. The results for the microscopic local-field correction factors ℓ_{ii} are:

$$\ell_{zz} = 1/(1-\zeta_0\alpha_{zz}/a^3)\,, \tag{6.6a}$$

$$\ell_{xx} = \ell_{yy} = 1/(1+\zeta_0\alpha_{xx}/2a^3)\,, \tag{6.6b}$$

where $\zeta_0 = -9.0336...$ [40]. In these calculations the microscopic polarizability in the laboratory frame $\boldsymbol{R}\alpha\boldsymbol{R}^{-1}$ was assumed to be diagonal. The image-dipole contribution from the glass substrate is omitted in Eq.(6.6) as it is assumed to be negligible [35].

With the local-field correction factors given above, one obtains for the second-harmonic field components generated in the monolayer:

$$E_i(2\omega) = AL_{ii}(2\omega)\ell_{ii}(2\omega)\chi^{(2)}_{ijk}(2\omega,\omega,\omega)L_{jj}(\omega)\ell_{jj}(\omega)E_{0,j}(\omega)L_{kk}(\omega)\ell_{kk}(\omega)E_{0,k}(\omega). \tag{6.7}$$

Here L_{xx} is a geometrical factor given by Eq.(6.1), ℓ_{xx} is a microscopic local-field correction factor as given by Eq.(6.6), and $E_{0,j}$ is the externally applied field along j. Each local-field correction factor needs to be evaluated at the appropriate frequency. $\chi^{(2)}$ is the macroscopic second-order nonlinear susceptibility, and A is a proportionality factor, containing the direction and

distance dependence of the emitted field $E_i(2\omega)$.

6.3.3. The isotropic monolayer model

For a numerical evaluation of the the dipolar sum in Eq.(6.2) we need information concerning the orientation of the dipoles in the monolayer. This input is provided by a well-known model for a homogeneous Langmuir-Blodgett monolayer of rod-like molecules [41]. In this model, shown in Fig. 6.2, the long axis of the dye units are assumed to have the same tilt angle ψ with respect to the surface normal z, but random projection angles ϕ onto the substrate plane x-y. In the density regime studied no correlations are supposed to exist between the orientations of neighbouring dye units. In the molecular frame of the dye units, the *dominant* linear and second-order tensor-components are assumed to be oriented along the ξ-axis.

The long hydrophobic alkyl chains, necessary for acquiring a stable Langmuir-Blodgett monolayer, are not shown in Fig. 6.2, and their contribution to the local-field effect is neglected.

We now proceed by presenting the details of a calculation of the second-harmonic intensity in monolayers.

The second-order nonlinear polarization component induced at site n is

$$p_i^n(2\omega) = \chi_{ijk}^{(2)^n} : E_{loc,j}^n(\omega) E_{loc,k}^n(\omega) \,, \tag{6.8}$$

where the superscript n refers to the particular molecule at site n. The direction and magnitude of the microscopic local-field at site n are determined by both the orientation of and the distance between neighbouring molecules. On the other hand, the Cartesian components of the microscopic hyperpolarizability $\chi_{ijk}^{(2)^n}$ (in the laboratory frame) only depend on the orientation of a particular molecule at site n. We therefore may write for the average induced polarization at frequency 2ω:

$$P_i(2\omega) = N_s < p_i^n(2\omega) > = N_s < \chi_{ijk}^{(2)^n} > : < E_{loc,j}^n(\omega) E_{loc,k}^n(\omega) > \quad (6.9a)$$

$$= \chi_{ijk}^{(2)} : < E_{loc,j}^n(\omega) E_{loc,k}^n(\omega) > , \quad (6.9b)$$

where $N_s < \chi_{ijk}^{(2)} > \equiv \chi_{ijk}^{(2)}$ is given below, N_s is the surface density, and the brackets denote averaging over all sites n.

The linear and second-order susceptibility tensor elements of the isotropic monolayer just described, can easily be calculated. Averaging over all sites n implies averaging over ϕ and leaves only two independent nonvanishing components for $\chi^{(1)}$ and $\chi^{(2)}$:

$$\chi_{xx}^{(1)} = \chi_{yy}^{(1)} = \tfrac{1}{2} N_s \sin^2\psi \alpha_{\xi\xi} , \quad (6.10a)$$

$$\chi_{zz}^{(1)} = N_s \cos^2\psi \alpha_{\xi\xi} , \quad (6.10b)$$

$$\chi_{zxx}^{(2)} = \chi_{zyy}^{(2)} = \tfrac{1}{2} N_s \sin\psi \cos^2\psi \beta_{\xi\xi\xi} , \quad (6.10c)$$

$$\chi_{zzz}^{(2)} = N_s \cos^3\psi \beta_{\xi\xi\xi} . \quad (6.10d)$$

Here $\alpha_{\xi\xi}$ is the dominant component of the molecular linear polarizability, and $\beta_{\xi\xi\xi}$ the dominant component of the molecular second-order polarizability.

From Eq.(6.10) it is clear that in the absence of local-field corrections, due to interaction between the molecules in the layer, $\chi^{(1)}$ and $\chi^{(2)}$ are linear functions of surface density. Note that the off-diagonal elements of $\chi^{(1)}$ vanish in this particular coordinate system, implying that the net dipolar-reaction field is parallel to the inducing field.

In the calculation of the induced polarization $P_i(2\omega)$ (Eq.6.9) the average of the product of the fundamental field components $< E_{loc,j}^n(\omega) E_{loc,k}^n(\omega) >$ is required. The product of off-diagonal elements of the microscopic *linear* susceptibility $\boldsymbol{R\alpha R^{-1}}$ contained in this term does not vanish, as would be the case when $< E_{loc,j}^n(\omega) E_{loc,k}^n(\omega) >$ were to be factored into the product $< E_{loc,j}^n(\omega) > < E_{loc,k}^n(\omega) >$. As will be shown later, the contributions due to the off-diagonal elements of $\boldsymbol{R\alpha R^{-1}}$ cannot be neglected at high surface densities.

In evaluating the second-harmonic intensity from the induced polarization $P_i(2\omega)$ of Eq.(6.9), the local-field at this frequency also needs to be considered. The microscopic local-field at the harmonic frequency can be

calculated by considering the monolayer as a system of dipoles, radiating at frequency 2ω. This local-field is independent of the way the dipoles originally are induced. Averaging over all sites n can therefore be separated from the averaging procedures at the fundamental frequency ω.

An analytical expression for the local-field cannot be obtained in this model due to a random angle ϕ. The local-field in the isotropic monolayer was calculated using the Monte-Carlo technique as follows. All molecules were placed on a lattice randomly with respect to ϕ, but with a fixed tilt angles ψ. A lattice of 30x30=900 sites was used. Density variations were simulated by incomplete padding of this lattice. In order to avoid errors in the calculation of the reaction field for dipoles close to the edges of the central dipole lattice, the partially occupied lattice was surrounded with identical lattices. Clearly, the calculation can be considered reliable only if the central lattice is taken large enough. A size of about one thousand lattice points was found to be sufficiently large. The spatial extension of this central lattice is still much less than the wavelength, which justifies the neglect of retardation. The local-field components at each site n of the central lattice were calculated iteratively until convergence was obtained. All field components thus obtained were stored to be used for calculation of an average value afterwards. The above procedure was repeated fifty times whereby each time the central lattice was filled up in a random manner. The final values of the local-field components were obtained from an average over these fifty runs and had reached their convergent values at this point.

The limitations of the above approach should also be mentioned. The local-field corrections are only calculated through the linear polarizability, neglecting higher order contributions. Simply the near-field of the induced dipoles is used, neglecting the imaginary part [13,34], and therefore disregarding the self-field of the dipole [33]. Furthermore $\alpha_{\xi\xi}$ is assumed to be real. This is a reasonable assumption for the off-resonance fundamental frequency ω, but questionable for the pre-resonant harmonic frequency 2ω. A further restriction is the use of point-dipoles in the calculation of the local-field. The dimensions of the induced dipoles, however, are of the same magnitude as the distances between the dipoles.

Despite these limitations, the attractive feature of the above approach is

that only one free (scaling) parameter is used in the calculations. This will be shown in section **6.5.**

6.3.4 Numerical results

The effect of the dipolar reaction-field on the macroscopic polarization $P_z(2\omega)$, induced through $\chi^{(2)}_{zyy}$, was calculated for different tilt angles.

In case of the crystal model the induced macroscopic polarization $P_z(2\omega)$ is assumed to be [2],

$$P_z(2\omega) = i(4\pi\omega/c)\tan\theta L_{zz}(2\omega)\ell_{zz}(2\omega)\,½N_s\sin^2\psi\cos\psi\beta_{\xi\xi\xi} \\ \times L^2_{yy}(\omega)\ell^2_{yy}(\omega)E_{0,y}(\omega)E_{0,y}(\omega)\,, \qquad (6.11)$$

where θ is the angle of incidence, and ϕ was taken to be 45°. In the crystal model other components of $\chi^{(2)}$ exist, which are neglected in Eq.(6.11). There is no a priori justification in neglecting these components, but it will be seen that Eq.(6.11) does predict qualitatively the correct behaviour.

The value of $P_z(2\omega)$ as a function of surface density is shown in Fig.6.3. Note that in general $P_z(2\omega)$ is a nonlinear function of surface density. Note also that the nonlinear behaviour of $P_z(2\omega)$ with surface density depends on the tilt angle ψ. For instance, in the case of flat lying dye-molecules $P_z(2\omega)$ continues to increase in a nonlinear fashion with increasing surface coverage (see fig.6.3, for instance $\psi = 80°$), while in case of more erect standing dye-molecules $P_z(2\omega)$ levels off (see Fig.6.3, for instance $\psi = 10°$).

For tilt angles around 50° the dependence of $P_z(2\omega)$ on surface density is rather linear. Near the magic tilt-angle the local-field factors are substantially different from unity, but it so happens that the product of the local-field factors $\ell_{zz}(2\omega)\ell^2_{yy}(\omega)$ in Eq.(6.11) is about one.

The behaviour of $P_z(2\omega)$ as a function of the surface density is also calculated using the isotropic monolayer model. Qualitatively, the shape of $P_z(2\omega)$ as a function of surface density at a given tilt angle is similar to that predicted by the crystal model. However, pronounced differences appear at higher surface densities. Examples are given in Figs.6.4, 6.5, and 6.6. In Fig.6.4 we

plot $P_z(2\omega)$ according to the two models for a tilt angle of 10°. Using the isotropic monolayer model the amplitude of $P_z(2\omega)$ (solid line) starts to level off at lower surface densities than predicted by the crystal–model (dashed line). In other words, the isotropic monolayer model yields a more pronounced deviation from linear dependence on surface density than the crystal model. The behaviour of $P_z(2\omega)$ in case of a tilt angle close to the magic angle is shown in Fig. 6.5. Again the behaviour of $P_z(2\omega)$ in either model is qualitatively the same. In case of a tilt angle larger than 40° (Fig. 6.6) the isotropic monolayer model predicts a steeper rise of $P_z(2\omega)$ as a function of surface density than the crystal model does. Here the calculated value of $P_z(2\omega)$ exceeds the value of the crystal model by a factor of two at surface densities around $3*10^{14}$ cm^{-2}.

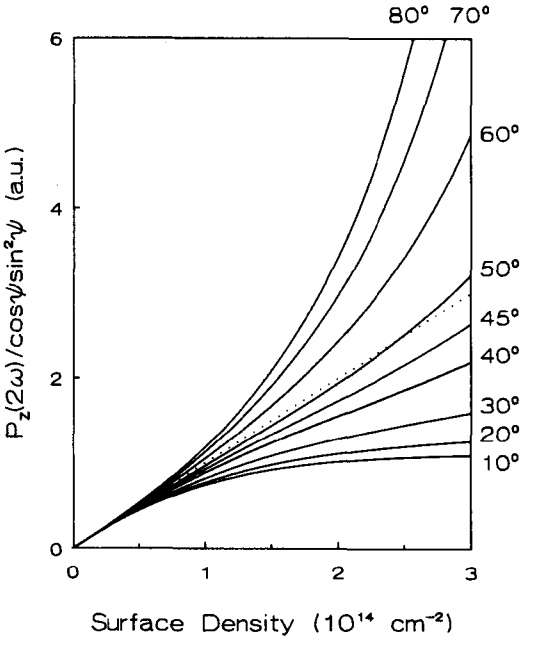

Figure 6.3: *Normalized values of $P_z(2\omega)$ calculated according to Eq.(6.11) as a function of surface density. The different traces are labelled by the tilt angles of the dye units with respect to the surface normal. The dotted line denotes the (linear) behaviour in case local–fields are neglected. A linear polarizability of 40 Å^3 was used in the calculations.*

It is of interest to ascertain whether in the calculations of the local-field factors according to the isotropic monolayer model the dominant contributions stem from density variations, or from the proper evaluation of the product $<E^n_{loc,j}(\omega)E^n_{loc,k}(\omega)>$. The factorization of the fundamental field components $<E^n_{loc,j}(\omega)E^n_{loc,k}(\omega)>$ into $<E^n_{loc,j}(\omega)><E^n_{loc,k}(\omega)>$ essentially means disregarding the off-diagonal components of the linear microscopic polarizability tensor $\boldsymbol{R}\alpha\boldsymbol{R}^{-1}$. On factorization, the off-diagonal components of $\boldsymbol{R}\alpha\boldsymbol{R}^{-1}$ average out. In Figs.6.4 to 6.6 the dash-dotted line is the result of setting $<E^n_{loc,j}(\omega)E^n_{loc,k}(\omega)>$ to $<E^n_{loc,j}(\omega)><E^n_{loc,k}(\omega)>$. From these calculations it is seen that factorization is only allowed for tilt angles close to 10°.

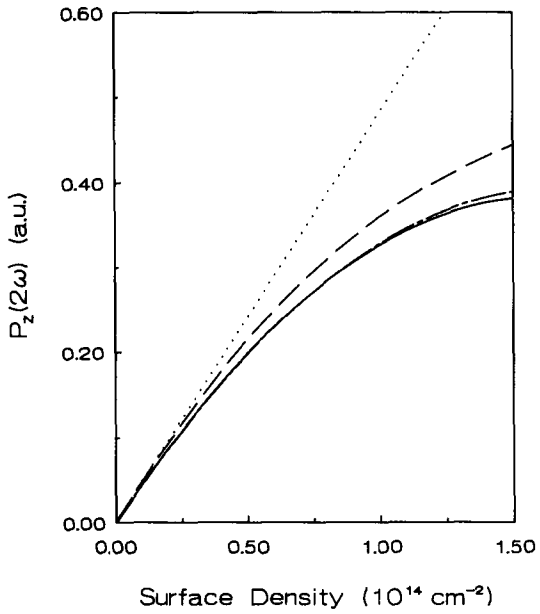

Figure 6.4: *Calculated values of* $P_z(2\omega)$ *according to the isotropic monolayer model (solid line) and the crystal model (dashed line), for a tilt angle of* 10°. *The dash-dotted line is the result according to the isotropic monolayer model in case the off-diagonal components of the microscopic linear polarizability are neglected. The linear behaviour (dotted line) is the result of disregarding the microscopic local-field. A linear polarizability of* 40 Å^3 *was used in the calculations.*

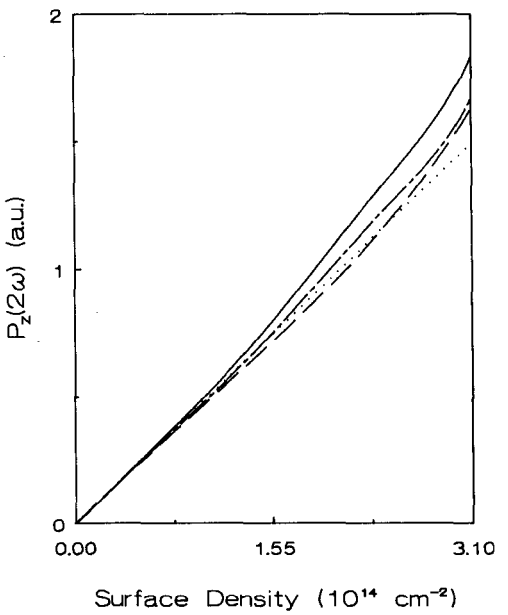

Figure 6.5: *Calculated values of $P_z(2\omega)$ according to the isotropic monolayer model (solid line) and the crystal model (dashed line), for a tilt angle of 50°. The dash-dotted line is the result according to the isotropic monolayer model in case the off-diagonal components of the microscopic linear polarizability are neglected. The linear behaviour (dotted line) is the result of disregarding the microscopic local-field. A linear polarizability of 40 Å^3 was used in the calculations.*

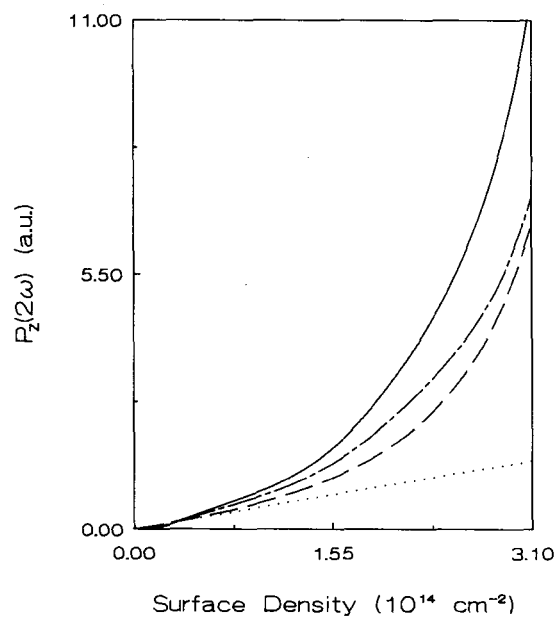

Figure 6.6: *Calculated values of* $P_z(2\omega)$ *according to the isotropic monolayer model (solid line) and the crystal model (dashed line), for a tilt angle of* 80°. *The dash-dotted line is the result according to the isotropic monolayer model in case the off-diagonal components of the microscopic linear polarizability are neglected. The linear behaviour (dotted line) is the result of disregarding the microscopic local-field. A linear polarizability of* 40 Å^3 *was used in the calculations.*

Summarizing: large differences (up to 100%) exist in the calculation of the local-field effects for the isotropic monolayer model compared to the crystal model. Both models, however, show qualitatively the same dependence on surface density. The nonlinear polarization in the isotropic monolayer model shows often a more pronounced deviation from a linear dependence on surface density than the crystal model. In general, local-field corrections are more pronounced in the isotropic monolayer model than in the crystal model. The effect of the nondiagonal terms in the Cartesian polarizability tensor is small when the tilt angle is close to zero.

6.4 Experimental

The optical nonlinear molecules used in this work are 4-(4-didecylaminostyryl)-N-methylpyridiniumiodide (dye **I**, see also Fig. 6.1), S-4-(4'-(1-pyrrolidine-3-palmitoate)phenylazo)-3-nitro-benzoic acid (dye **II**, Fig. 6.1) and (S,S)-4'-(4-(1-pyrrolidine-3,4-dipalmitoate)-phenylazo-3-nitro-benzoic acid (dye **III**, Fig. 6.1). Dye **I** was purchased from Molecular Probes Inc., and used without further purification. The synthesis of dyes **II** and **III** will be published elsewhere [42].

Preparation and deposition of the monolayers was established with a commercially available trough (Lauda Langmuir Balance). The Langmuir-Blodgett monolayers were deposited on Corning 7059 glass microscope slides. These substrates were cleaned in chromic acid (at least 16 hours, 20 °C), and rinsed ultrasonically with milli-Q water, acetone, chloroform and hexane.

A specific surface density of either dye **I**, **II** or **III** was obtained by dissolving known amounts of dye and arachidic acid (Fluka AG) in chloroform. The 10^{-3}M chloroform solution was spread onto an aqueous subphase.

In case of dye **I** the subphase contained 10^{-2}M potassium iodide, the pH was about 5.8, and the temperature 19 ± 1 °C. The resulting monolayers were compressed and stabilized at a pressure of 10 mN/m, and were deposited at this pressure by withdrawal of the hydrophilic substrate from the subphase at a rate of 4 mm/min. The dye is chemically unstable, and therefore sample preparation and handling were done in the dark, and all measurements were performed within one hour after preparation. The number of molecules per surface unit was determined from the compression-isotherm, taken at a rate of 5 Å^2 per molecule per minute.

For the preparation of monolayers of dye **II** $CdCl_2$ was added to the subphase upto a concentration of 10^{-3} M, the pH was raised to a value of 8.2 by addition of NaOH. The temperature of the suphase was 19 ± 1 °C. Monolayers were compressed and stabilized at a pressure of 28 mN/m. Deposition onto the glass substrate took place at a rate of 4 mm/min [43]. In case of dye **III** the suphase was higly purified water (milli-Q), having a temperature of 19 ± 1 °C. The deposition rate was 2 mm/min. A specific surface density of either dye **II** or **III** was obtained in the same fashion as for dye **I**. The dye systems are very stable, and optical measurements performed immediately or two weeks after preparation of the

monolayer gave identical results.

Prior to any measurements we removed the monolayer at the backside of the substrate by wiping with lens tissues soaked in acetone and in chloroform. This in order to prevent interference between signals arising from monolayers at the front and backside of the substrate.

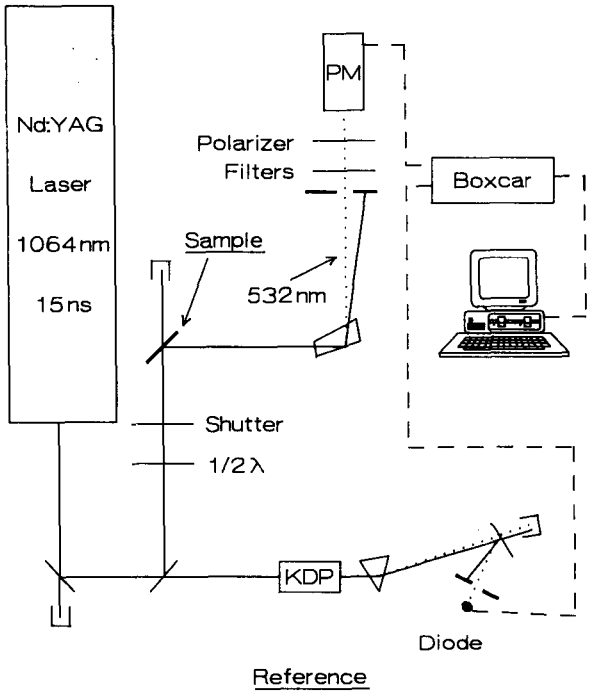

Figure 6.7: *Schematic of the S.H.G. measuring set-up.*

In the second-harmonic-generation experiment we used the linearly polarized fundamental output (1064nm) of a Q-switched Nd^{3+}:YAG laser (Molectron Corporation). The polarization of the fundamental beam could be rotated by means of a halve-wave plate. The fundamental beam was directed onto the sample with an angle of incidence of 45°. The frequency doubled light (532 nm) was detected in reflection by a photomultiplier. Reflections from the backside of the substrate were spatially separated from frontside reflections by pasting the backside of

the substrate with indexmatching oil to a thick piece of glass. Separation of the harmonic from the fundamental beam was accomplished by a Pellin–Broca prism and suitable colour filters. The polarization direction of the second-harmonic beam was determined with a sheet polarizer (Melles–Griot). Signal sampling, averaging, and recording took place with a boxcar (Princeton Applied Research, model 162) and computer. The signal was divided by the reference signal from a KDP doubling crystal. With the pulse energies used (1.5 – 5 mJ), the nonlinear contribution of the glass substrate covered with a monolayer of arachidic acid was below the detection limit.

The size of the error–bars indicated in Figs. 6.13–6.16 is determined mainly by statistical noise in the experimental setup, due to amongst others laser amplitude fluctuations.

The absorption spectra of the monolayers were measured on a Pye Unicam SP8–200 UV/VIS spectrophotometer. Absorption spectra of the charge–transfer transition of the dye monolayers were also measured as a function of the angle of incidence. In these measurements we used a collimated polarized beam from a tungsten lamp. A double–array optical multichannel–analyzer (Princeton Instruments, Inc.) was used to record the absorption spectra. In order to obtain the internal absorbance of the monolayer the total absorption has to be corrected for reflection losses at every angle of incidence. Reflection losses were measured using a reference object consisting of a glass slide covered with a monolayer of pure arachidic acid.

The numerical calculations described in section **6.3** were done on a Convex 230 *mini–supercomputer*.

6.5 Experimental results

6.5.1 General aspects

The second–harmonic intensity was measured in reflection with an incident angle of 45°. For all dye systems the following set of second–harmonic intensities were measured: $I_{pp}(2\omega)$, $I_{ps}(2\omega)$, $I_{qp}(2\omega)$, $I_{qs}(2\omega)$, $I_{sp}(2\omega)$ and $I_{ss}(2\omega)$. Here, the first and second subscript label the input and output

polarization directions, respectively. p and s refer, respectively, to the polarization directions parallel and perpendicular to the plane of incoming and outgoing beams (the x–z plane). The polarization direction in between s and p is denoted as q, i.e. 45° with respect to the plane of incidence.

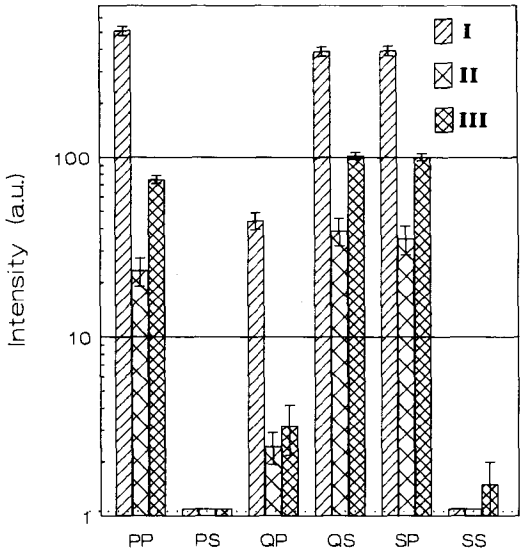

Figure 6.8: *Histogram of the observed p- and s-polarized second-harmonic intensities as measured in reflection for different polarization directions of the fundamental beam. Full monolayer coverage signal strengths are given. The dotted line indicates the detection limit.*

A typical result obtained for both dye systems is shown in Fig. 6.8. $I_{ss}(2\omega)$ and $I_{ps}(2\omega)$ are found to be two orders or magnitude smaller than the other polarization combinations, confirming the uniaxial symmetry of the system (Fig. 6.2) [2,44]. The uniaxiality of the system derives further support from polarized absorption measurements.

For all three dye systems the second-harmonic intensities $I_{pp}(2\omega)$, $I_{ps}(2\omega)$, $I_{qp}(2\omega)$, $I_{qs}(2\omega)$, $I_{sp}(2\omega)$, and $I_{ss}(2\omega)$ were measured as a function of density of the dye molecules. Figure 6.13 displays the observed relation for $\sqrt{I_{sp}}$ in the case of dye system **I**. Clearly, $\sqrt{I_{sp}}$ is not linear in surface density. It is

tempting to interpret this behaviour in terms of a local-field effect, but in order to draw this conclusion two other effects that could influence second-harmonic generation have to be ruled out. First, aggregation could occur at high surface densities. This possibility is considered in the next section. Second, the tilt angle of the dye units might change as a function of surface density. An investigation concerning this problem is described in the section **6.5.3**. After having addressed these problems and concluded that neither effect plays a role in the monolayers studied, we continue in section **6.5.4** with a discussion of the density dependence of the second-harmonic intensity.

6.5.2 Aggregation

We recall that $I_{ss}(2\omega)$ and $I_{ps}(2\omega)$ were found to be two orders of magnitude

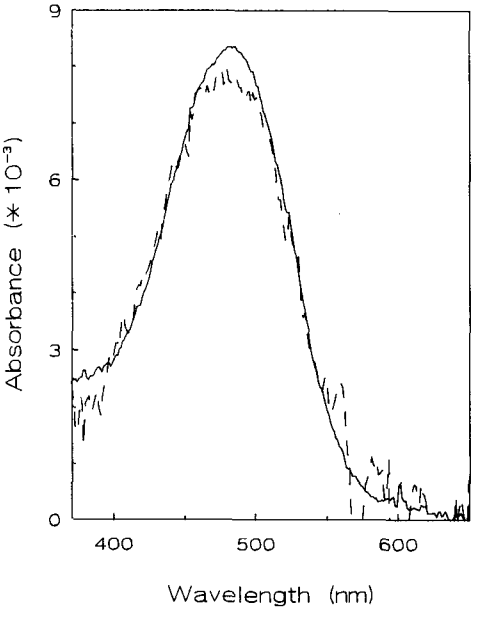

Figure 6.9: *Absorption spectra of dye* **I** *at full monolayer coverage* ($1.5055*10^{14}\ cm^{-2}$, *solid line*) *and at low surface density* ($0.36*10^{14}\ cm^{-2}$, *dashed line*). *The absorbance scale corresponds to the full monolayer case.*

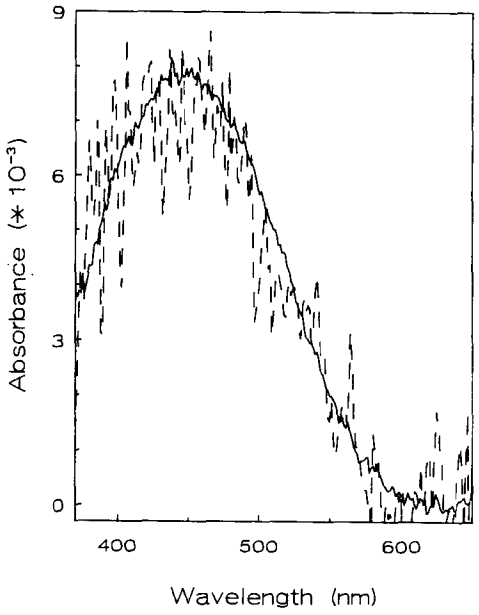

Figure 6.10: *Absorption spectra of dye* **II** *at full monolayer coverage* ($3.03*10^{14}$ cm^{-2}, *solid line*) *and at low surface density* ($0.41*10^{14}$ cm^{-2}, *dashed line*). *The absorbance scale corresponds to the full monolayer case.*

smaller than the other second-harmonic intensities. This fact indicates that the samples are macroscopically isotropic with respect to the substrate plane and that aggregate formation is highly unlikely [45]. The near-equality of the intensities of $I_{qs}(2\omega)$ and $I_{sp}(2\omega)$ further supports this assumption [46]. Further evidence for the absence of aggregation stems from the density dependence of the absorption spectra. Figures 6.9, 6.10, and 6.11 display these spectra for low surface coverage (dashed line) and maximum surface density (solid line). It is clear that the spectra show no broadening and/or shift of the charge-transfer band in the regime of densities studied. These findings strongly suggest that the optical excitations in these films can effectively be considered as localized, implying that the local inhomogeneity exceeds by far the dipolar coupling between the sites. The assumption of localized excitations in these Langmuir-Blodgett films is basic to the local-field approach taken in

this chapter. It should be noted, however, that for substrates that were not cleaned immediately prior to use, a blue shift of the absorption band can be observed in case of dye **I**, which is indicative of H–aggregate formation [24].

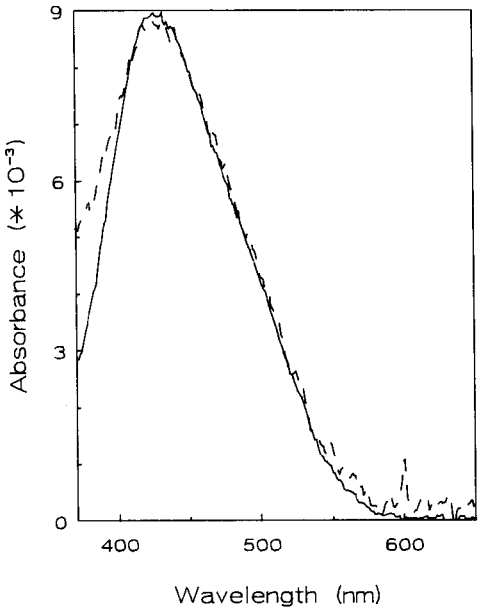

Figure 6.11: *Absorption spectra of dye* **III** *at full monolayer coverage* ($2.19*10^{14}$ cm^{-2}, *solid line*) *and at low surface density* ($0.23*10^{14}$ cm^{-2}, *dashed line*). *The absorbance scale corresponds to the full monolayer case.*

The change in surface acidity resulting from dilution of the dye molecules with arachidic acid has no effect on the absorption spectrum, as expected for the molecules under study [44,47]. Its effect on the nonlinear optical properties can therefore be neglected.

6.5.3 The tilt angle

Knowledge of the tilt angle ψ of the dye unit is essential to predicting the second–harmonic intensity as a function of the surface density. In principle

the tilt angle ψ can be determined by second-harmonic generation. However, in case local-field corrections are important, this calculation is extremely laborious for the following reasons. First, the tilt angle itself is an important parameter in the calculation of macroscopic field corrections of Eq.(6.1). The dielectric constant of the monolayer ε' in Eq.(6.1c) is a rather critical parameter [46], and depends on the tilt angle through Eq.(6.10a) [45]. Small modifications of the dielectric constant lead to substantial changes in the obtained tilt angle [46]. Second, also the microscopic local-field correction is rather sensitive to the tilt angle, as follows from the numerical calculations of section **6.3.4** (c.f. Figs. 6.3, 6.4, 6.5, 6.6). The microscopic local-field will also influence the dielectric constant of the monolayer. Third, the optical nonlinearities often allow two possible solutions for the tilt angle ψ and additional information is needed to make a choice.

Clearly, it would be extremely valuable if another independent method could give an initial estimate of the tilt angle. For our systems a polarization-dependent study of the optical density turns out to be extremely useful. The anisotropy of the absorbance stems from the fact that the transition dipole moment of the charge-transfer transition is directed along the ξ-axis. The derivation of the relevant formula for the angular-dependent absorption is given in the Appendix, at the end of this chapter. In calculating the tilt angle from linear spectroscopy the dielectric constant of the monolayer is also requested, but its precise value is not so important to the outcome. In case no spectral shifts occur, the microscopic local-field has no influence on the optical density [48].

For all three dye systems the tilt angles were determined by the optical-density method, and were found to be $80^{\circ}(\pm 5)$ for dye **I**, $50^{\circ}(\pm 2)$ for dye **II**, and $60^{\circ}(\pm 2)$ in case of dye **III**. A tilt angle of 80° for dye **I** agrees well with a report [44,49], for a similar molecule. For dyes **II** and **III** an estimation of ψ indicates that the tilt angle is close to the magic angle (54.7°), making a calculation of ψ virtually independent of the choice of the dielectric constant ε' of the monolayer. For a magic tilt-angle the optical-density is independent of the angle of incidence on the substrate. The difference in tilt angle found for dye systems **II** and **III** must be ascribed to the additional hydrophobic chain in compound **III**.

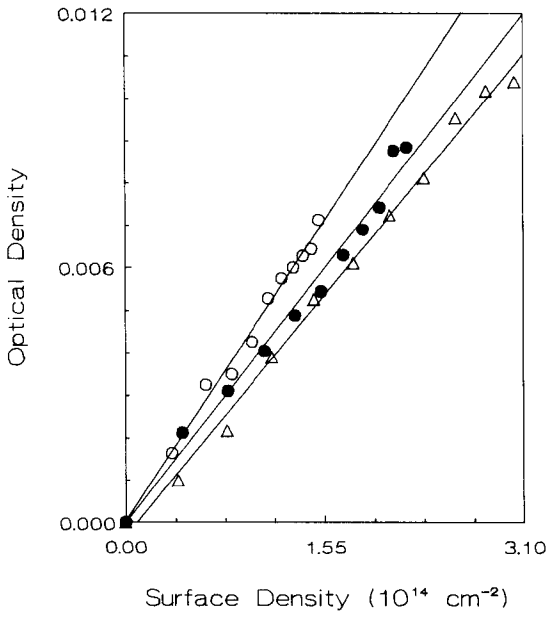

Figure 6.12: *Measurement of the optical density for dye* **I** *(open circles), dye* **II** *(open triangles), and dye* **III** *(closed circles) as a function of surface density, measured at a perpendicular angle of incidence. The straight lines are least square fits to the measurements.*

From angular–dependent absorption measurements it was concluded that the tilt angle is independent of the surface density. Confirmation of this fact comes from a plot of the optical density versus surface density. The results are shown in Fig. 6.12. For all three dyes a linear behaviour is found, indicating that the respective tilt angles of the dye units do not change with surface coverage in the density regime studied.

The tilt–angles determined in this way are in complete agreement with the ones obtained from a second–harmonic generation experiment, once the local–field corrections are incorporated. For the calculation of ψ from SHG data, the dielectric constants of the monolayer are important. The values $\varepsilon'_{zz}(2\omega)$=2.66 and $\varepsilon'_{zz}(\omega)$=2.50 were used for a monolayer of dye **II** [50]. The ratio $\varepsilon'(2\omega)/\varepsilon'(\omega)$ is in excellent agreement with the ratio obtained from $I_{qs}(2\omega)$ and $I_{sp}(2\omega)$ [46].

The z-component of ε' has been used in the calculations [5]. For dye **I** the dielectric constant ε'_{zz} was supposed to be close to 1, because of the large tilt angle ψ. In case of dye **III** we used $\varepsilon_{zz}(\omega)$=2.25 and $\varepsilon_{zz}(2\omega)$=2.40. The tilt angle deduced from SHG data is not very sensitive to the microscopic local-field corrections ($\pm 5^{\circ}$). We found this to be true for both the crystal model as well as the isotropic monolayer model. In case of dye **I** the tilt angle deduced from SHG changes 5° using the microscopic local-field correction factors. The smallest differences ($\approx 2^{\circ}$) are found for tilt angles close to 50°. These findings corroborate the results of Heinz et al. [41] who found that tilt angles hardly depend on microscopic local-field corrections.

The difference in tilt angles of the chromophores also manifests itself in the maximum surface density that can be reached, before the monolayer collapses or aggregation occurs. For almost flat lying dye-molecules, like **I**, less high surface densities ($1.5055 \cdot 10^{14}$ cm^{-2}) can be reached than for the more erect ones like **II** ($3.03 \cdot 10^{14}$ cm^{-2}). In case of dye **III** the maximum attainable surface density is determined by the area of the two alkyl chains (≈ 45 Å^2) and not by the area of the dye unit.

In summary the tilt angles deduced from absorption and second-harmonic generation (SHG) measurements are in excellent agreement with one another. The advantage of the absorption method as compared to the SHG measurements is that the deduced tilt angle is not very sensitive to the value of the monolayer dielectric constant.

6.5.4 Microscopic local-fields: dependence of $\chi^{(2)}$ on surface density

For dye **I** (ψ=80°) the measured and calculated relation between $\sqrt{I_{sp}}$ and increasing surface density is shown in Fig. 6.13. Scatter in the data is ascribed to the chemical instability of the dye unit. Note from Eq.(6.11) that $\sqrt{I_{sp}}$ is proportional to the amplitude of $P_z(2\omega)$ (i.e. the effective value of $\chi^{(2)}_{zyy}$). The observed second-harmonic efficiency (triangular points) increases in a nonlinear fashion with surface density. As argued in preceding sections, no hints of aggregation occur, while also the tilt angle is independent of the surface density. We therefore conclude that this nonlinear behaviour is due to

local–field effects. The result of the Monte–Carlo calculations based on the isotropic monolayer model (solid line) is in excellent agreement with the measurements. The crystal–model calculation (dashed line) also yields a good description except for high surface densities. Analogous results have been found for $\sqrt{I_{pp}}$.

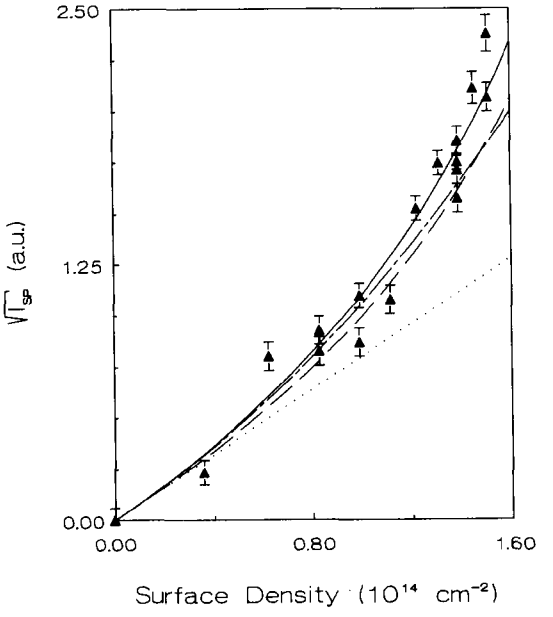

Figure 6.13: *Measured values of* $\sqrt{I_{sp}}$ *for monolayers of dye* **I** *as a function of surface density (triangular points). Also shown are the results of the calculations according to the isotropic monolayer model (solid line), the crystal model (dashed line), and in case the off–diagonal components of the linear microscopic polarizability are neglected (dash–dotted line). The dotted line is the result of disregarding the microscopic local–field. In the calculations a linear polarizability of* 50 Å^3 *was used.*

We emphasize that only one free parameter, the molecular hyperpolarizability $\beta_{\xi\xi\xi}$, enters into the calculation of the local–field, the rest of the parameters are either measured or known. For dye **I** a lattice constant of 8.15 Å was calculated from the compression–isotherm. For the

molecular polarizability $\alpha_{\xi\xi}$ a value of $50\,\text{Å}^3$ was taken at the harmonic as well as at fundamental frequency [51]. The dispersion in $\alpha_{\xi\xi}$ is neglected, because of the fact that the results of the calculations are not very critical to the value of the linear polarizability.

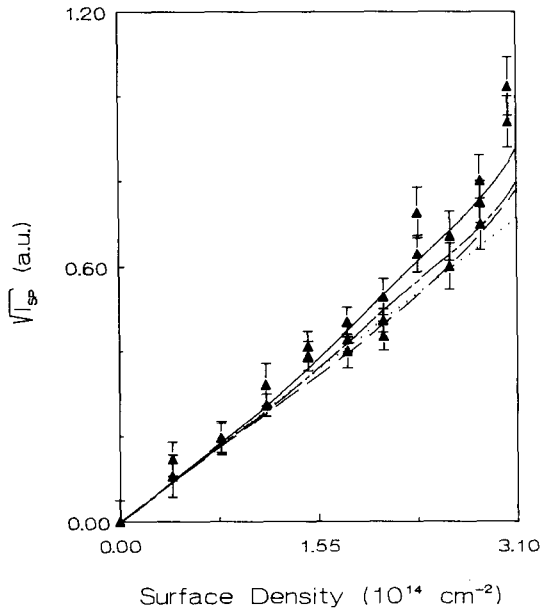

Figure 6.14: *Measured values of* $\sqrt{I_{sp}}$ *for monolayers of dye* II *as a function of surface density (triangular points). Also shown are the results of the calculations according to the isotropic monolayer model (solid line), the crystal model (dashed line), and in case the off-diagonal components of the linear microscopic polarizability are neglected (dash-dotted line). The dotted line is the result of disregarding the microscopic local-field. In the calculations a linear polarizability of* $40\,\text{Å}^3$ *was used.*

The value of the molecular hyperpolarizability $\beta_{\xi\xi\xi}$, as inferred from the measured $\chi^{(2)}_{zyy}$, differs (at full coverage) by a factor two from the local-field corrected value (dotted line, Fig. 6.13). The microscopic local-field can be the reason for the exceptionally large $\chi^{(2)}$ measured for monolayers of dye I [17,44].

For dye **II** a tilt angle ψ of 50° was found. The experimentally observed behaviour of $\sqrt{I_{sp}}$ for dye **II** as a function of surface density is given in Fig. 6.14. Indeed, as might be expected for a tilt angle of 50° (see Fig. 6.3) a rather linear dependence of $\sqrt{I_{sp}}$ on surface density is observed. The isotropic monolayer model, at high surface densities, still yields a better fit (solid line), than provided by the crystal model (dashed line). The lattice constant for this dye was determined to be 5.74 Å, and the molecular polarizability was taken to be 40 Å^3 [52,53].

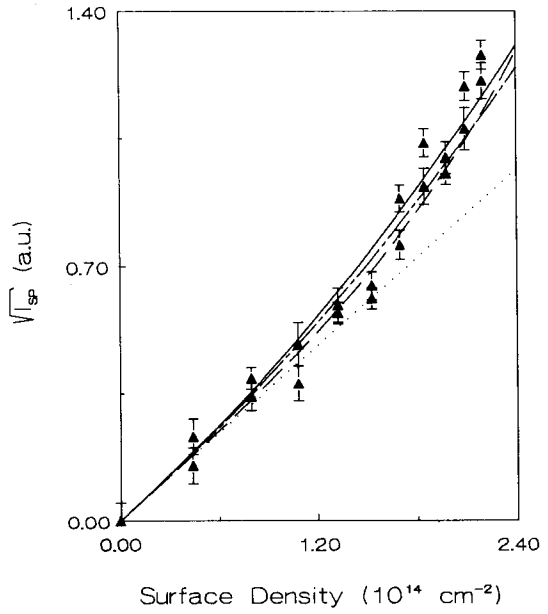

Figure 6.15: *Measured values of* $\sqrt{I_{sp}}$ *for monolayers of dye* **III** *as a function of surface density (triangular points). Also shown are the results of the calculations according to the isotropic monolayer model (solid line), the crystal model (dashed line), and in case the off-diagonal components of the linear microscopic polarizability are neglected (dash-dotted line). The dotted line is the result of disregarding the microscopic local-field. In the calculations a linear polarizability of* 40 Å^3 *was used.*

The small deviation from linear behaviour might suggest that the

local–field corrections are of minor importance in this case [29,54]. The linear–like behaviour, however, is due to the fact that near the magic tilt angle a cancellation of local–field correction factors occurs. The field along the y–axis (parallel to the substrate) is about 1.4 times the applied field, while the field along z (i.e. perpendicular to the substrate) is calculated to be about 0.5 times the applied field.

In case of dye **III** (tilt angle of 60°) again a nonlinear increase of $\chi^{(2)}_{zyy}$ with surface density is observed. A quantitative agreement is found between the measured $\chi^{(2)}_{zyy}$ and the Monte–Carlo calculations based on the isotropic monolayer model. A lattice constant of 6.75 Å was used. The different values of $\beta_{\xi\xi\xi}$ obtained for dye systems **II** and **III** at maximum surface density, is attributed to the microscopic local–field. At low surface densities, where the microscopic local–field can be neglected, a small difference in $\beta_{\xi\xi\xi}$ remains. This difference arises because monolayers of dye **II** need to be prepared under basic circumstances, at which the carbon–acid group is completely deprotonated [43]. Dye **III** exists in its protonated form. Deprotonation causes an additional negative charge at the benzoic–acid group, reducing the asymmetric charge distribution in the system, leading to a decrease of $\beta_{\xi\xi\xi}$ [55]. The different surface density dependence of $\chi^{(2)}_{zyy}$ for dye systems **II** and **III** can be completely attributed to the microscopic local–field effect. The difference in local–field factors is caused by a difference in tilt angles (Fig. 6.3).

For dye **II** the measured and calculated behaviour of $\sqrt{I_{pp}}$ with surface density is given in Fig. 6.16. For this polarization combination the fundamental and second–harmonic beams are both polarized parallel to the plane of incidence. The fundamental field can be decomposed into a parallel ($E_x(\omega)$) and perpendicular ($E_z(\omega)$) electric field component to the substrate surface. The emitted second–harmonic signal is then proportional to the difference between the two nonlinearly induced polarizations $P_x(2\omega)$ and $P_z(2\omega)$. The off–diagonal components of the *linear* susceptibility tensor $\boldsymbol{R\alpha R}^{-1}$ (Eq.(6.9)) also yield a contribution to the fundamental field along the y–axis ($< E^n_{loc,y}(\omega) E^n_{loc,y}(\omega) >$). This latter quantity contributes through $\chi^{(2)}_{zyy}$ to the second–harmonic polarization $P_z(2\omega)$. This additional contribution to $P_z(2\omega)$ reduces the difference between $P_x(2\omega)$ and $P_z(2\omega)$ and therefore leads to a measurable decrease of $\sqrt{I_{pp}}$ at high surface densities (solid line). In case the

off-diagonal elements of $R\alpha R^{-1}$ are neglected (dash-dotted line), a steeper increase of $\sqrt{T_{pp}}$ is calculated. The result of the computations according to the crystal model are plotted as the dashed line. It is clear that in this case the contribution of the off-diagonal terms of $R\alpha R^{-1}$ cannot be disregarded at higher surface densities.

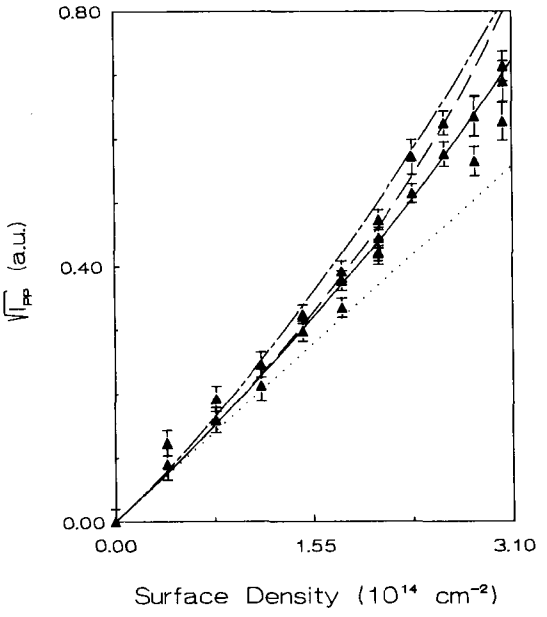

Figure 6.16: *Measured values of* $\sqrt{T_{pp}}$ *for monolayers of dye* **II** *as a function of surface density (triangular points). Also shown are the results of the calculations according to the isotropic monolayer model (solid line), the crystal model (dashed line), and in case the off-diagonal components of the linear microscopic polarizability are neglected (dash-dotted line). The dotted line is the result of disregarding the microscopic local-field. In the calculations a linear polarizability of* 40 Å^3 *was used.*

6.6 Discussion and Conclusions

In this chapter we showed that a Monte–Carlo calculation of the local–field in a monolayer of rod–shaped chromophores yields good agreement between theory and experiment in second–harmonic generation experiments. We found that Monte–Carlo calculations of the local–field can differ up to a factor of 2 from what is obtained by using a crystal model. The qualitative behaviour of $\chi^{(2)}$ versus surface density in both models, however, is the same. These results are clearly relevant when SHG is used in a determination of the molecular hyperpolarizability $\beta_{\xi\xi\xi}$. The values reported in the literature for $\beta_{\xi\xi\xi}$ have often been obtained from Langmuir–Blodgett monolayers at maximum surface density using the 3–dimensional Lorentz–Lorenz expressions for the local–field, or by using local–field corrections based on the crystal model. Our work shows that by this approach the value of $\beta_{\xi\xi\xi}$ can be overestimated or underestimated depending on the spatial orientation of the optical nonlinearity.

In the systems studied no additional broadening of the experimental spectra at high surface density could be observed within experimental accuracy (about 200 cm^{-1}). However, a broadening of approximately 1500 cm^{-1} due to dipolar interactions is calculated for a simple two–level system [15]. The absence of such a large broadening is attributed to inhomogeneous broadening of the optical transition, which *at resonance* considerably reduces the dipolar–coupling. Off–resonance however, the molecular polarizability may be assumed to be site independent. Hence, in our local–field calculations the effect of inhomogeneous broadening on dipolar interactions was neglected.

To calculate the microscopic local–field a large number of parameters are needed: 1) the dielectric constants $\varepsilon'(\omega)$, $\varepsilon'(2\omega)$ of the monolayer at the fundamental and the second harmonic frequency, 2) the polarizability $\alpha_{\xi\xi}$ at ω and 2ω, 3) the tilt angle of the dye molecules, 4) the mean distance between the dye units, and 5) the absolute value of $\beta_{\xi\xi\xi}$. To complicate matters further, both ε' and $\boldsymbol{\alpha}$ can be complex. In addition, ε' will depend on the surface density, while also the tilt angle may be a function of surface density. In this paper the number of free parameters could successfully be restricted to one, namely the absolute value of the molecular hyperpolarizability $\beta_{\xi\xi\xi}$. The value of the other parameters were known or could be determined independently. Despite

these complications our Monte-Carlo calculations reproduce extremely well the experimentally observed behaviour of the different $\chi^{(2)}$ components, justifying our approach.

Note added in proof: Recent work of J. Knoester [56] justifies the use of the local-field theory as described in this chapter, because only a single resonance occurs in these particular experiments.

Appendix

The optical density of a transition is proportional to $(\boldsymbol{\mu}.\boldsymbol{E})^2$, where $\boldsymbol{\mu}$ is the transition dipole moment and $\boldsymbol{E}$ the electromagnetic field. The relation between the components of the transition dipole moment in the laboratory frame and the molecular frame is given by (see Fig. 6.2):

$$\boldsymbol{\mu} = \begin{pmatrix} \cos\phi\sin\psi \\ \sin\phi\sin\psi \\ \cos\psi \end{pmatrix} \boldsymbol{\mu}_0 . \qquad \text{(A.6.1)}$$

Here $\boldsymbol{\mu}_0$ is the transition dipole moment directed along the molecular ξ-axis. The angles ψ and ϕ are shown in Fig. 6.2.

For a parallel-polarized light beam the electric field in the film is given by:

$$\boldsymbol{E} = \begin{pmatrix} \cos\theta' \\ 0 \\ \sin\theta' \end{pmatrix} \boldsymbol{E}_0 = \begin{pmatrix} (\varepsilon' - \sin^2\theta)^{1/2} \\ 0 \\ \sin\theta \end{pmatrix} \boldsymbol{E}_0/\sqrt{\varepsilon'} , \qquad \text{(A.6.2)}$$

where θ is the angle of incidence on the sample, θ' the angle of refraction in the monolayer, and ε' is the dielectric constant of the monolayer, which for simplicity is supposed to be isotropic.

The optical density for a parallel polarized light beam (OD_p) is calculated as:

$$OD_p = Q(\theta) < (\boldsymbol{\mu}.\boldsymbol{E})^2 > \tag{A.6.3}$$

$$= \frac{Q}{\cos\theta} \{½\sin^2\psi + (\cos^2\psi - ½\sin^2\psi)\sin^2\theta/\varepsilon'\}, \tag{A.6.4}$$

where < > means averaging over ϕ. The proportionality constant $Q(\theta)$ contains, amongst others, the number of molecules in the beam, which depends on the angle of incidence θ. By varying θ, the number of absorbing molecules is changed. To correct for this effect, $Q(\theta)$ is divided by $\cos\theta$.

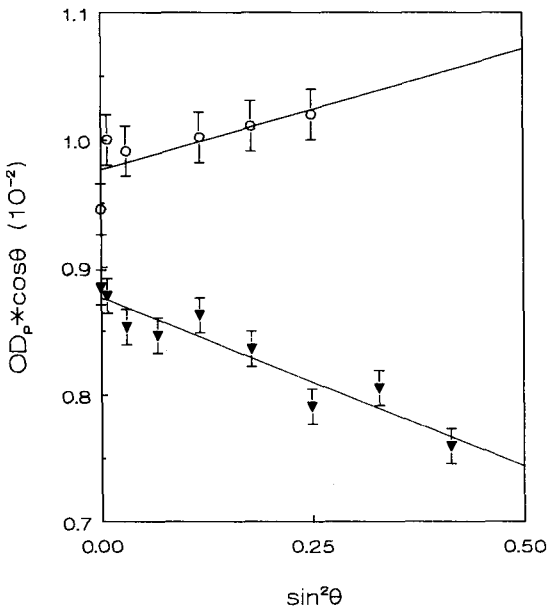

Figure A.6.1: *Measurement of the optical density of the charge-transfer transition of monolayers of dye* II *(open circles) and dye* III *(closed triangles), plotted as a function of the sine squared of the angle of incidence. The drawn lines are least square fits to the measurements. See text for further explanations.*

A plot of $OD_p * \cos\theta$ against $\sin^2\theta$ should give a straight line. The tilt angle ψ can be determined from the ratio of the slope S and the abscissa A:

$$\tan^2\psi = 2/\{(S/\varepsilon' A)+1\}\,, \qquad \text{(A.6.5)}$$

in which case Q is divided out. Changes in reflection losses, upon varying the angle of incidence, are corrected for by subtraction of a reference spectrum of a virgin glass slide.

As an example a plot of the optical densities versus $\sin^2\theta$ for monolayers of dye systems **II** and **III** is shown in Fig.A.6.1. From this plot we calculate tilt angles of 50° and 60° for dyes **II** and **III**, respectively. The sign of the slope depends on whether the tilt angle of the dye unit is larger or smaller than the magic angle value of 54.7°.

References

[1] Y.R. Shen, *Nature (London)* **337**, 519 (1989).

[2] Y.R. Shen, *Annu. Rev. Phys. Chem.* **40**, 327 (1989).

[3] C.K. Chen, T.F. Heinz, D. Ricard, and Y.R. Shen, *Phys. Rev.* **B27**, 1965 (1983).

[4] G.T. Boyd, Th. Rasing, J.R.R. Leite, and Y.R. Shen, *Phys. Rev.* **B30**, 519 (1984).

[5] T.F. Heinz, *PhD thesis*, Univ. of Calif., Berkeley (1982).

[6] G.J Kovacs, R.O. Loufty, P.S. Vincent, C. Jennings, and R. Aroca, *Langmuir* **2**, 689 (1986).

[7] T.M. Cotton, R.A. Uphaus, and D. Möbius, *J. Phys. Chem.* **90**,6071 (1986).

[8] K.E. Drabe, G. Cnossen, and D.A. Wiersma, *Opt. Commun.* **73**, 91 (1989).

[9] K.E. Drabe, G. Cnossen, and D.A. Wiersma, *Chem. Phys. Lett.* **169**, 416 (1990).

[10] C.K. Carniglia, L. Mandel, and K.H. Drexhage, *J. Opt. Soc. Am.* **62**, 479 (1972).

[11] P. Guyot–Sionnest, Y.R. Shen, and T.F. Heinz, *Appl. Phys.* **B42**, 237 (1987).

[12] J. Knoester and S. Mukamel, *J. Opt. Soc. Am.* **B6**, 643 (1989).

[13] J.D. Jackson, *Classical Electrodynamics*, 2nd ed. (J. Wiley and Sons, New York, 1975).

[14] B.F. Levine and C.G. Bethea, *J. Chem. Phys.* **63**, 2666 (1975).

[15] J.J. Maki, M.S. Malcuit, J.E. Sipe, and R.W. Boyd, *Phys. Rev. Lett.* **67**, 972

(1991).

[16] H. Hsiung, G.R. Meredith, H. Vanherzeele, R. Popovitz–Biro, E. Shavit, and M. Lahav, *Chem. Phys. Lett.* **164**, 539 (1989).

[17] D. Lupo, W. Prass, U. Scheunemann, A. Leschewsky, H. Ringsdorf, and I. Ledoux, *J. Opt. Soc. Am.* **B5**, 300 (1988).

[18] F.C. Spano and S. Mukamel, *Phys. Rev.* **A40**, 5783 (1989), **A41**, 5243 (E) (1990).

[19] F.C. Spano and S. Mukamel, *Phys. Rev. Lett.* **66**, 1197 (1991).

[20] L.M. Hayden, *Phys. Rev.* **B38**, 3718 (1988).

[21] K. Shirota, K. Kajikawa, H. Takezoe, and A. Fukada, *Jpn. J. Appl. Phys.* **29**, 750 (1990).

[22] K. Kajikawa, K. Shirota, H. Takezoe, and A. Fukada, *Jpn. J. Appl. Phys.* **29**, 913 (1990).

[23] K. Kajikawa, H. Takezoe, and A. Fukuda, *Jpn. J. Appl. Phys.* **30**, 1050 (1991).

[24] J.S. Schildkraut, T.L. Penner, C.S. Willand, and A. Ulman, *Opt. Lett.* **13**, 134 (1988).

[25] G. Marowsky and R. Steinhoff, *Opt. Lett.* **13**, 707 (1988).

[26] I.R. Girling, N.A. Cade, P.V. Kolinsky, R.J. Jones, I.R. Peterson, M.M. Ahmad, D.B. Neal, M.C. Petty, G.G. Roberts, and W.J. Feast, *J. Opt. Soc. Am.* **B4**, 950 (1987).

[27] A. Scheelen, P. Winant and A. Persoons, *Conjugated Polymeric Materials: Opportunities in Electronics, and Molecular Electronics*, edited by J.L. Bredas and R.R. Chance (Kluwer Academic Publishers, Dordrecht, 1990), p443.

[28] P. Winant, A. Scheelen and A. Persoons, *Nonlinear Optical Effects in Organic Polymers*, edited by J. Messier et al. (Kluwer Academic Publishers, Dordrecht, 1989), p219.

[29] G. Berkovic, Th. Rasing, and Y.R. Shen, *J.Opt. Soc. Am.* **B4**, 945 (1987).

[30] J. Bauer, P. Jeckeln, D. Lupo, W. Prass, U. Scheunemann, R. Keosian, and G. Khanarian, *Organic Materials for Non–linear Optics*, edited by R.A. Hann and D. Bloor (The Royal Society of Chemistry, London, 1989), p348.

[31] A. Bagchi, R.G. Barrera, and R. Fuchs, *Phys. Rev.* **B25**, 7086 (1982).

[32] A. Bagchi, R.G. Barrera, and B.B. Dasgupta, *Phys. Rev. Lett.* **44**, 1475 (1980).

[33] D. Bedeaux and N. Bloembergen, *Physica (Utrecht)* **69**, 57 (1973).

[34] J. Van Kranendonk and J.E. Sipe, *Progress in Optics*, edited by E. Wolf (North–Holland, Amsterdam, 1977), vol. 15, p245.

[35] P. Ye and Y.R. Shen, *Phys. Rev.* **B28**, 4288 (1983).

[36] W.H. de Jeu and P. Bordewijk, *J. Chem. Phys.* **68**, 109 (1978).

[37] M. Orrit, D. Möbius, U. Lehmann, and H. Meyer, *J. Chem. Phys.* **85**, 4966 (1986).

[38] H. Hoek, *Dissertation*, Univ. of Leiden, Leiden (1939).

[39] F. Reiche, *Ann. d. Physik* **50**, 1, 121 (1916).

[40] J. Topping, *Proc. Roy. Soc. (London) Ser.* **A114**, 67 (1927).

[41] T.F. Heinz, H.W.K. Tom, and Y.R. Shen, *Phys. Rev.* **A28**, 1883 (1983).

[42] J.B.E. Hulshof, E.P. Schudde, B.L. Feringa, M.A. Schoondorp, and A.J. Schouten, to be published.

[43] M.A. Schoondorp, A.J. Schouten, J.B.E. Hulshof, and B.L. Feringa, to be published.

[44] G. Marowsky, L.F. Chi, D. Möbius, R. Steinhoff, Y.R. Shen, D. Dorsch, and B. Rieger, *Chem. Phys. Lett.* **147**, 420 (1988).

[45] O.A. Aktsipetrov, N.N. Akhmediev, J.M. Baranova, E.D. Mishina, and V.R. Novak, *Sov. Phys. JETP* **62**, 524 (1985).

[46] T.G. Zhang, C.H. Zhang, and G.K. Wong, *J. Opt. Soc. Am.* **B7**, 902 (1990).

[47] X. Xiao, V. Vogel, and Y.R. Shen, *J. Chem. Phys.* **94**, 2315 (1991).

[48] M.R. Philpott, *J. Chem. Phys.* **61**, 5306 (1974).

[49] R.W.J. Hollering and W.J.O.V. Teesselink, *Opt. Commun.* **79**, 224 (1990).

[50] N.J. Geddes, M.C. Jurich, J.D. Swalen, R. Twieg, and J.F. Rabolt, *J. Chem. Phys.* **94**, 1603 (1991).

[51] B.F. Levine, C.G. Bethea, E. Wasserman, and L. Leenders, *J. Chem. Phys.* **68**, 5042 (1978).

[52] H. Kuhn and A. Schweig, *Chem. Phys. Lett.* **1**, 255 (1967).

[53] G. Khanarian, A. Artigliere, R. Keosian, E.W. Choe, R. DeMartino, D. Stuetz, and C.C. Teng, *Proc. SPIE. Int. Soc. Opt. Eng.* **682** (Mol. Polym. Optoelectron. Mater.: Fundam. Appl.), 153 (1986).

[54] Th. Rasing, G. Berkovic, Y.R. Shen, S.G. Grubb, and M.W. Kim, *Chem. Phys. Lett.* **130**, 1 (1986).

[55] D.J. Williams, Editor, *Nonlinear Optical Properties of Organic and*

Polymeric Materials, ACS Symposium series, No. 233, American Chemical Society, Washington, D.C., (1983).

[56] J. Knoester, *Phys. Rev.* **A**, submitted for publication.

CHAPTER 7

Second-harmonic generation in front of a mirror

7.1 Abstract

7.2 Introduction

7.3 Experimental

7.4 Results and discussion

7.4.1 Second-harmonic generation as a function of surface density

7.4.2 Second-harmonic generation as a function of distance to the mirror

References

7.1 Abstract

In this chapter we study the influence of an aluminum substrate on the second-order nonlinear optical properties of dye-doped monolayers. The behaviour of $\chi^{(2)}(2\omega,\omega,\omega)$ is measured as a function of surface density on aluminum and on glass substrates. For a given distance of the layer to the substrate the behaviour of $\chi^{(2)}(2\omega,\omega,\omega)$ as a function of surface density on either aluminum or glass substrates can be quantitatively explained by taking into account local-field corrections in a manner previously described.

The second-harmonic generation efficiency was found to depend on monolayer-aluminum distance. Close to the metal substrate a decrease in efficiency is observed, which is not reproduced by local-field calculations. The distance dependence could be attributed to energy transfer to the metal.

7.2 Introduction

The second-order nonlinear optical susceptibility of non-centrosymmetric dye molecules is frequently studied by preparing a monolayer of the compound using the Langmuir-Blodgett dipping technique [1,2]. The substrate used is often an amorphous glass and its contribution to the second-harmonic signal can be neglected for symmetry reasons. However, in case of metallic substrates quadrupole contributions can be of importance [3]. Another consequence of using metal instead of glass substrates is that the *macroscopic* local-field in the monolayer is different [4]. For metal substrates the dominant field component is perpendicular to the surface, while the component parallel to the surface is an order of magnitude smaller. In case of glass substrates the perpendicular and parallel electric field components are of comparable magnitude. Besides the macroscopic local-field, also the *microscopic* local-field is different. On glass substrates only induced-dipole induced-dipole interactions within the monolayer are of importance, while for metal substrates also the interaction with induced

image dipoles should be included. These interactions lead to frequency shifts, and affect the excited state lifetime. The frequency shift can be neglected for monolayer-metal distances larger than a few angstroms. For these larger distances the interaction of a dipole with the real part of the reaction field of its own mirror image is effectively counteracted by the opposing field of neighbouring image dipoles [5,6]. Energy transfer has a longer range and cannot be neglected. Energy transfer reduces the excited state lifetime by several orders of magnitude for monolayer-metal distances smaller than 10 nm. In general, an inverse cube dependence of the energy transfer rate with distance is found [7,8]. Energy transfer will influence linear as well as nonlinear optical properties. The increased damping rate is expected to decrease the second-harmonic generation (SHG) efficiency for monolayers close to metal substrates.

In this work we study the SHG efficiency of dye doped monolayers both as a function of surface density on, and as a function of distance to flat aluminum substrates. The results are compared with previous experiments on glass substrates. In case of glass substrates a deviation from the expected linear behaviour of $\chi^{(2)}(2\omega,\omega,\omega)$ on surface density was previously reported [9,10]. The deviation was interpreted in terms of induced-dipole induced-dipole interactions. The size of the deviation was found to depend on the orientation of the dye molecules in the monolayer. In the present work, the surface density dependence for a given monolayer-metal distance is measured and calculated. A less pronounced deviation on surface density is found. We also measured the second-harmonic generation efficiency, as a function of monolayer-aluminum distance for various surface densities. The monolayer-Al distance was varied by the application of polymer spacer layers, achieving a spatial resolution of 1 nm thickness. $\chi^{(2)}(2\omega,\omega,\omega)$ was found to decrease for small monolayer-metal distances.

7.3 Experimental

Substrates were prepared by evaporation, at a pressure of 10^{-5}Torr, of

thick aluminum layers onto Corning 7059 amorphous glass slides. The slides were cleaned before use in chromic acid, and were rinsed ultrasonically with milli-Q water, acetone, chloroform, and hexane.

The spacer layer consisted of amylose-acetate ester, and was applied by the Langmuir-Blodgett technique at a surface pressure of 7 mN/m [11]. The subphase was highly purified water (milli-Q), at a temperature of 22 °C. Monolayers were transferred during every upstroke.

The optical nonlinear molecules studied in this work are 4-(4-didecylaminostyryl)-N-methylpyridiniumiodide (dye **I**, see the inset of Fig. 7.2) and (S,S)-4'-[4-(1-pyrrolidine-3,4-dipalmitoate)-phenylazo-3-nitro-benzoic acid (dye **II**, see the inset of Fig. 7.3). Dye **I** was purchased from Molecular Probes, Inc., and was used without further purification. Preparation of monolayers of dye **I** has been described in reference [9]. The synthesis [12] and the preparation of monolayers [13] of dye **II** will be published elsewhere.

A specific surface density of either dye **I** or **II** was obtained by dissolving known amounts of dye and arachidic acid (Fluka AG) in chloroform before spreading onto the aqueous subphase.

For the second-harmonic-generation experiment we used the linearly polarized fundamental output (1064 nm) of a Q-switched Nd^{3+}:YAG laser (Molectron Corporation), which was incident on the sample under 45 degrees. The frequency doubled light (532 nm) was detected in the reflected direction. All measurements were done within one hour after preparation.

7.4 Results and discussion

7.4.1 Second-harmonic generation as a function of surface density

The macroscopic surface nonlinear susceptibility $\chi_s^{(2)}$ of a molecular monolayer on a substrate can be separated into three parts [1]:

$$\chi_s^{(2)} = \chi_{ss}^{(2)} + \chi_m^{(2)} + \chi_i^{(2)}, \qquad (7.1)$$

where $\chi_{ss}^{(2)}$ is the bare substrate nonlinear susceptibility, $\chi_m^{(2)}$ is the nonlinearity of the isolated monolayer, and $\chi_i^{(2)}$ accounts for the interaction between monolayer and substrate. $\chi_i^{(2)}$ will generally be distance dependent. In the systems studied the optical nonlinearity of the dye molecules is dominant. The nonlinear contribution of the bare (amorphous) aluminum substrate ($\chi_{ss}^{(2)} \approx 9*10^{-14}$ esu [14]) is an order of magnitude smaller than the isolated monolayer nonlinearity ($\chi_m^{(2)} \approx 10^{-12}$ esu). We neglect the interaction term $\chi_i^{(2)}$.

For the calculation of the second-harmonic field strength we assume an azimuthal isotropic ordering of rigid-rod shaped dye molecules. For this ordering the tilt angle ψ of the dye unit with respect to the surface normal (the z-axis) is the same for every molecule, while the distribution of projection angles ϕ in the azimuthal plane (the substrate surface) is random (isotropic monolayer model) [9,15]. For axially symmetric dye molecules as studied in this chapter, the dominant molecular linear and second-order polarizability component is along the long axis (ξ-axis) of the dye unit. For this system one calculates for the parallel polarized second-harmonic field strength, induced by a parallel polarized fundamental beam [1]:

$$
\begin{aligned}
E_{pp}(2\omega) = \frac{i4\pi\omega}{c}\tan\theta \Big\{ & L_{zz}(2\omega) < E^n_{loc,z}(2\omega) > \chi^{(2)}_{zzz} L^2_{zz}(\omega) < E^n_{loc,z}(\omega) E^n_{loc,z}(\omega) > \sin^2\theta \\
& + \big[L_{zz}(2\omega) < E^n_{loc,z}(2\omega) > \chi^{(2)}_{zxx} L^2_{xx}(\omega) < E^n_{loc,x}(\omega) E^n_{loc,x}(\omega) > \\
& - 2L_{xx}(2\omega) < E^n_{loc,x}(2\omega) > \chi^{(2)}_{xzx} L_{zz}(\omega) L_{xx}(\omega) < E^n_{loc,z}(\omega) E^n_{loc,x}(\omega) > \big] \cos^2\theta \Big\} E_0^2(\omega) ,
\end{aligned}
\tag{7.2}
$$

where θ is the angle of incidence on the sample, ω the fundamental frequency, and c the speed of light. The capital L's are Fresnel transmission coefficients (macroscopic local-field factors) containing the dielectric constants of substrate, monolayer, and superstrate [1]. The distance dependence of these macroscopic local-field factors can be neglected for the studied monolayer-aluminum distance regime (1 – 6 nm). The dielectric constant and the angle of refraction are complex numbers in case of metal substrates. The subscripts denote projections on the (Cartesian) laboratory axis system, where the z-axis is perpendicular to the substrate surface, and the x-axis is parallel

to the substrate plane and the plane of incidence. On metal substrates, $|L_{zz}|$ is usually an order of magnitude larger than $|L_{xx}|$. For a perfect mirror $|L_{xx}|$ is even zero, and the terms between square brackets diminish. However, for real metallic substrates and in case of large tilt angles this term may become comparable to the first term in Eq.(7.2), and should not be neglected. Expressions between triangular brackets denote ensemble averaged microscopic local-field components [9].

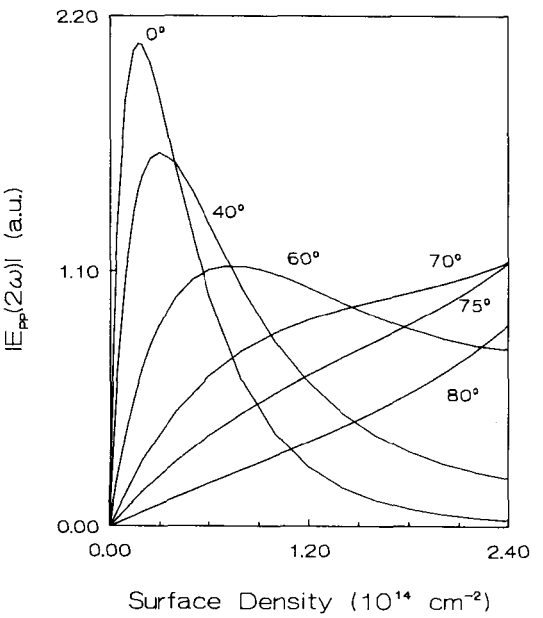

Figure 7.1: *The dependence of the second-harmonic field strength on surface density as predicted by Eq.(7.2). The different traces are labelled by the tilt angle of the dye unit with respect to the surface normal. A linear polarizability of* $40\,\text{Å}^3$ *was used in the calculations.*

In Eq.(7.2), the ensemble averaged microscopic local-field components $<E^n_{loc,j}>$ and $<E^n_{loc,j}E^n_{loc,k}>$ along $j,k=x,y,z$ were calculated iteratively for a random and partially filled lattice of dye molecules, arranged according to the above described isotropic monolayer model [9,16]. The sum of the applied field

and the total reaction field of surrounding dipoles was calculated for each lattice site n, and averaged over the lattice, followed by averaging over a large number of different ensembles. Density variations were simulated by an incomplete occupation of the lattice. In the calculations only near-field contributions of surrounding dipoles to the total reaction field are considered. Calculations show that the contribution of induced image dipoles to the local-field can be neglected for distances larger than a few tens of a nanometer [17], in agreement with previous work of Ye et al. [6] and Levine et al. [5].

The above described local-field calculations have been successfully applied to the description of nonlinear optical properties of monolayers on glass substrates [9,10]. In this chapter an extension is made to the second-harmonic efficiency of monolayers on aluminum substrates.

The SHG efficiency is calculated by multiplication of Eq.(7.2) with its complex conjugate. The results are given in Fig.7.1, where $|E_{pp}(2\omega)|$ is plotted against surface density. The different traces are labelled by the tilt angle of the dye molecules. Except for molecules oriented almost parallel to the metal substrate, a maximum in SHG efficiency is found. The surface density at which the maximum occurs depends on the tilt angle: the maximum shifts to higher surface densities for larger tilt angles.

The appearance of a maximum in the SHG efficiency is due to the microscopic local-field. In case of metal substrates, the projection on the surface normal of the induced dipoles in the monolayer is an order of magnitude larger than other components, and consequently the applied field at site n is opposed by the reaction field of surrounding dipoles [5]. For molecules with a larger tilt the opposing reaction field along the surface normal is smaller compared to the reaction field of more erect molecules. Therefore the maximum in SHG efficiency appears only at higher surface densities. In case of molecules oriented almost parallel to the substrate, the induced component perpendicular to the substrate surface (first term of Eq.(7.1)) can be neglected compared to the small component parallel to the substrate. Consequently a nonlinear increase of the SHG intensity with surface density is calculated (see Fig.7.1, trace labelled 80°). Note that for large tilt angles the second-harmonic efficiency at low surface densities is very sensitive to small variations in tilt angle.

In Fig.7.2 we plotted for dye **I** the square root of the second-harmonic intensity as a function of surface density. Assuming a tilt angle of 80° (the same value as determined in case of glass substrates) [9], good agreement

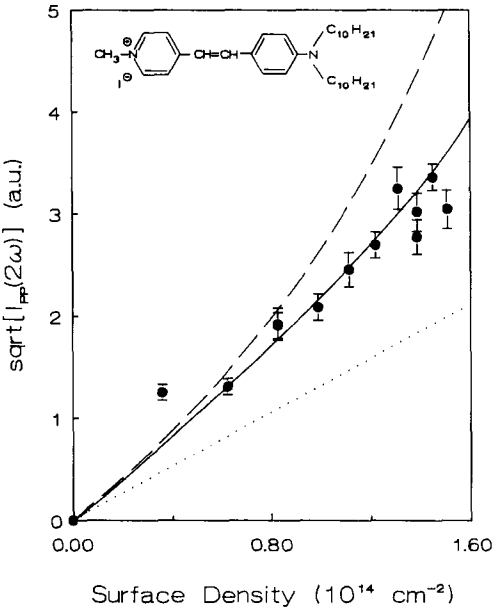

Figure 7.2: *Square root of the measured values of* $I_{pp}(2\omega)$ *for monolayers of dye* **I** *on amorphous aluminum substrates (circular points) as a function of surface density. Shown in the inset is the structural formula of dye* **I**. *Also shown are results of calculations according to the isotropic monolayer model* [9] *in case of aluminum substrates (solid line) and glass substrates (dashed line). In these calculations we used a tilt angle of* 80° *for the dye units on both types of substrates. The dotted line is the result of disregarding the microscopic local-field. In the calculations a linear polarizability of* 50 Å^3 *was used.*

between calculations (drawn line) and experimental data is found. Compared to glass substrates (broken line), a less pronounced deviation from a linear behaviour (dotted line) with surface density is found. A similar kind of

behaviour is found for the azo-dye **II** (Fig.7.3). In case of glass substrates a tilt angle of 60° is determined [10]. However, for the case of aluminum substrates agreement between experiment and calculations is reached assuming a tilt angle of 80°. The reason for this change in tilt angle is not clear. From

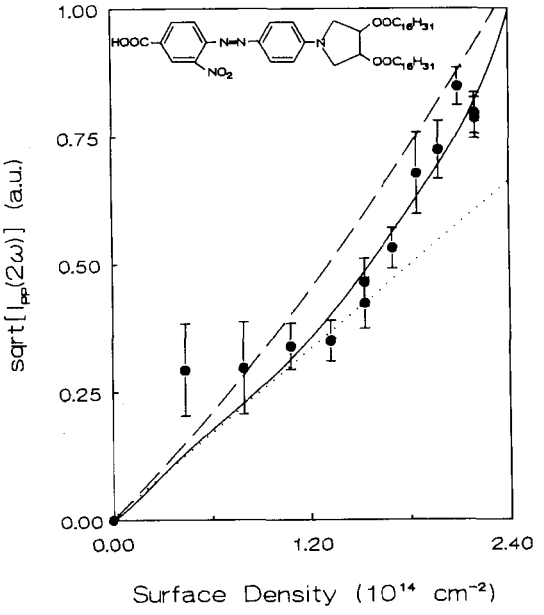

Figure 7.3: *Square root of the measured values of* $I_{pp}(2\omega)$ *for monolayers of dye* **II** *deposited on amorphous aluminum substrates (circular points) as function of surface density. Shown in the inset is the structural formula of dye* **II**. *Also shown are results of calculations according to the isotropic monolayer model* [9] *in case of aluminum substrates (solid line) and glass substrates (dashed line). In these calculations we used a tilt angle of* 80° *for the dye units in case of aluminum substrates and* 60° *when using glass substrates. The dotted line is the result of disregarding the microscopic local-field. In the calculations a linear polarizability of* 40 Å^3 *was used.*

molecular modelling however, it appears that some freedom exists for the dye unit to reorient itself. The occupied surface area per molecule (≈ 45 Å^2) is

determined by the two alkyl chains and not by the dye unit. Deviations from the calculated behaviour at low surface density are possibly due to small variations in tilt angle. As follows from Fig.7.1, the signal strength is very sensitive to small changes in tilt angle for molecules oriented almost parallel to the substrate.

The same type of behaviour of $|E_{pp}(2\omega)|$ with surface density is found at larger distances (2–6 nm) from the mirror. However, the measured intensity does depend on distance from the surface, which is the subject of the next section.

7.4.2 Second-harmonic generation as a function of distance to the mirror.

In figure 7.4 we plotted for dye **II** the square root of the SHG intensity, normalized with respect to the square root of the intensity at infinite distance from the mirror, as a function of monolayer–mirror distance. For small distances a decrease of the SHG efficiency is found. A similar behaviour is found at other surface densities. In case of glass substrates, the SHG efficiency is independent of monolayer–substrate distance. Several mechanisms can be proposed for the observed decrease in harmonic intensity at small distances from the mirror surface.

A possible explanation is given by Antoniewicz [18], who describes the interaction between the molecule and the substrate in terms of induced–dipole – image–dipole interactions. By incorporating the oscillation of the induced dipole moment around the center of mass of the molecule, the generation of harmonic components is described in a monolayer of centrosymmetric molecules on rough silver surfaces [19]. However, rather small distances between the molecules and the substrate need to be chosen to yield the observed signal strength. In case of distances larger than about 1 nm, this contribution to the second–order susceptibility is calculated to be about four orders of magnitude smaller than the inherent molecular nonlinearity, and can therefore be neglected for the studied distance regime in this work.

Ye et al [6] considered the spatial variation of the local–field at the metal surface. The strong variation of the field is expected to change molecular

nonlinear polarizabilities, and affects the observed signal strength. For distances larger than about 0.5 nm from the mirror, however, the spatial variation of the local-field can be neglected, as follows from our calculations [17], and also from the work of Ye et al. [6]. For this reason the above mentioned mechanism does also not apply to the distance regime studied in this chapter.

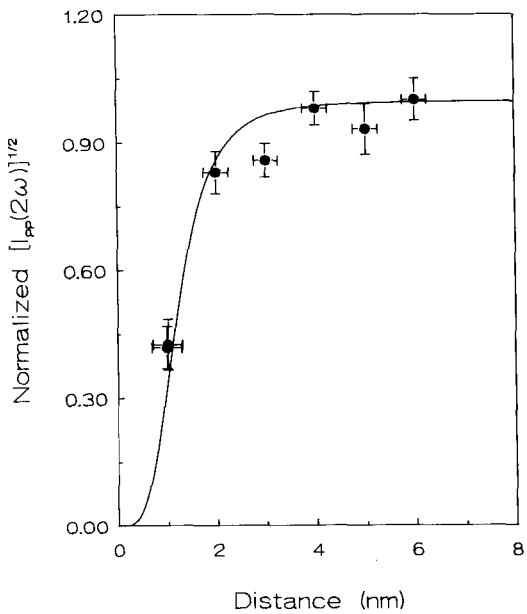

Figure 7.4: *Experimental values of the square root of the second-harmonic intensity as a function of monolayer-aluminum distance (closed circles). The data are normalized with respect to the value at infinite distance from the mirror. Also shown (solid line) is the calculated distance behaviour if energy transfer is incorporated (see text for details).*

We propose that energy transfer to the metal substrate is the main reason for the observed distance behaviour. Energy transfer is caused by the coupling of the near field of an oscillating dipole with the metal electron gas, where energy is dissipated through various scattering processes. In order to estimate

the efficiency of energy transfer the imaginary part of the reflected field needs to be calculated [7]. Energy transfer did not appear in the above calculations, because only the real part of the reflected field was considered.

The drawn curve in Fig.7.4 is the result of calculations were the effect of energy-transfer has been included in the damping term, which appears in the denominator of the nonlinear susceptibility. In this section we discuss the effect of energy transfer on first-order nonlinear optical properties of monolayers.

The effect of energy transfer on *linear* optical properties has been studied extensively during past decades [7,20]. Energy transfer dominates optical properties for molecules close (<10 nm) to metal surfaces. A decrease of the excited state lifetime by several orders of magnitude is observed, and is attributed to the presence of a continuum of nonradiative decay channels. The reduced excited state lifetime leads to a broadening of the transition if the excited state lifetime becomes of the order of magnitude of the pure dephasing time, which is the case for directly adsorbed molecules [21,22].

In order to incorporate energy transfer in the second-order susceptibility $\chi^{(2)}(2\omega,\omega,\omega)$ we use a two-level approximation [23], which is justified by the large and highly anisotropic polarizability and hyperpolarizability. Energy transfer will influence the homogeneous damping rate Γ of the optical transition, which appears in the common denominator $[(\omega_0-\omega+i2\pi\Gamma)(\omega_0-2\omega+i2\pi\Gamma)]^{-1}$ of the expression for the second-harmonic field strength of Eq.(7.2) [23]. Here ω is the (fundamental) laser frequency, and ω_0 the centre frequency of the homogeneous transition.

In order to calculate the second-harmonic field strength we have to sum over the nonlinear contribution of single molecules in the inhomogeneous distribution of oscillators. Assuming a Gaussian inhomogeneous distribution one then obtains for the second-harmonic field strength:

$$E_{pp}(2\omega) \propto \int_{+\infty}^{-\infty} \frac{\exp(-\Delta^2/\sigma^2)\,d\Delta}{(\Omega_0-\Delta-\omega+i2\pi\Gamma)(\Omega_0-\Delta-2\omega+i2\pi\Gamma)}, \qquad (7.3)$$

where Ω_0 is the center frequency of the inhomogeneously broadened absorption line, Δ the detuning from Ω_0, and σ the width of the Gaussian inhomogeneous distribution of optical oscillators.

The homogeneous damping rate Γ is given by [24]:

$$\Gamma = (2T_1)^{-1} + (T_2^*)^{-1} \ , \tag{7.4}$$

where T_1 is the excited state lifetime, and T_2^* the pure dephasing time (transverse relaxation time). T_2^* is presumed to be independent of emitter-mirror distance. Energy transfer will reduce T_1 by several orders of magnitude according to [21]:

$$T_1^{-1}(d,\omega) \approx T_r^{-1}\left\{1+\frac{\eta}{8}(dk)^{-3}\left[2\mathrm{Im}\left(\frac{\varepsilon_m(\omega)-\varepsilon_1}{\varepsilon_m(\omega)+\varepsilon_1}\right)+6\xi\frac{1}{k_F d}\frac{\omega}{\omega_p}+18\frac{\omega_F}{\omega_p}\frac{\omega}{\omega_p}\frac{1}{k_F d}\right]\right\}, \tag{7.5}$$

where T_r is the radiative lifetime in the absence of the mirror, d is the distance between the nonlinear monolayer and the aluminum surface, k is the magnitude of the wavevector at the emitted frequency ω (in this case the second-harmonic frequency), $\varepsilon_m(\omega)$ is the (complex) metal dielectric constant, ε_1 is the dielectric constant of the medium in which the dipole is embedded, and η is an orientational parameter ($\eta = {}^3/_2$ for a perpendicular dipole and $\eta = {}^3/_4$ for a parallel dipole). Some typical metallic electron gas parameters are contained in the last two terms between square brackets, where k_F is the Fermi wavevector, ω_F the Fermi frequency, ω_p the plasma frequency, and $\xi \approx 1$ is a constant which depends on the electron gas density [21]. For a complete derivation and discussion of the different terms in Eq.(7.5) we refer to the work of Persson et al. [21,25]. Eq.(7.5) has been applied successfully to the interpretation of fluorescence properties of rhodamine 6G monolayers close to aluminum surfaces [22].

For a calculation of the distance dependence of the second-harmonic efficiency (solid line in Fig7.4) we evaluated Eq.(7.3) numerically. In the calculations we used $\eta = {}^3/_4$ (the dye units are nearly parallel to the surface), $T_r = 2.8$ ns, $\Omega_o = 4.28{*}10^{15}$ rad/s (corresponding to a center wavelength of 440 nm),

$\sigma = 10^{14}$ rad/s, $\varepsilon(2\omega) = -33 + i10$ [26], $\varepsilon_1 = 1.3$, $k_F = 1.75*10^{10}$ m^{-1}, $\omega_F = 1.7774*10^{16}$ rad/s, and $\omega_p = 2.39*10^{16}$ rad/s [27]. The value for T_r was estimated from the Einstein A coefficient [24] using a transition dipole moment of $3.14*10^{-29}$ Cm, which was determined from the integrated absorption spectrum. Furthermore, we used a value of 1 ps for T_2^*, the same value as used previously in a study of the optical properties of dye monolayers on aluminum substrates [22]. The results of calculations were found to be practically independent of the value for the inhomogeneous width σ. In the monolayer–mirror distance we included, as in previous work [22], a native oxide layer of 1 nm thickness [28]. This oxide layer is formed within two hours of exposure to air, and continues to grow very slowly and reaches its final value of about 4 nm after one month. Oxidation is unavoidable due to the application of spacer layers by the Langmuir–Blodgett technique.

From the above results we conclude that energy transfer theory predicts quantitatively the correct behaviour of $\chi^{(2)}(2\omega,\omega,\omega)$ as a function of distance from the aluminum surface.

In summary, we measured the SHG efficiency of monolayers of dye molecules on aluminum substrates as a function of surface density, and as a function of monolayer–aluminum distance. Deviations from the expected linear behaviour in surface density were found and attributed to the microscopic local-field. The deviations were less pronounced as in case of glass substrates, due to the difference in macroscopic local-field factors. At a fixed surface density the SHG efficiency was found to decrease for small monolayer–aluminum distances. This decrease is possibly caused by energy transfer through the near-field of the induced dipoles to the aluminum substrate.

References

[1] Y.R. Shen, *Ann. Rev. Phys. Chem.* **40**, 327 (1989).

[2] *Langmuir–Blodgett films*, edited by G. Roberts (Plenum Press, London, 1990).

[3] N. Bloembergen, R.K. Chang, S.S. Jha, and C.H. Lee, *Phys. Rev.* **174**, 813

(1968); **178**, 1528(E) (1969).

[4] P. Guyot-Sionnest and Y.R. Shen, *Phys. Rev.* **B35**, 4420 (1987).

[5] B.F. Levine, C.V. Shank, and J.P. Heritage, *IEEE J. Quantum Electron.* **QE-15**, 1418 (1979).

[6] P. Ye and Y.R. Shen, *Phys. Rev.* **B28**, 4288 (1983).

[7] R.R. Chance, A. Prock, and R. Silbey, *Adv. Chem. Phys.* **37**, 1 (1978).

[8] P.M. Whitmore, H.J. Robota, and C.B. Harris, *J. Chem. Phys.* **77**, 1560 (1982).

[9] G. Cnossen, K.E. Drabe, and D.A. Wiersma, *J. Chem. Phys.*, submitted for publication. See also chapter 6 of this thesis.

[10] G. Cnossen, K.E. Drabe, D.A. Wiersma, M.A. Schoondorp, A.J. Schouten, J.B.E. Huslhof, and B.L. Feringa, to be published.

[11] M.A. Schoondorp, E.J. Vorenkamp, and A.J. Schouten, *Thin Solid Films* **196**, 121 (1991).

[12] J.B.E. Hulshof, E.P.Schudde, B.L. Feringa, M.A. Schoondorp, and A.J. Schouten, to be published.

[13] M.A. Schoondorp, A.J. Schouten, J.B.E. Hulshof, and B.L. Feringa, to be published.

[14] S. Govorkov, N.I. Koroteev, I.L. Shumay, and V.V. Yakovlev, *J. Opt. Soc. Am.* **B8**, 1023 (1991).

[15] T.F. Heinz, H.W.K. tom, and Y.R. Shen, *Phys. Rev.* **A28**, 1883 (1983).

[16] J. Van Kranendonk and J.E. Sipe, in *Progress in Optics*, edited by E. Wolf (North-Holland, Amsterdam, 1977), vol.XV, p245.

[17] G. Cnossen, K.E. Drabe, and D.A. Wiersma, unpublished results.

[18] P.R. Antoniewicz, *Phys. Rev.* **B26**, 2285 (1982).

[19] T.F. Heinz, C.K. Chen, D. Ricard, and Y.R. Shen, *Chem. Phys. Lett.* **83**, 180 (1981).

[20] X.L. Zhou, X.Y. Zhu, and J.M. White, *Surf. Sci. Rep.* **13**, 75 (1992) and references therein.

[21] Ph. Avouris and B.N.J. Persson, *J. Phys. Chem.* **88**, 837 (1984).

[22] G. Cnossen, K.E. Drabe, and D.A. Wiersma, to be published, see also chapter 5 of this thesis.

[23] Y.R. Shen, *The Principles of Nonlinear Optics* (John Wiley & Sons, Inc, New

York, 1984).

[24] see for example L. Allen and J.H. Eberly in *Optical Resonance and Two-Level Atoms* (John Wiley & Sons, Inc., New York, 1975).

[25] - B.N.J. Persson and N.D. Lang, *Phys. Rev.* **B26**, 5409 (1982).
- B.N.J. Persson and M. Persson, *Surf. Sci.* **97**, 609 (1980).
- B.N.J. Persson, *J. Phys. C.* (*Solid State Phys.*) **11**, 4251 (1978).

[26] C.C. Zheng and J.T. Lue, *Phys. Rev.* **A39**, 191 (1989).

[27] N.W. Ashcroft and N.D. Mermin in *Solid State Physics* (Saunders College, Philadelphia, 1976).

[28] G. Hass and N.W. Scott, *J. Phys. Rad.* **11**, 394 (1950).

Samenvatting

In dit proefschrift worden experimenten beschreven waarin de optische eigenschappen van kleurstof-bevattende dunne lagen zijn bestudeerd. Onder een dunne laag wordt verstaan een film met een dikte minder dan 10 micrometer. Twee soorten dunne lagen zijn bestudeerd, namelijk polymere films met een dikte van ongeveer 2 micrometer, en monomoleculaire lagen met een dikte in de orde van 2,5 nanometer (1 nanometer is éénmiljoenste millimeter). In de experimenten staat de invloed van quantumelectrodynamische interacties tussen moleculen en hun omgeving op de optische eigenschappen van deze dunne lagen centraal.

Het eerste deel van dit proefschrift behandelt het effect van een spiegel op de intensiteit en kleurinhoud (spectrum) van het door de kleurstofmoleculen uitgezonden licht. Hierbij speelt de interactie tussen de moleculen en hun spiegelbeeld een belangrijke rol. Manipulatie van deze interactie is mogelijk door de afstand tussen de kleurstoflaag en de spiegel te variëren. In het tweede deel staat de interactie tussen kleurstofmoleculen onderling centraal. Het effect van de onderlinge afstand en orientatie op de efficiëntie van optisch niet-lineaire processen wordt nader behandeld. Kennis van de interacties tussen moleculen is van belang voor een beter begrip van de relatie tussen macroscopische waarnemingen en moleculaire eigenschappen.

In het navolgende zal een beknopte samenvatting van de verschillende hoofdstukken worden gegeven en zal de relatie tussen de hoofdstukken nader worden toegelicht.

Na de introductie in hoofdstuk 1 is *hoofdstuk* 2 gewijd aan effect van een spiegel op het emissiespectrum uitgezonden door kleurstofmoleculen die zijn opgelost in een polymere film (2 micrometer dik). Deze film werd direct aangebracht op een vlakke aluminium spiegel, of met behulp van een transparante polymeer laag (1 tot 20 micrometer dik) van de spiegel gescheiden. De oscillaties, die in het emissiespectrum worden waargenomen, zijn het gevolg van een tweetal interferentie effecten. In de eerste plaats wordt er een rooster van geëxciteerde moleculen gevormd als gevolg van interferentie tussen de directe en de aan de spiegel gereflecteerde laserbundel. Vanaf dit rooster vindt fluorescentie plaats, waarbij interferentie optreedt tussen direct uitgezonden licht en licht dat via de spiegel de detector bereikt. De vorming van het rooster is essentieel om de genoemde oscillaties spectraal te kunnen oplossen.

Tevens dient de afstand tussen de emitterende moleculen en de spiegel niet groter te zijn dan een aantal malen de golflengte van het uitgezonden licht (570 nanometer).

Bij gebruik van een gepulste laser als excitatiebron, in plaats van een continu lasersysteem, is het mogelijk om tijdens de opbouw van het rooster informatie te verkrijgen over faserelaxatie (defasering) ten gevolge van fase-verstorende wisselwerking met de polymere matrix. Defasering treedt op gedurende het tijdsverschil tussen de directe exciterende puls en de aan de spiegel gereflecteerde puls. Door de afstand tussen kleurstoflaag en spiegel te veranderen kan de tijdsduur tussen deze twee pulsen gevarieerd worden. Defasering resulteert in een slechter contrast van de eerdergenoemde spectrale oscillaties.

In *hoofdstuk* 3 wordt een experiment beschreven waarin dit contrast wordt gemeten als functie van het tijdsverschil tussen de twee exciterende laserpulsen. Als excitatiebron fungeert een ultrasnelle gepulste laser met een pulsduur van 45 femtoseconden (1 femtoseconde is 0,000000000000001 seconde). Met deze techniek wordt een defaseringstijd van 100 femtoseconden bij kamertemperatuur gemeten voor de kleurstof Nile Blue opgelost in poly(4-vinylpyridine). Het voordeel van deze nieuwe techniek ten opzichte van conventionele foton-echo technieken is dat er met veel lagere laservermogens gewerkt kan worden, waardoor degradatie van het monster niet optreedt.

In *hoofdstuk* 4 worden de coherentie eigenschappen behandeld van het licht dat wordt uitgezonden door een dunne fluorescerende film (2 micrometer dik) voor een spiegel. De correlatie tussen het uitgezonden electromagnetisch veld op verschillende punten in de tijd en de ruimte wordt berekend. Het blijkt dat deze correlatiefunctie afwijkt van die van een zwarte straler (bijvoorbeeld een gloeilamp). Het gevolg hiervan is dat het spectrum verandert tijdens propagatie door de ruimte, hetgeen bij een zwarte straler niet het geval is. Voor een zwarte straler geldt dat het spectrum onafhankelijk van is van het observatiepunt. Metingen bevestigen de verandering van het spectrum tijdens propagatie.

In de hierboven beschreven experimenten is de afstand tussen de kleurstofmoleculen en de spiegel groter dan de golflengte van het uitgezonden licht. Voor deze afstanden kan energie-overdracht naar de spiegel toe verwaarloosd worden. Energie-overdracht wordt veroorzaakt door de interactie van

de aangeslagen moleculen met het electronengas van het metaal. Energie-overdracht is afstandsafhankelijk en leidt tot een verkorting met enkele ordes van grootte van de levensduur van de aangeslagen toestand. Het effect van energie-overdracht op de fluorescerende eigenschappen van moleculen die minder dan 10 nanometer van de spiegel verwijderd zijn, is het onderwerp van *hoofdstuk* 5. Een monolaag van fluorescerende kleurstofmoleculen wordt hiertoe gescheiden van een aluminium spiegel door monomoleculaire transparante polymeerlagen. Op deze wijze kan de afstand tussen de fluorescerende laag en de spiegel in stapjes van 1 nanometer worden vergroot. De fluorescentielevensduur en het emissiespectrum worden gemeten als functie van de afstand tussen de kleurstoflaag en de spiegel. Bij een afstand kleiner dan 2 nanometer tot de spiegel wordt een levensduur gemeten die 4 ordes van grootte korter is dan de levensduur bij een oneindige afstand van de spiegel. Tevens wordt een verbreding van het spectrum gevonden voor kleurstof-spiegel afstanden kleiner dan 4 nanometer. Deze verbreding wordt toegeschreven aan de korte levensduur van de aangeslagen toestand. Uit de verbreding van het spectrum kan tevens informatie worden verkregen over de defaseringstijd van de kleurstofmoleculen in de monolaag. Direct op het metaaloppervlak wordt de defaseringstijd bepaald op 100 femtoseconden, terwijl voor een kleurstoflaag die door polymere monolagen van de spiegel wordt gescheiden een defaseringstijd van 1 picoseconde wordt afgeleid (1 picoseconde is 1000 femtoseconden). Het verschil in defaseringstijd moet worden toegeschreven aan de interacties met het metaaloppervlak.

In het tweede deel van dit proefschrift worden intermoleculaire interacties bestudeerd met behulp van harmonische generatie. Het proces van harmonische generatie is vergelijkbaar met de productie van boventonen in een muziekinstrument. Gemeten wordt de hoeveelheid licht van de dubbele frequentie die door een intense laser, werkend op de fundamentele frequentie, in een monolaag van cylindervormige kleurstofmoleculen wordt gegenereerd. De sterkte van het signaal is afhankelijk van het aantal moleculen per oppervlakte-eenheid (oppervlaktedichtheid), van de orientatie van de moleculen in de monolaag en van de intermoleculaire interacties. In de afwezigheid van intermoleculaire interacties is de wortel uit het signaal (efficiëntie) lineair in de oppervlaktedichtheid. De sterkte van de intermoleculaire interacties hangt af van de afstand tussen de moleculen en de onderlinge orientatie.

In *hoofdstuk* 6 worden resultaten van computersimulaties beschreven waarin de signaalsterkte wordt berekend als functie van de oppervlaktedichtheid en als functie van de orientatie van de moleculen in de monolaag. Quantumelectrodynamische interacties tussen de moleculen worden meegenomen. Uit de berekeningen volgt dat voor moleculen die vrijwel evenwijdig aan het substraat georiënteerd zijn de signaalsterkte niet–lineair toeneemt met de oppervlaktedichtheid. Voor moleculen die een positie innemen vrijwel loodrecht op het substraat, treedt er een verzadiging van het signaal op bij hoge oppervlaktedichtheden. In het geval dat de moleculen een orientatie innemen die het midden houdt tussen loodrecht en parallel, wordt een vrijwel lineair gedrag van het signaal als functie van de oppervlaktedichtheid berekend. Dit lineaire gedrag betekent echter niet dat de intermoleculaire interacties verwaarloosd kunnen worden. Voor drie verschillende soorten kleurstofmoleculen, elk met een andere orientatie, worden monolagen geprepareerd. De orientatie van de moleculen wordt via een nieuwe methode bepaald, gebruikmakend van lineaire absorptiespectroscopie. De efficiëntie van frequentieverdubbeling wordt gemeten als functie van de oppervlaktedichtheid, waarbij de afstand tussen de kleurstofmoleculen wordt gevarieerd door deze te mengen met optisch–neutrale vetzuurmoleculen. In alle gevallen wordt een quantitatieve overeenkomst verkregen tussen de experimentele resultaten en de berekeningen. De enige vrije parameter hierbij is een schalingsconstante tussen theorie en experiment. Alle overige parameters kunnen onafhankelijk worden gemeten of werden verkregen uit de literatuur.

In *hoofdstuk* 7 wordt harmonische generatie voor een spiegel behandeld. Voor een spiegel zijn zowel de aangelegde veldcomponenten als de gegenereerde veldcomponenten verschillend in grootte in vergelijking met dezelfde situatie voor een glas–substraat. Bovendien moet voor afstanden kleiner dan 5 nanometer tot de spiegel het effect van energie–overdracht worden meegenomen. De efficiëntie van harmonische generatie wordt opnieuw gemeten als functie van de oppervlaktedichtheid, bij een vaste afstand tot de spiegel. Vergeleken met een glas–substraat worden kleinere afwijkingen van lineair gedrag gevonden. De overeenkomst met de theorie is goed. De efficiëntie van frequentieverdubbeling wordt tevens gemeten als functie van de afstand tot de spiegel, bij een vaste oppervlaktedichtheid. Een afname van de signaalsterkte ten opzichte van het geval van een oneindige kleurstoflaag–spiegel afstand wordt gevonden voor

afstanden kleiner dan 2 nanometer. De afname wordt verklaard in termen van energie–overdracht. Energie–overdracht leidt tot een verhoogde demping van de oscillerende kleurstofmoleculen, hetgeen aanleiding geeft tot een minder efficiënte harmonische generatie. Uit de afname van de signaalsterkte kan een defaseringstijd van 1 picoseconde worden afgeleid, in overeenstemming met het resultaat van de metingen beschreven in hoofdstuk 5.